Title
Computational Investigations of Organic Reactions on Graphene, Fullerenes, and Carbon Nanotubes

Author
Cao, Yang

Publication Date
2014

Peer reviewed|Thesis/dissertation

UNIVERSITY OF CALIFORNIA

Los Angeles

Computational Investigations of Organic Reactions on Graphene, Fullerenes, and Carbon Nanotubes

A dissertation submitted in partial satisfaction of the requirements

for the degree of Doctor of Philosophy

in Chemistry

By

Yang Cao

2014

ABSTRACT OF THE DISSERTATION

Computational Investigations of Organic Reactions on Graphene,

Fullerene, and Carbon Nanotubes

by

Yang Cao

Doctor of Philosophy in Chemistry

Unversity of California, Los Angeles, 2014

Professor Kendall N. Houk, Chair

This dissertation involves explorations of on surfaces and on carbon-based nanomaterials, especially graphene, using quantum chemical calculations. The work evaluates energetics of cycloaddition reactions on different sites of graphene, improving the understanding of graphene chemistry and guiding experiments.

Chapter 1 to 3 describes theoretical investigations of 1,3-dipolar cycloadditions, Diels-Alder reactions, (2+2) cycloadditions, (4+4) cycloadditions and non-covalent interactions to graphene models. Reaction energetics have been obtained and showed that edge areas of graphene are much more favorable reaction sites than the center sites. Results indicate that graphene edges may be functionalized by a series of small molecule functional groups through cycloaddition reactions, while the interior regions cannot react. Non-covalent complexation is much more favorable than cycloaddition reactions on interior bonds of graphene. Furthermore,

the Hückel molecular orbital (HMO) localization energy calculations could be used as a tool to estimate the reactivities of various polycyclic aromatic hydrocarbon molecules for experimental guidance.

Chapter 4 illustrates the Diels-Alder reactions of pentacene, bistetracene and their derivatives with fullerene. Reaction barriers and free energies have been obtained to assess the effects of frameworks and substituent groups on the Diels-Alder reactivity and product stability. Surprisingly, calculations predict that the bulky silylethynyl substituents of pentacene and bistetracene have only a small influence on reaction barriers. However, the silylethynyl substituents significantly destabilize the corresponding products due to steric repulsions in the adducts. This is confirmed by experimental results from collaborators.

Chapter 5 reports theoretical investigations of (1+2) cycloadditions of carbene, nitrene, and oxygen with fullerene, carbon nanotube and graphene models. The results suggest that closed bond adducts are much more preferred on graphene models.

Chapter 6 describes a new method to quickly estimate the reaction energetics on large carbon nanomaterials. For the same addition reaction or cycloaddition, the reaction energetics on benzene was found to perfectly correlate with those on carbon allotrope models. Based on these linear correlation equations, it is possible to quickly estimate cycloaddition or addition reaction energies on different sites of carbon-based nanomaterials by simply calculating these reactions on benzene.

The dissertation of Yang Cao is approved.

Anastassia N. Alexandrova

Yu Huang

Kendall N. Houk, Committee Chair

University of California, Los Angeles

2014

DEDICATION

To my husband and my parents

TABLE OF CONTENTS

LIST OF FIGURES

Chapter 1

Chapter 2

Chapter 5

LIST OF TABLES

ACKNOLEDGEMENTS

First and foremost I would like to express my sincere gratitude to my advisor, Professor Kendall N. Houk for his excellent guidance, patience and financial support. He also gave me the freedom to work in my own time and enormous opportunities to explore careers beyond academia. Dr. Houk has provided me the excellent example as a successful scientist and a great person, which will inspire my whole life.

I would like to thank professor Robin Garrell for accepting me in the Material Creation Training Program, a highly competitive two-year interdisciplinary program for material science. Under her great leadership, this program has provided me a collaborative research environment, professional support and diverse cultural exposure.

I would like to thank my husband Guangye Zhang for his unconditional support and love. He is my best friend and my source of energy. I could not complete the whole process without his accompany.

I would like to thank the Houk group for their encouragement and great friendship. A special acknowledge goes to Dr. Yong Liang for his insightful suggestions and consistent guidance.

Last but not least, I would like to thank my committee, UCLA chemistry department and all my collaborators.

Chapter 1 is a version of Yang Cao, K. N. Houk *J. Mater. Chem.* **2011**, *21*, 1503.

Chapter 2 is a version of Yang Cao, Sílvia Osuna, Yong Liang, Robert C. Haddon, K. N. Houk *J. Am. Chem. Soc.* **2013**, *135*, 17643, a collaboration with Prof. Robert C. Haddon at University of California, Riverside.

Chapter 3 is a version of Shudan Bian, Amy M. Scott, Yang Cao, Yong Liang, Sílvia Osuna, K. N. Houk, and Adam B. Braunschweig, *J. Am. Chem. Soc.* **2013**, *135*, 9240. Yang Cao, Yong Liang, Sílvia Osuna and K. N. Houk were responsible for the computational work. Shudan Bian, Amy M. Scott and Adam B. Braunschweig were responsible for the experimental work.

Chapter 4 is a revised version of Yang Cao, Yong Liang, Lei Zhang, Sílvia Osuna, Andra- Lisa M. Hoyt, Alejandro L. Briseno, K. N. Houk *J. Am. Chem. Soc.* **2014**, *136*, 10743-10751. Yang Cao, Yong Liang, Sílvia Osuna and K. N. Houk were responsible for the computational work. Lei Zhang, Andra- Lisa M. Hoyt and Alejandro L. Briseno were responsible for the computational work.

VITA

2008-2009	Research Fellow
	Cross-disciplinary Scholars in Science and Technology program
	University of California, Los Angeles
	Los Angeles, California
2009	B. S. Chemistry
	University of Science and Technology of China
	Heifei China
2009-present	Graduate Student
	Department of Chemistry and Biochemistry
	University of California, Los Angeles
	Los Angeles, California
2009-2013	Teaching Assistant
	Department of Chemistry and Biochemistry
	University of California, Los Angeles
	Los Angeles, California

PUBLICATIONS

Computational Assessment of 1,3-Dipolar Cycloadditions to Graphene
Yang Cao, and Kendall N. Houk, *J. Mater. Chem.* **2011**, 21, 1503-1508.

Creating Favorable Geometries for Directing Organic Photoreactions in Alkanethiolate Monolayers
Moonhee Kim, J. Nathan Hohman, **Yang Cao**, Kendall N. Houk, Hong Ma, Alex K.-Y. Jen, and Paul S. Weiss *Science* **2011**, *331*, 1312-1315.

Computational Methods to Calculate Accurate Activation and Reaction Energies of 1,3-Dipolar Cycloadditions of 24 1,3-Dipoles
Yu Lan, Lufeng Zou, Yang Cao, Kendall N. Houk *J. Phys. Chem. A.* **2011**, *115*, 13906-13920.

Covalently Patterned Graphene Surfaces by a Force Accelerated Diels-Alder Reaction
Shudan Bian, Amy M. Scott, Yang Cao, Yong Liang, Sílvia Osuna, K. N. Houk, and Adam B. Braunschweig *J. Am. Chem. Soc.* **2013**, *135*, 9240-9243.

Diels-Alder Reactions of Graphene: Computational Predictions of Products and Sites of Reaction
Yang Cao, Sílvia Osuna, Yong Liang, Robert C. Haddon, and K. N. Houk *J. Am. Chem. Soc.* **2013**, *135*, 17643-17649.

Why Bistetracenes Are Much Less Reactive than Pentacenes in Diels-Alder Reactions of Fullerenes
Yang Cao, Yong Liang, Lei Zhang, Silvia Osuna, Andra-Lisa M. Hoyt, Alejandro L. Briseno, K. N. Houk *J. Am. Chem. Soc.* **2014**, *136*, 10743-10751.

Chemically Stable, Unconventional Soluble Linear Polycyclic Aromatic Hydrocarbons: From Molecular Design to Device Applications
Lei Zhang, Yang Cao, Nicholas S. Colella, Yong Liang, Jean-Luc Brédas, Kendall N. Houk, and Alejandro L. Briseno. *Acc. Chem. Res.* Submitted.

Chapter 1 Computational Assessment of 1,3-Dipolar Cycloadditions to Graphene

1.1 Abstract

The 1,3-dipolar cycloadditions of azomethine ylide and carbonyl ylide to models of graphene have been investigated with density functional theory. Reaction energetics have been obtained and show that edge areas of graphene are much more favorable reaction sites than the center sites. Azomethine ylide cannot directly react at the center area, while carbonyl ylides are promising reagents for functionalization of graphene. The influence of some 1,3-dipole substituents is also evaluated.

1.2 Introduction

The extraordinary structures and properties of fullerenes and single-walled carbon nanotubes have had an important impact on nanotechnology.[1–5] These compounds exhibit outstanding mechanical and electronic properties,[6–10] and have attracted large numbers of experimental investigations.

During the past decades, thorough efforts have been devoted to fullerene and carbon nanotubes, especially on covalent functionalization methods that moderate intermolecular interactions and solubilities.[11–15] The 1,3-dipolar cycloaddition has proven a powerful way to functionalize conjugated π systems:[16–23] convenient synthetic applications of 1,3-dipolar cycloadditions to fullerenes and carbon nanotubes have led to many applications in various areas like solar cells and biotechnology.[4, 23–25]

Graphene is a two-dimensional planar sheet of sp^2 hybridized carbon atoms, the basic structural element for graphite and carbon nanotubes.[26, 27] Graphene is considered one of the most

robust nano-scale materials since it was first synthesized in the laboratory in 2004.[28–32] However, there are two main obstacles holding back rapid applications of graphene: difficulties in producing high quality single-layered graphene sheets,[27] and difficulties in functionalization due to the perfect planar morphology and aromaticity of graphene.[33, 34] Inspired by the success of some 1,3-dipolar cycloadditions to fullerenes and nanotubes, we decided to explore this class of reactions with graphene surfaces. Recently, two experimental groups have reported the functionalizations of graphene by 1,3-dipolar cycloadditions of azomethine ylides generated in situ.[34, 35] Georgakilas et al.[35] reported that an excess of *N*-methyl-glycine and 3,4-dihydroxybenzaldehyde mixed in DMF and refluxed gave an azomethine ylide intermediate which functionalized graphene. The covalently modified graphene is easily dispersible in polar organic solvents, and even in water.[35] Once graphene is soluble, properties can be studied more easily. This methodology opens new doors to processible graphene sheets with new functionalities. Prato et al. made graphene adducts of a different azomethine ylide and reported that although the sheet edges are thought to be the most reactive sites, the center region of the graphene also becomes functionalized.[34, 36, 37]

We have explored the reactivity and regioselectivity of several 1,3-dipolar cycloadditions to graphene models by means of density functional theory calculations. Two highly reactive 1,3-dipolar species, azomethine ylide and carbonyl ylide, were explored (Figure 1.1). Cycloadditions with several models for graphene were studied. The cycloadditions of azomethine ylides (Prato reaction)[16] are the most extensively studied reactions on fullerenes and carbon nanotubes.[16–23] Amino acids react with aldehydes, and decarboxylation gives ylides that react readily with fullerenes. According to calculations from Osuna in our group,[38] the cycloaddition of azomethine ylide to C_{60} fullerene is exothermic by about 54 kcal/mol. We also studied carbonyl ylide,

because it is predicted to be even more reactive than azomethine ylide. From unpublished results from our group,[39] the reaction enthalpy of azomethine ylide to ethylene is -65 kcal/mol and that of carbonyl ylide to ethylene is -90 kcal/mol using high-accuracy CBS-QB3 calculations. This shows that carbonyl ylide is a promising reagent for modification of graphene. Although at present carbonyl ylide itself has not been studied experimentally, quite a number of derivatives are available.[40–42]

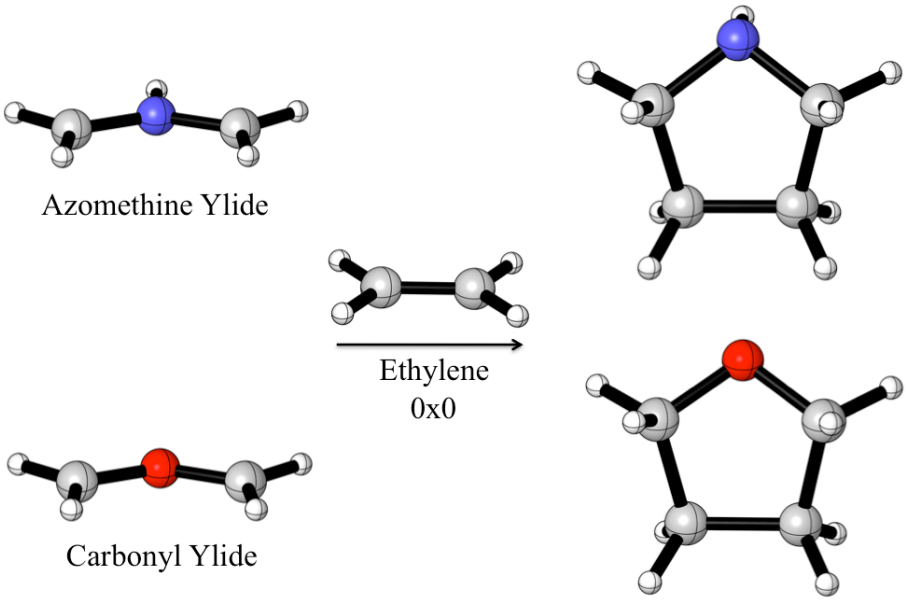

Figure 1.1 Azomethine ylide and carbonyl ylide, react with ethylene to form pyrrolidine and tetrahydrofuran, respectively.

1.3 Computational methodology

All the systems were performed with the Gaussian 03 suite of programs.[43] Our group has extensively studied different levels of methods and basis sets for 1,3-dipolar cycloadditions.[44–46] We investigated three main classes of 1,3-dipolar cycloadditions, including diazonium, nitrilium

and azomethine betaine classes, on ethylene and acetylene. CBS-QB3 reaction energetics were used as a standard.[44, 47, 48] The B3LYP/6-31G(d) method and basis set perform reasonably well for reaction energetics, with a mean absolute deviation (MAD) of 2.4 kcal/mol by comparing to CBS-QB3 results.[44]

Osuna and Houk[38] have explored transition states of 1,3- dipolar cycloadditions on fullerene and single-wall nanotubes with B3LYP/6-31G(d). These results were interpreted with the distortion/interaction model.[45, 46] Previous work has shown that B3LYP/6-31G(d) is relatively accurate, although the reaction exothermicities are underestimated by about 5 kcal/mol.

The electronic properties of graphene models like large oligoacenes and nanoribbons have been investigated theoretically by a number of groups. Bendikov et al. predicted, through various computational methods, that oligoacenes possesses an open-shell singlet diradical ground state.[49] We investigated these systems with both restricted and unrestricted B3LYP/6-31G(d). Full geometry optimizations were computed with restricted and unrestricted methods. In some cases, HF optimizations were used to obtain geometries for DFT calculations. The larger size graphene models (4x4, 5x5, 6x6) have open-shell singlet ground states with polyradical character. Basis set superposition errors (BSSE) on reaction energies were also calculated.

1.4 Results and discussions

The Huisgen 1,3-dipolar cycloaddition[42, 50–55] involves the reaction between a 1,3-dipole and a dipolarophile to form a heterocyclic five-membered ring. This is one of the most versatile and useful class of reactions and is utilized in almost every field of chemistry and biology.

Our graphene models include benzene and polybenzenoid hydrocarbons with up to 36 benzene rings, terminated by hydrogen atoms (ethylene, benzene, 2x2, 3x3, 4x4, 5x5, 6x6). 2x2 system means two condensed benzene rings in row and two in line, four condensed benzene

rings in total. The structures are shown in Figure 1.2. The larger the system is, the closer it resembles graphene, although graphene typically has thousands of carbon atoms.

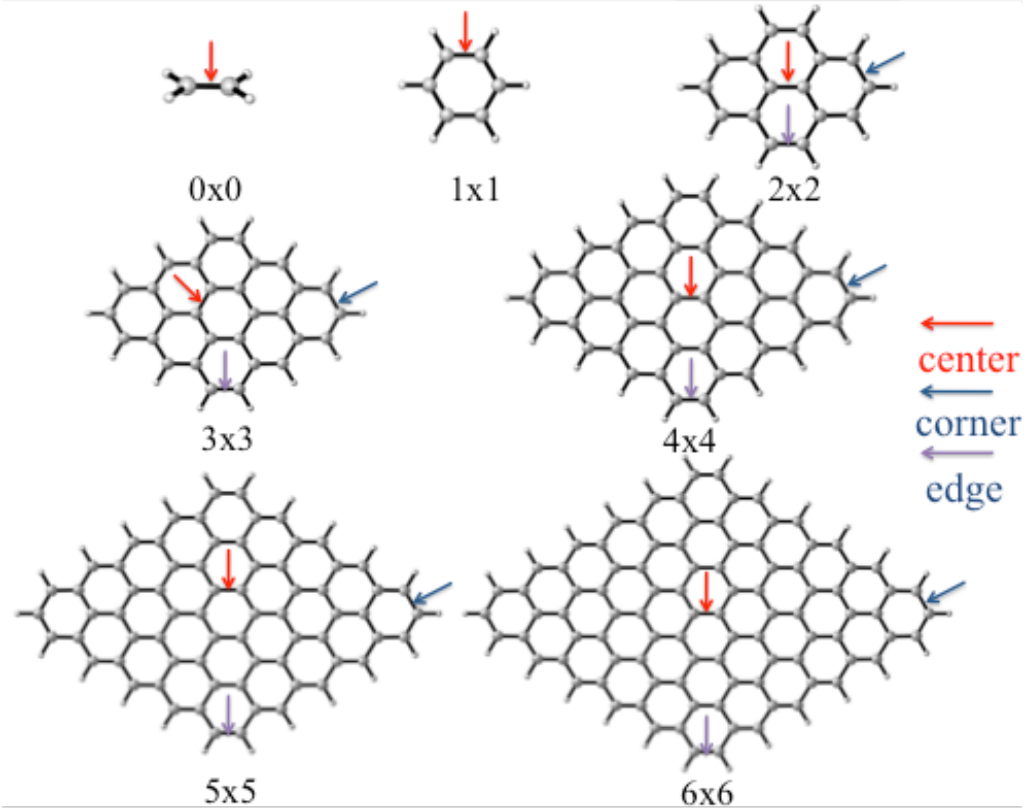

Figure 1.2 Representations of seven optimized dipolarophiles, expanded gradually from 0x0 (0 aromatic ring in row and line, ethylene) to 6x6 (6 aromatic rings in row and line, 36 aromatic rings in total) systems. Three types of bonds are explored: center, corner and edge.

We begin with ethylene, the simplest dipolarophile. Cycloaddition reactions on ethylene are expected to be most exothermic. Since 1,3-dipolar cycloadditions to ethylene have been studied previously,[38,44–46] many results are available as benchmarks for our results. Benzene (1x1 system, one benzene-ring in both row and line) is the simplest aromatic system and unit of

graphene. The cycloaddition reaction destroys its aromaticity and is thus less exothermic than with ethylene.

As mentioned in the introduction, Georgakilas et al.[35] reported a derivative of azomethine ylide, N-methyl-1-(3,4-dihydroxy)-phenyl azomethine ylide, reacting with graphene. We took a simplified form of this dipole, N-methyl-1-phenyl azomethine ylide, and calculated its reaction energy with ethylene. The reaction energy is -65.7 kcal/mol with N-methyl-1-phenyl azomethine ylide with ethylene, comparable to -68.6 kcal/mol for azomethine ylide with ethylene. The difference is only 2.9 kcal/mol. The phenyl functional group stabilizes azomethine ylide, but maintains its high reactivity.

For the case of carbonyl ylide, no experimental data are available. Therefore, we compare reaction energetics with its two derivatives, tetracyanocarbonyl ylide (TCCY)[40,41] and 1-cyano-1,2-diphenyl carbonyl ylide (CDPCY),[42] both of which are quite common derivatives (shown in Figure 1. 3 and Table 1.1). Derivatives TCCY and CDPCY are stabilized by conjugating and electron withdrawing groups. They have more or less half the reaction energy of carbonyl ylide, and the energetics are quite comparable to that of azomethine ylide.

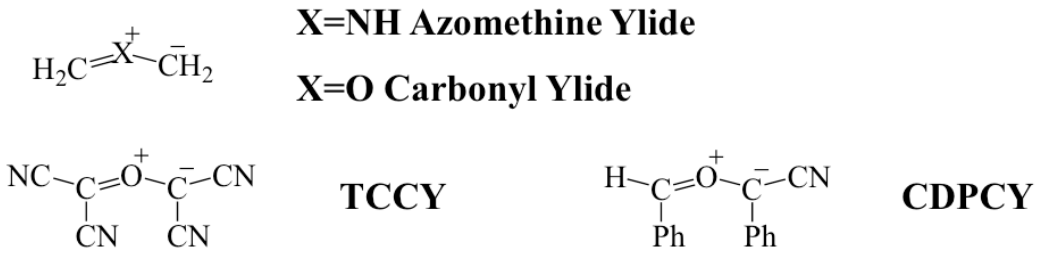

Figure 1.3 Four 1,3-dipoles.

Table 1.1 Energetics of reactions using UB3LYP/6-31G(d) of four 1,3-dipoles with benzene.

1,3-Dipoles	Reaction Energy ΔE (kcal/mol)
Carbonyl Ylide	-51.7
Azomethine Ylide	-26.8
TCCY	-17.8
CDPCY	-26.9

Two cycloaddition products on benzene are shown in Figure 1.4. Although they are products of two different 1,3-dipoles, they have almost the same bond lengths and angles. Parameters around carbon atoms that have undergone reaction are listed in the figure. As shown by these numbers, cycloaddition on benzene breaks its aromaticity. For the purpose of simplicity, we only show the products of carbonyl ylide cycloadditions for the larger systems. Azomethine ylide produces very similar structures.

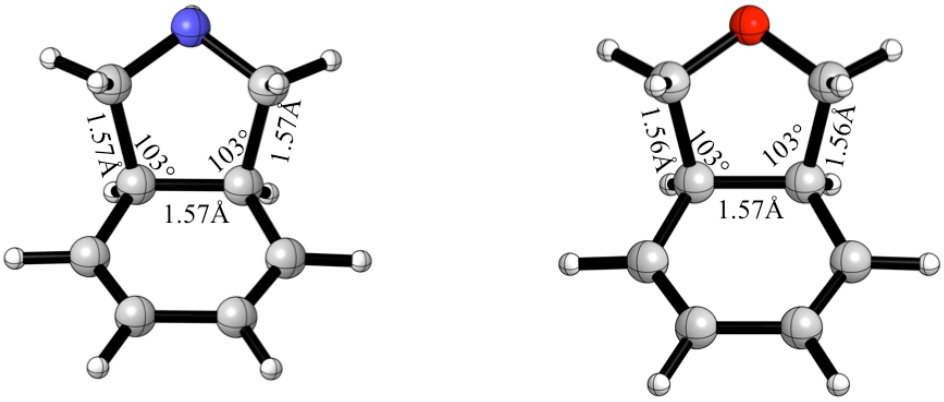

Figure 1.4 Products of azomethine ylide and carbonyl ylide cycloadditions to benzene.

There are many types of double bonds in large systems, and we explored only three of them defined as center, corner and edge, as shown in Figure 1.2. Center bonds of 5x5 and 6x6

systems will behave most like graphene. Two aromatic rings share each center bond. Reactions change the π bond into a σ bond, and two carbon atoms are changed from sp^2 into sp^3 hybridization. Reactions on the center bond have a direct effect on four benzene rings by eliminating their aromaticity and reducing π–π conjugation. The dramatic change of the planar morphology of graphene induces curvature (Figure 1.5). The 2D structure of graphene is severely distorted around the center bond after reaction. Therefore, the reactions of the center bond are expected to be least exothermic.

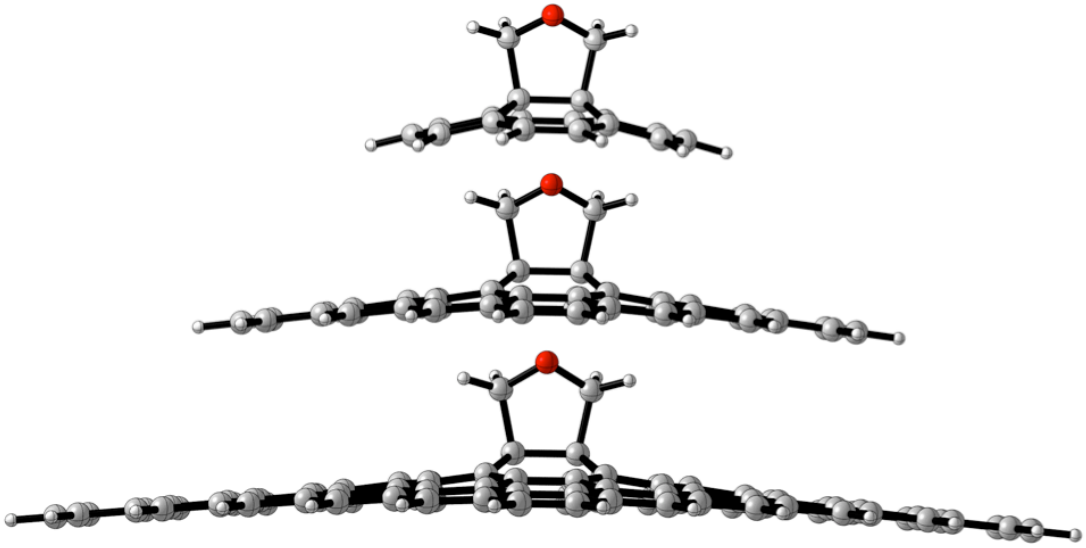

Figure 1.5 Side views of carbonyl ylide cycloadditions products on 2x2, 4x4, 6x6 systems on center bonds.

Reactions on corner and edge bonds will be more favored energetically as they are all shared by only one benzene ring. Reactions on them will have a direct effect in only one ring. The distortion of that ring will have very limited affect on the total morphology of graphene. In Figure 1.5, the side views of products of carbonyl ylide cycloadditions on center bonds of 2x2,

4x4, 6x6 graphene models are shown. The products show obvious curvature originating from the tetrahedral atoms where cycloaddition occurred. Distortion decreases π orbital overlap and weakens the conjugation. From this point of view, reactions on the center area of graphene need to be very exothermic in order to compensate for the product distortions.

Figure 1.6 shows side views of carbonyl ylide cycloaddition products on other types of bonds: corner and edge. The products of corner and edge bonds have significant differences from those in center cases. Reaction only distorts the ring that reacts, while other areas are unaffected. Reactions on corner and edge, the periphery of the graphene, are much easier than reactions at the center areas.

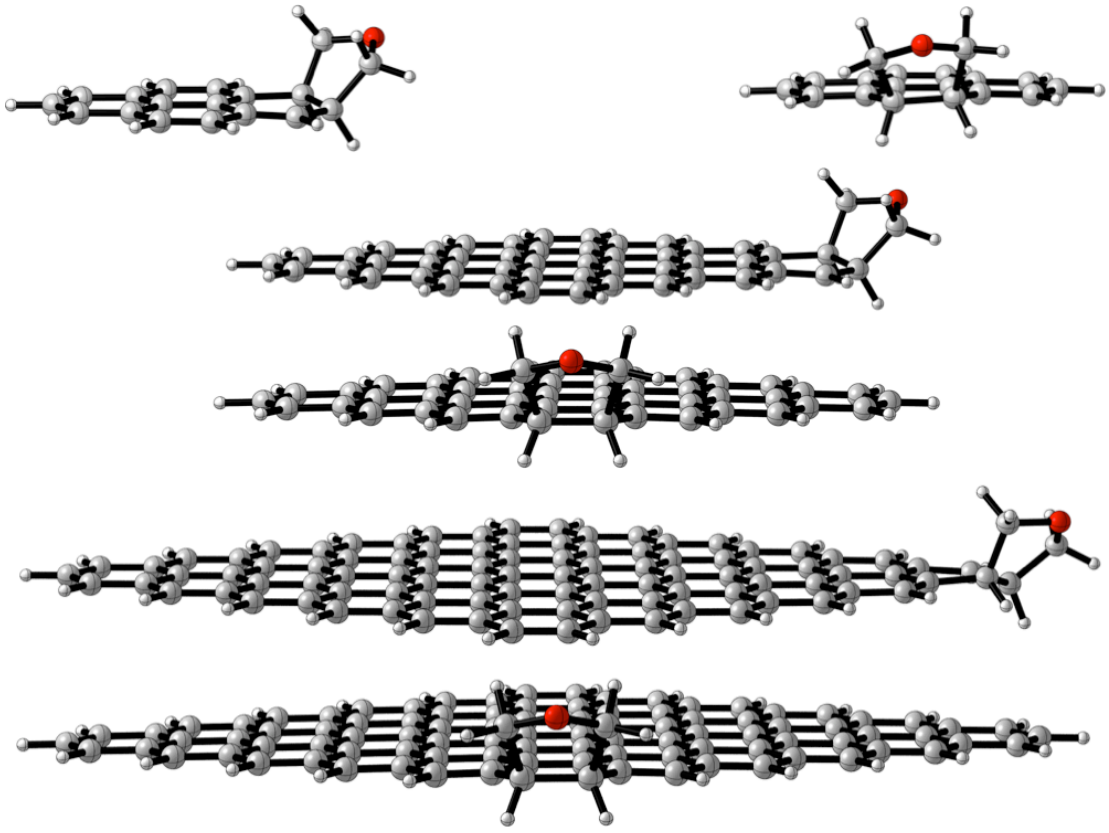

Figure 1.6 Side views of carbonyl ylide cycloaddition products on 2x2, 4x4, 6x6 systems on corner and edge bonds.

Table 1.2 summarizes reaction energetics of 1,3-dipolar cycloadditions of azomethine ylide and carbonyl ylide on our seven models, with (ΔE^{BSSE}) and without BSSE (ΔE) from UB3LYP calculations, and reaction energies without BSSE from RB3LYP calculations (ΔE^{RB3LYP}). Due to difficult convergence and time limitations, unrestricted reaction energies of azomethine ylide on 6 x 6 edge bonds were not obtained. We tested whether BSSE could influence the computed reaction energies. BSSE are, in our cases, all in the range of 6.0–8.5 kcal/mol, which makes it indispensable for absolute accuracy, although the general trends of the reaction energetics are conserved. The following discussions are mostly based on the results of ΔE^{BSSE}. Small systems up to the 3x3 model possess singlet closed-shell ground states. ΔE and ΔE^{RB3LYP} therefore are the same. Diradical character becomes evident in larger systems (4x4, 5x5, 6x6). Singlet open-shell states are more stable than closed-shell. The energy gap between the two states of 4x4 model is 2.3 kcal/mol; for 5x5 it is 11.3 kcal/mol; and for 6x6 it is 22.6 kcal/mol. Reactants and products are both lower in energy by similar amounts, which makes the differences of ΔE and ΔE^{RB3LYP} small. When dealing with large graphene flakes, ΔE^{RB3LYP} is able to give reasonable results rapidly, although energies of reactants and products are both too high. Figure 1.7 gives the trends of reaction energetics for increasingly large models based on unrestricted results. Ethylene (0x0), benzene (1x1), 2x2, 3x3, 4x4, 5x5, 6x6, correspond to **1-7**, respectively. The Y-axis is the total electronic reaction energy. Dashed lines are determined as the electronic energy difference between products and reactants. Full lines include one more term, BSSE corrections.

Table 1.2 Reaction energetics for cycloadditions of azomethine and carbonyl ylides to seven models at UB3LYP/6-31G(d) level, ΔE and ΔE^{BSSE}, and at B3LYP/6-31G(d) level, ΔE^{RB3LYP}. Energies in kcal/mol.

	ΔE	BSSE	ΔE^{BSSE}	ΔE^{RB3LYP}
Azomethine ylide + 0x0	-68.6	6.6	-62.0	-68.4[b]
Carbonyl ylide + 0x0	-93.8	5.9	-87.9	-93.8[b]
Azomethine ylide + 1x1	-26.8	6.9	-19.9	-26.2[b]
Carbonyl ylide + 1x1	-51.7	6.4	-45.3	-50.4[b]
Azomethine ylide + 2x2 center	12.2	7.4	19.6	12.2[b]
Azomethine ylide + 2x2 corner	-27.9	7.2	-20.7	-23.8[c]
Azomethine ylide + 2x2 edge	-42.5	7.3	-35.2	-39.2[c]
Carbonyl ylide + 2x2 center	-10.2	6.7	-3.5	-10.2[b]
Carbonyl ylide + 2x2 corner	-52.8	6.5	-46.3	-48.9[c]
Carbonyl ylide + 2x2 edge	-67.8	6.7	-61.1	-65.3[c]
Azomethine ylide + 3x3 center	10.9	7.3	18.2	10.9[b]
Azomethine ylide + 3x3 corner	-29.5	7.2	-22.3	-21.4[c]
Azomethine ylide + 3x3 edge	-45.4	7.3	-38.1	-39.3[c]
Carbonyl ylide + 3x3 center	-11.9	6.7	-5.2	-11.9[b]
Carbonyl ylide + 3x3 corner	-54.4	6.6	-47.8	-46.6[c]
Carbonyl ylide + 3x3 edge	-70.6	6.7	-63.9	-64.7[c]
Azomethine ylide + 4x4 center	6.1	7.2	13.3	7.1[b]
Azomethine ylide + 4x4 corner	-34.5	7.3	-27.3	-17.0[c]
Azomethine ylide + 4x4 edge	-44.7	7.3	-37.4	-33.3[c]
Carbonyl ylide + 4x4 center	-16.8	6.6	-10.2	-15.8[c]
Carbonyl ylide + 4x4 corner	-59.7	8.5	-51.2	-42.2[c]
Carbonyl ylide + 4x4 edge	-68.4	6.7	-61.7	-59.4[c]
Azomethine ylide + 5x5 center	7.2	7.2	14.4	13.5[c]
Azomethine ylide + 5x5 corner	-35.5	7.3	-28.1	-29.4[c]
Azomethine ylide + 5x5 edge	-44.9	7.3	-37.5	-45.8[c]
Carbonyl ylide + 5x5 center	-15.7	6.6	-9.1	-9.7[c]
Carbonyl ylide + 5x5 corner	-60.6	6.7	-53.9	-54.5[c]
Carbonyl ylide + 5x5 edge	-69.4	6.7	-62.7	-71.1[c]
Azomethine ylide + 6x6 center	10.1	7.1	17.2	7.7[c]
Azomethine ylide + 6x6 corner	-35.3	7.3	-28.1	-30.4[c]
Azomethine ylide + 6x6 edge	---[a]	---[a]	---[a]	-44.1[c]
Carbonyl ylide + 6x6 center	-12.7	6.5	-6.2	-15.9[c]
Carbonyl ylide + 6x6 corner	-60.4	6.9	-53.5	-55.0[c]
Carbonyl ylide + 6x6 edge	-69.8	6.7	-63.1	-70.9[c]

[a] Due to computational limitation, ΔE^{BSSE} and ΔE for azomethine ylide on 6x6 edge bonds are not included. [b] Full geometry optimization by B3LYP/6-31G(d). [c] Full geometry optimization by HF/STO-3G and single point energy calculation on B3LYP/6-31G(d).

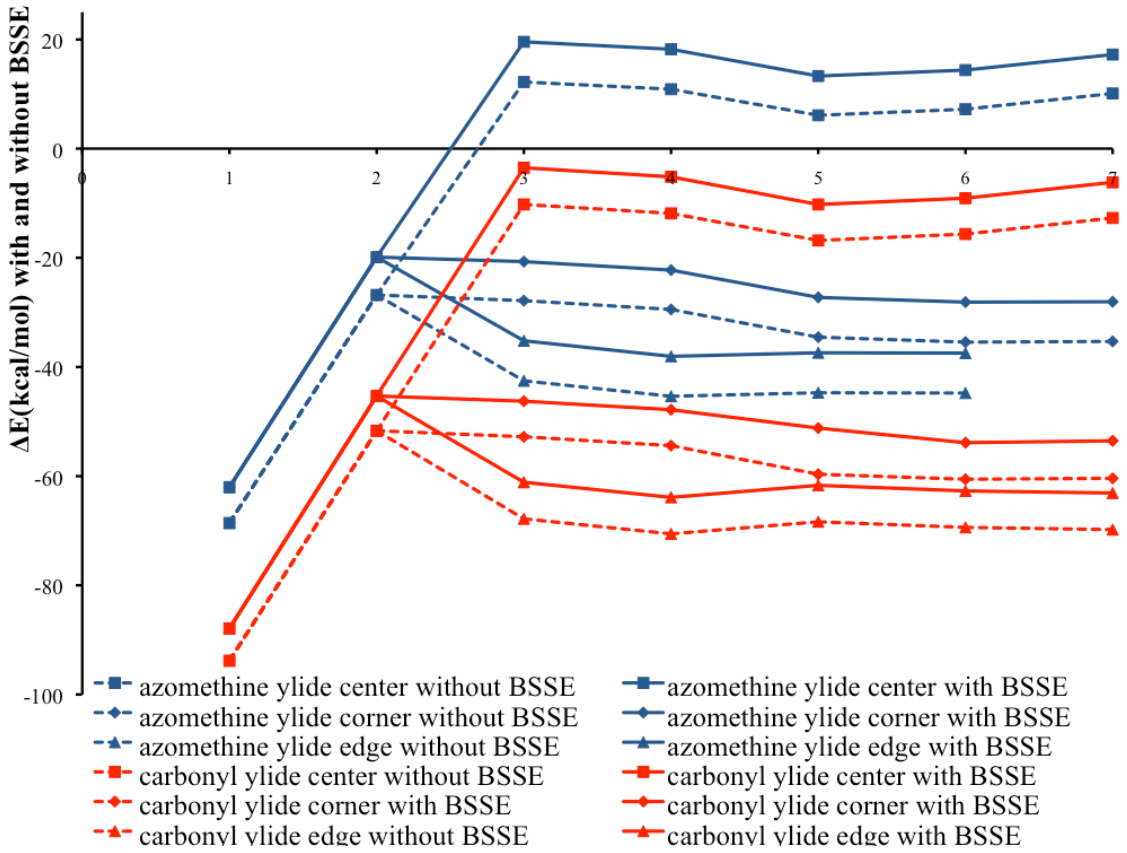

Figure 1.7 Reaction energetics for azomethine and carbonyl ylide cycloadditions to seven graphene models at center, corner and edge bonds before (dashed line) and after (closed line) BSSE. These models are shown in Figure 1.2.

Ethylene and benzene each have only one possible product. As expected, the cycloaddition on ethylene is most exothermic: -62.0 kcal/mol with azomethine ylide and -87.9 kcal/mol with carbonyl ylide. Reactions on benzene are less favorable than ethylene as the aromaticity is interrupted. Nevertheless, they are still quite exothermic: -19.9 kcal/mol with azomethine ylide and -45.3 kcal/mol with carbonyl ylide. Osuna previously reported azomethine ylide cycloadditions to ethylene and benzene.[38] The results are similar to our results.

The introduction of azomethine ylide on center bonds on graphene models starting from 2x2 to 6x6 are all endothermic: 19.6 kcal/mol for 2x2, 18.2 kcal/mol for 3x3, 13.3 kcal/mol for 4x4, 14.4 kcal/mol for 5x5, and 17.2 kcal/mol for 6x6 system. It should be noted that the Gibbs free energies for these reactions are more positive than electronic energies by the entropy penalty ($\Delta G=\Delta H-T\Delta S$, $-T\Delta S$ is positive for cycloadditions). We calculated entropy contributions $-T\Delta S$ for ethylene (13.6 kcal/mol) and benzene (14.1 kcal/mol) reactions. Although our graphene model systems differ in size, we estimate that entropy contributions are in the range of 12 to 15 kcal/mol. That means the calculated free energy of the introduction of azomethine ylide to center of infinite graphene is greater than 30 kcal/mol. Such a reaction is unfavorable and cannot happen spontaneously. In the two experimental papers[34, 35] about the functionalization of graphene via azomethine ylide derivatives, the authers propose that modification occurs in the center areas as well as on the edges. We think none of these reactions near the center are feasible. To support this point, we calculated the reaction of N-methyl-1-phenyl azomethine ylide on the 5x5 graphene model. This reaction (without BSSE correction) is endothermic by 26.6 kcal/mol. The majority of modifications are likely to happen on edges and near edges.

On the other hand, the reactions of carbonyl ylide on center bonds (red line with square dots) are exothermic: -3.5 kcal/mol for 2x2, -5.2 kcal/mol for 3x3, -10.2 kcal/mol for 4x4, -9.1 kcal/mol for 5x5, and -6.2 kcal/mol for 6x6 system. We expect the whole systems have $-T\Delta S$ contributions in the range of 12 to 15 kcal/mol. B3LYP tends to underestimate exothermic reaction energy by around 5 kcal/mol, and sometimes errors are as large as 10 kcal/mol.[44, 56] Taking into account the entropy contribution and B3LYP corrections, these reactions have Gibbs free energies near 0. Thus, although the functionalization on graphene is difficult, there are still very good possibilities for carbonyl ylides to overcome the distortion (shown in Figure 1.5)

necessary to react. Here, we predict that, carbonyl ylide or dipoles with comparable reactivities could functionalize the center area of graphene, although less readily than near edges.

The cycloadditions to corner and edge bonds are exothermic, both for azomethine ylide and carbonyl ylide. They are all spontaneous reactions, and much more favorable than attack on center bonds. The distortion energy is much smaller than for reactions on the center region. Our results show that the azomethine ylide functionalizations of graphene reported by two groups should happen mostly on the outer edges of graphene with center areas left untouched. Reaction energies on the periphery gradually converge to a constant number. The edge reaction is more favorable than corner by about 10–15 kcal/mol. In future work, we will explore larger models for the reactions on center areas.

As previously mentioned, Osuna and Houk[38] have explored 1,3-dipolar cycloadditions on single-wall nanotubes with B3LYP/6-31G(d). Their results are comparable with ΔE^{RB3LYP} in Table 1.2. Reactions on center bonds of our largest graphene models (6x6) are analogous to that on single-wall nanotubes. In their report, the most favorable reaction on nanotube has elec- tronic reaction energy -26.3 kcal/mol. While ΔE^{RB3LYP} for azomethine ylide on 6x6 center is 7.7 kcal/mol. The curved geometry present in carbon nanotubes weakens π-π conjugation. More importantly, the strained geometry makes distortion towards the transition state and product much easier.

1.5 Conclusion

We have reported a comparative study of the addition of azomethine and carbonyl ylide to graphene models with DFT calculations. Three types of bonds have been explored: center, corner and edge. Reaction on the center area will have significant effect on the morphology of

graphene and change the planar structure into a bent structure, breaking local π-π conjugation. Reactions on corner and edge bonds only distort the reacting benzene ring and keep the overall planar structure elsewhere. Azomethine ylide reactions on center bonds of graphenes are endothermic. Carbonyl ylide reactions on center bonds have free energies around 0 kcal/mol. The outer layer of graphene is more reactive than center areas. Reactions on corner and edge bonds are all exothermic on graphene both for azomethine ylide and carbonyl ylide cases. Based on this, we predict that reagents as reactive as carbonyl ylide should be effective modifiers of graphene. Previous modifications of graphene[34, 35] by azomethine ylides are most likely in the edge areas.

Our future studies will explore larger graphene models and reactions with a wide variety of 1,3-dipoles.

1.6 References

1 Tans, S. J., Verschueren, A. R. M., Dekker, C., *Nature*, 1998, **393**, 49-52.

2 Kong, J., Franklin, N. R., Zhou, C. W., Chapline, M. G., Peng, S., Cho, K. J., Dai, H. J., *Science*, 2000, **287**, 622-625.

3 Postma, H. W. C., Teepen, T., Yao, Z., Grifoni, M., Dekker, C., *Science*, 2001, **293**, 76-79.

4 Wudl, F., *J. Mater. Chem.*, 2002, **12**, 1959-1963.

5 Qureshi, A., Kang, W. P., Davidson, J. L., Gurbuz, Y., *Diamond Relat. Mater.*, 2009, 1401-20.

6 Dresselhaus, M. S., Dresselhaus, G., Rao, A. M., Eklund, P. C., *Synth. Met.*, 1996, **78**, 313-325

7 Schon, J. H., Kloc, C., Batlogg, B., *Science*, 2001, **293**, 2432-2434.

8 Tang, X. P., Kleinhammes, A., Shimoda, H., Fleming, L., Bennoune, K. Y., Sinha, S., Bower, C., Zhou, O., Wu, Y., *Science*, 2000, **288**, 492-494.

9 Majumdar, H. S., Baral, J. K., Osterbacka, R., Ikkala, O., Stubb, H., *Org. Electron.*, 2005m, **6**, 188-192.

10 Yamamoto, T., Watanabe, K., Hernandez, E. R., *Carbon Nanotubes. Advanced Topics in the Synthesis, Structure, Properties and Applications*, 2008, 165-94.

11 Dyke, C. A., Tour, J. M., *J. Phys. Chem. A*, 2004, **108**, 11151-11159.

12 Dyke, C. A., Tour, J. M., *Chem. Eur. J.*, 2004, **10**, 813-817.

13 Tagmatarchis, N., Prato, M., *Fullerene-Based Materials: Structures and Properties*, 2004, **109**, 1-39.

14 Iehl, J., de Freitas, R. P., Nierengarten, J. F., *Tetrahedron Lett.*, 2008, **49**, 4063-4066.

15 N.Karousis, N. Tagmatarchis, D.Tasis, Chem. Rev., 2010, 110, 5366-5397

16 Maggini, M., Scorrano, G., Prato, M., *J. Am. Chem. Soc.*, 1993, **115**, 9798-9799.

17 Prato, M., Maggini, M., *Acc. Chem. Res.*, 1998, **31**, 519-526.

18 Georgakilas, V., Kordatos, K., Prato, M., Guldi, D. M., Holzinger, M., Hirsch, A., *J. Am. Chem. Soc.*, 2002, **124**, 760-761.

19 Tagmatarchis, N., Prato, M., *Pure Appl. Chem.*, 2005, **77**, 1675-1684.

20 Langa, F., Oswald, F., *C. R. Chim.*, 2006, **9**, 1058-1074.

21 Wang, X. Q., Jiang, D. E., Dai, S., *Chem. Mater.*, 2008, **20**, 4800-4802.

22 Ghini, G., Luconi, L., Rossin, A., Bianchini, C., Giambastiani, G., Cicchi, S., Lascialfari, L., Brandi, A., Giannasi, A., *Chem. Commun.*, 2010, **46**, 252-254.

23 Kharisov, B. I., Kharissova, O. V., Gomez, M. J., Mendez, U. O., *Industrial & Engineering Chemistry Research*, 2009, **48**, 545-571.

24 Bosi, S., Da Ros, T., Spalluto, G., Prato, M., *Eur. J. Med. Chem.*, 2003, **38**, 913-923.

25 Bakry, R., Vallant, R. M., Najam-Ul-Haq, M., Rainer, M., Szabo, Z., Huck, C. W., Bonn, G. K., *Int. J. Nanomed.,* 2007, **2**, 639-649.

26 Geim, A. K., Novoselov, K. S., *Nat. Mater.*, 2007, **6**, 183-191.

27 Allen, M. J., Tung, V. C., Kaner, R. B., *Chem. Rev.*, 2010, **110**, 132-145.

28 Novoselov, K. S., Geim, A. K., Morozov, S. V., Jiang, D., Zhang, Y., Dubonos, S. V., Grigorieva, I. V., Firsov, A. A., *Science*, 2004, **306**, 666-669.

29 Novoselov, K. S., Geim, A. K., Morozov, S. V., Jiang, D., Katsnelson, M. I., Grigorieva, I. V., Dubonos, S. V., Firsov, A. A., *Nature*, 2005, **438**, 197-200.

30 Zhang, Y. B., Tan, Y. W., Stormer, H. L., Kim, P., *Nature*, 2005, **438**, 201-204.

31 Novoselov, K. S., Jiang, Z., Zhang, Y., Morozov, S. V., Stormer, H. L., Zeitler, U., Maan, J. C., Boebinger, G. S., Kim, P., Geim, A. K., *Science*, 2007, **315**, 1379-1379.

32 Ruoff, R., *Nat. Nanotechnol.*, 2008, **3**, 10-11.

33 Denis, P. A., Iribarne, F., *Int. J. Quantum Chem.*, 2010, **110**, 1764-1771.

34 Quintana, M., Spyrou, K., Grzelczak, M., Browne, W. R., Rudolf, P., Prato, M., *Acs Nano*, 2010, **4**, 3527-3533.

35 Georgakilas, V., Bourlinos, A. B., Zboril, R., Steriotis, T. A., Dallas, P., Stubos, A. K., Trapalis, C., *Chem. Commun.*, 2010, **46**, 1766-1768.

36 Lin, T. T., Zhang, W. D., Huang, J. C., He, C. B., *J. Phys. Chem. B,* 2005, **109**, 13755-13760.

37 Jiang, D. E., Sumpter, B. G., Dai, S., *J. Chem. Phys.*, 2007, 126.

38 Osuna, S., Houk, K. N., *Chem. Eur. J.*, 2009, **15**, 13219-13231.

39 Lan, Y., Houk, K. N., unpublished results

40 Linn, W. J., Benson, R. E., *J. Am. Chem. Soc.*, 1965, **87**, 3657-3665.

41 Linn, W. J., *J. Am. Chem. Soc*., 1965, **87**, 3665-3672.

42 (a). Huisgen, R., Markowski, V., *J. Chem. Soc*., *Chem. Commun*., 1977, 440-442. (b). Markowski, V., Huisgen, R., *Tetrahedron Lett*., 1976, 4643-4646. (c). Markowski, V., Huisgen, R., *J. Chem. Soc*., *Chem. Commun*., 1977, 439-440.

43 Gaussian 03, Revision E.01, M. J. Frisch, G. W. Trucks, H. B. Schlegel, G. E. Scuseria, M. A. Robb, J. R. Cheeseman, J. A. Montgomery, Jr., T. Vreven, K. N. Kudin, J. C. Burant, J. M. Millam, S. S. Iyengar, J. Tomasi, V. Barone, B. Mennucci, M. Cossi, G. Scalmani, N. Rega, G. A. Petersson, H. Nakatsuji, M. Hada, M. Ehara, K. Toyota, R. Fukuda, J. Hasegawa, M. Ishida, T. Nakajima, Y. Honda, O. Kitao, H. Nakai, M. Klene, X. Li, J. E. Knox, H. P. Hratchian, J. B. Cross, V. Bakken, C. Adamo, J. Jaramillo, R. Gomperts, R. E. Stratmann, O. Yazyev, A. J. Austin, R. Cammi, C. Pomelli, J. W. Ochterski, P. Y. Ayala, K. Morokuma, G. A. Voth, P. Salvador, J. J. Dannenberg, V. G. Zakrzewski, S. Dapprich, A. D. Daniels, M. C. Strain, O. Farkas, D. K. Malick, A. D. Rabuck, K. Raghavachari, J. B. Foresman, J. V. Ortiz, Q. Cui, A. G. Baboul, S. Clifford, J. Cioslowski, B. B. Stefanov, G. Liu, A. Liashenko, P. Piskorz, I. Komaromi, R. L. Martin, D. J. Fox, T. Keith, M. A. Al-Laham, C. Y. Peng, A. Nanayakkara, M. Challacombe, P. M. W. Gill, B. Johnson, W. Chen, M. W. Wong, C. Gonzalez, and J. A. Pople, Gaussian, Inc., Wallingford CT, 2004.

44 Ess, D. H. and Houk, K. N., *J. Phys. Chem. A*, 2005, **109**, 9542-9553.

45 Ess, D. H. and Houk, K. N., *J. Am. Chem. Soc*., 2007, **129**, 10646-10647.

46 Ess, D. H. and Houk, K. N., *J. Am. Chem. Soc*., 2008, **130**, 10187-10198.

47 Guner, V., Khuong, K. S., Leach, A. G., Lee, P. S., Bartberger, M. D., Houk, K. N., *J. Phys. Chem. A*, 2003, **107**, 11445-11459.

48 Guner, V. A., Khuong, K. S., Houk, K. N., Chuma, A., Pulay, P., *J.Phys. Chem. A*, 2004, **108**, 2959-2965.

49 Bendikov, M., Duong, H. M., Starkey, K., Houk, K. N., Carter, E. A., Wudl, F., *J. Am. Chem. Soc.*, 2004, 126, 7416-7417.

50 Huisgen, R., *Angew. Chem., Int. Ed. Engl.*, 1963, **2**, 565-598.

51 Huisgen, R., *Angew. Chem., Int. Ed. Engl.*, 1963, **2**, 633-645.

52 Huisgen, R.; Gotthardt, H.; Bayer, H. O., *Angew. Chem., Int. Ed. Engl.*, 1964, **3**, 135.

53 Huisgen, R., Gashey, R., Hauck H., Seidl, H., *Chem. Ber.*, 1968, **101**, 2568-2584.

54 Huisgen, R., Gashey, R., Seidl, H., *Chem. Ber.*, 1968, **101**, 2548-2558.

55 Huisgen, R., Seidl, H., Gashey, R., *Chem. Ber.*, 1998, **101**, 2559-2567.

56 Wheeler, S. E., Moran, A., Pie, S. N., niazek, Houk, K. N., *J. Phys. Chem. A,* 2009, **113**, 10376-10384

Chapter 2 Diels-Alder Reactions of Graphene: Computational Predictions of Products and Sites of Reaction

2.1 Abstract

The cycloaddition reactions and non-covalent π interactions of 2,3-dimethoxybutadiene (DMBD), 9-methylanthracene (MeA), tetracyanoethylene (TCNE), and maleic anhydride (MA) with graphene models have been investigated using density functional theory (DFT) calculations. Reaction enthalpies have been obtained to assess the reactivity and selectivity of covalent and non-covalent functionalization. Results indicate that graphene edges may be functionalized by the four reagents through cycloaddition reactions, while the interior regions cannot react. Non-covalent complexation is much more favorable than cycloaddition reactions on interior bonds of graphene. The relative reactivities of different sites in graphene are related to loss of aromaticity, and can be predicted using Hückel molecular orbital (HMO) localization energy calculations.

2.2 Introduction

Chemical functionalization is a method to manipulate the electronic properties of graphene.[1] By forming covalent bonds and converting sp^2 into sp^3-hybridized carbons, the electronic properties of graphene can be tuned, and additional functionality can be incorporated. However, graphene is a highly stabilized, intrinsically inert, macromolecular aromatic material. To overcome the large reaction barrier, highly reactive chemical reagents or harsh reaction conditions are often required,[1-2] as in examples like oxidation,[3-5] fluorination,[6-8] hydrogenation,[9-11] and radical addition.[12-13] Inspired by well-established modifications of fullerenes and carbon nanotubes, cycloaddition reactions are another approach to the chemical functionalization of graphene. Nitrenes, which are reactive intermediates that can be obtained from decomposition of

azides, are reported to undergo (2+1) cycloaddition reactions on graphene and form aziridines.[14-15] Benzynes have been reported to modify graphene surfaces efficiently with a high degree of functionalization through (2+2) cycloaddition pathways.[16-17] The 1,3-dipolar cycloaddition of an azomethine ylide has also been reported to functionalize graphene.[18-19]

In 2011, Haddon's group reported a series of DA reactions on graphene.[20-21] It was reported that graphene reacts reversibly as a dienophile with 2,3-dimethoxybutadiene (DMBD) or 9-methylanthracene (MeA). The DA reaction of DMBD with graphene could be achieved both in solution at 120 °C and in gas phase at 50 °C. Both reactions are reported to reverse at 170 °C. MeA reacts with graphene in a solution of *p*-xylene at 130 °C, and the retro-DA reaction occurs at 160 °C. Graphene is also reported to react as a diene with tetracyanoethylene (TCNE) and with maleic anhydride (MA). The reaction with TCNE proceeds at room temperature and reverses at 100 °C. MA requires 120 °C for DA reaction and reverses at 150 °C. Raman spectroscopy was mainly employed to track the reaction process. The ratio of D to G band intensity (I_D/I_G) was considered as an index of the degree of functionalization.

The non-covalent functionalization of graphene by π complexes has also been studied extensively.[1] The graphene surface is known to adsorb many types of molecules through non-covalent interactions, from metal ions to small organic molecules to biomolecules such as DNA and proteins.[22-25] The electronic properties of graphene can be effectively modified by adding adsorbate molecules to the surface and forming charge transfer complexes.[26-27] Rao and co-workers found that TCNE and graphene formed a charge transfer complex in solution phase, where TCNE was an electron acceptor and graphene functioned as an electron donor.[28-31] Raman spectroscopy was again utilized as a major characterization tool.[28] Through comparing the Raman before and after the interaction with TCNE, they found that the intensity of D band

increased after the complex formation, as did the I_D/I_G ratio. The increased I_D/I_G ratio phenomenon was also observed in the interaction of graphene with electron donor molecules. Both covalent and non-covalent bonding could increase the D band intensity in the Raman spectrum.

To better understand the reactivity and selectivity of the four reagents (DMBD, MeA, TCNE, and MA) with graphene, we have performed a computational assessment through DFT calculations. Our graphene models are finite-size polybenzenoid (25 fused benzene rings) hydrocarbons with no considerations of complex defects. Reactivities in the interior and peripheral sites (zigzag and armchair edges) are considered. We evaluated the feasibility of (2+2), (4+2), and (4+4) cycloadditions, where graphene functions a 2π or 4π component. We also studied the non-covalent interactions of the four compounds with graphene. We assessed the radical character of graphene fragments by spin density calculations. HMO theory provides insights into relative reactivities of different sites in graphene.

Before the submission of this manuscript, Denis reported a study of Diels-Alder reactions of graphene with the same dienes or dienophiles studied here.[32] Although different models and density functional methods were used, the conclusions about the unreactivity of the interior portion of graphene in Diels-Alder reactions are congruent with our results.

2.3 Computational Models and Methods

Ideal graphene has a perfectly flat, single-layer structure; comprised of purely sp^2-hybridized carbons.[33] Graphene flakes generally have several thousand carbons. In a large graphene flake, the carbons are indistinguishable and packed into a honeycomb lattice with a C-C bond length of 1.42 Å.[34] However, real graphene samples inevitably have defects and vary in size, layers, and boundary conditions depending on their fabrication processes. Enormous efforts

at fabrication have been made in recent years to prepare pristine graphene, but still there are significant variations in graphene structures and qualities. Graphene samples with lateral dimensions ranging from 2 nm (a few hundred-carbon atoms)[35] up to 1 mm[36] have been reported. There are two basic shapes for graphene edges, zigzag and armchair.[36] A Previous study indicated that zigzag edges have multi-radical character and are predicted to have high reactivity.[37] Scott's group also reported the Diels-Alder reaction of acetylene to the armchair edge of aromatic hydrocarbons.[38] We have studied two graphene models containing both types of edges. They are polybenzenoid hydrocarbons $C_{70}H_{22}$ (25 fused benzene rings). Figure 2.1 shows structures of the two graphene models: model 1 terminates with a zigzag edge and model has armchair edges. They are both terminated with hydrogen atoms.[32] He also found that the presences of Stone-Wales translocations, 585 double vacancies, and 555-777 reconstructed double vacancies did not significantly change graphene reactivity.[32]

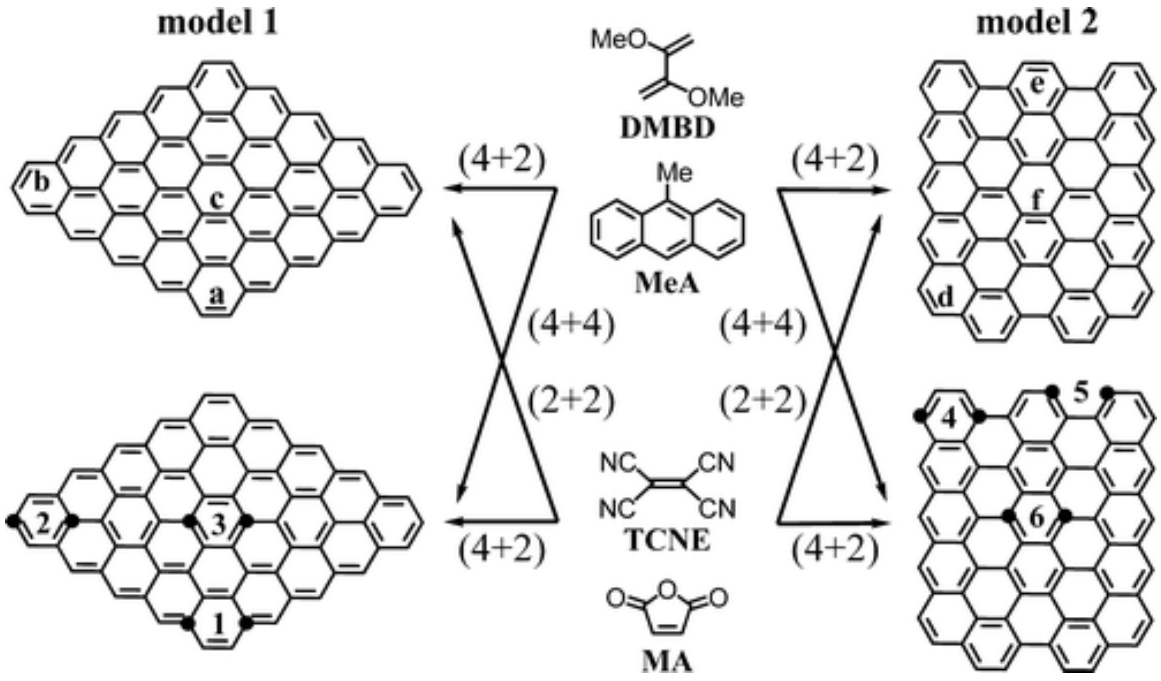

Figure 2.1 Two graphene models (Model 1 and Model 2) terminated with hydrogen atoms. Reaction sites including interior and peripheral bonds are considered. When graphene functions as the 2π component, six bonds from a to f are considered. When graphene functions as the 4π component, six reaction sites from 1 to 6 are calculated.

For computational investigations, the larger the model is, the more closely it resembles graphene. However, DFT computation times scale by about n^4 (n = number of atoms) as size increases, which greatly limits the size of models.[39-41] In previous study, we performed benchmarks regarding the size effects on graphene models.[42] It was found that, for both interior and peripheral bonds, the energetics quickly converged as the model size increases. This indicates that our finite-size models provide reliable energetics for both interior and peripheral bonds.

Reactions of interior and peripheral bonds in graphene are considered. When graphene functions as the 2π component, three representative bonds from each model were studied. The bonds a and b represent zigzag edges. Ideally, the two zigzag bonds are indistinguishable when the graphene model approaches infinite. Here, in our finite-size model, they differ in reactivity. Bonds a and b are most reactive in these two categories, respectively. The corner bond a in Model 1 can also be viewed as the joint part of zigzag and armchair edges of graphene. The interior bond c comprises the majority of bonds in graphene. Likewise, the peripheral bond d in Model 2 can be viewed as the joint part of zigzag and armchair edges of graphene. Due to the similarity of their structure environment, the d bond is expected to have a comparable reactivity with that of a. The edge bond e in Model 2 represents the armchair edge. The interior bond f represents graphene interior. In addition to the DA reactions ((4+2) reactions with DMBD and MeA), we also considered the possibilities of (2+2) cycloaddition reactions towards TCNE and MA. Likewise, when graphene functions as the 4π component, DFT calculations were conducted on another six sites. In particular, site 5 is a representative armchair edge that is similar to the bay region of Scott's models.[38] Interior sites 3 and 6 represent graphene interior. The (4+2) cycloaddition reactions with TCNE and MA, as well as the (4+4) reactions with DMBD and MeA, were conducted on these sites.

A previous computational study from our group indicates that polyacenes possess an open-shell singlet ground state.[43] The polyradical behavior was also found in graphene nanoflakes with system sizes on the order of 100 carbon atoms.[37] Our calculation is in agreement with previous findings that graphene models are more stable as open-shell singlet states than as closed-shell singlet and open-shell triplet states.[44] The open-shell character requires unrestricted DFT calculations for species involving graphene. All calculations were performed with Gaussian 09.[45]

The geometry optimizations of all the minima and transition states were carried out at the (U)M06-2X level of theory[46-47] with the 6-31G(d) basis set.[48] Single-point energy calculations were subsequently carried on the optimized structures at the (U)M06-2X and (U)ωB97X-D levels[49] with a larger basis set 6-311G(d,p). Both methods yield better results when describing medium to long-range electron correlation and dispersion effects than traditional hybrid methods like B3LYP.[46,49] M06-2X is reported to provide reliable energetics for cycloaddition reactions.[50] Very recently, M06-2X has also been demonstrated to generate good results for calculating the adsorption enthalpies of small organic molecules on graphene.[51] Vibrational frequencies were computed at the (U)M06-2X/6-31G(d) level to check whether each optimized structure is an energy minimum or a transition state and to evaluate zero-point vibrational energies (ZPVE) and thermal corrections at 298 K. Here only (U)M06-2X results will be discussed. The (U)ωB97X-D calculations were found to give similar energetics and the same general conclusions, thus not reported here.

It is well known that, for bimolecular reactions, the free energy term (ΔG) is unfavorable due to the entropy contribution ($\Delta G = \Delta H - T\Delta S$; $-T\Delta S$ is positive). Recently, it was reported that the entropy contribution is small (within 5 kcal/mol) from calculations calculations on free energies of the non-covalent association of graphene with small organic molecules.[25] This corresponds to a ΔS of about -15 eu (cal/(mol K)), appropriate for loss of one translational and two rotational degrees of freedom. Consequently, a complex of a small molecule at graphene will be exergonic if ΔH is about -5 kcal/mol or more exothermic. For a covalent cycloadduct, the ΔS will be -30 eu or even more negative so that a ΔH of reaction of -10 kcal/mol or more exothermic will be necessary for an exergonic reaction. We use enthalpies to evaluate the feasibility of

reactions, as the entropy term in ΔG is overestimated by gas phase calculations based on harmonic frequencies.

2.4 Results and discussions

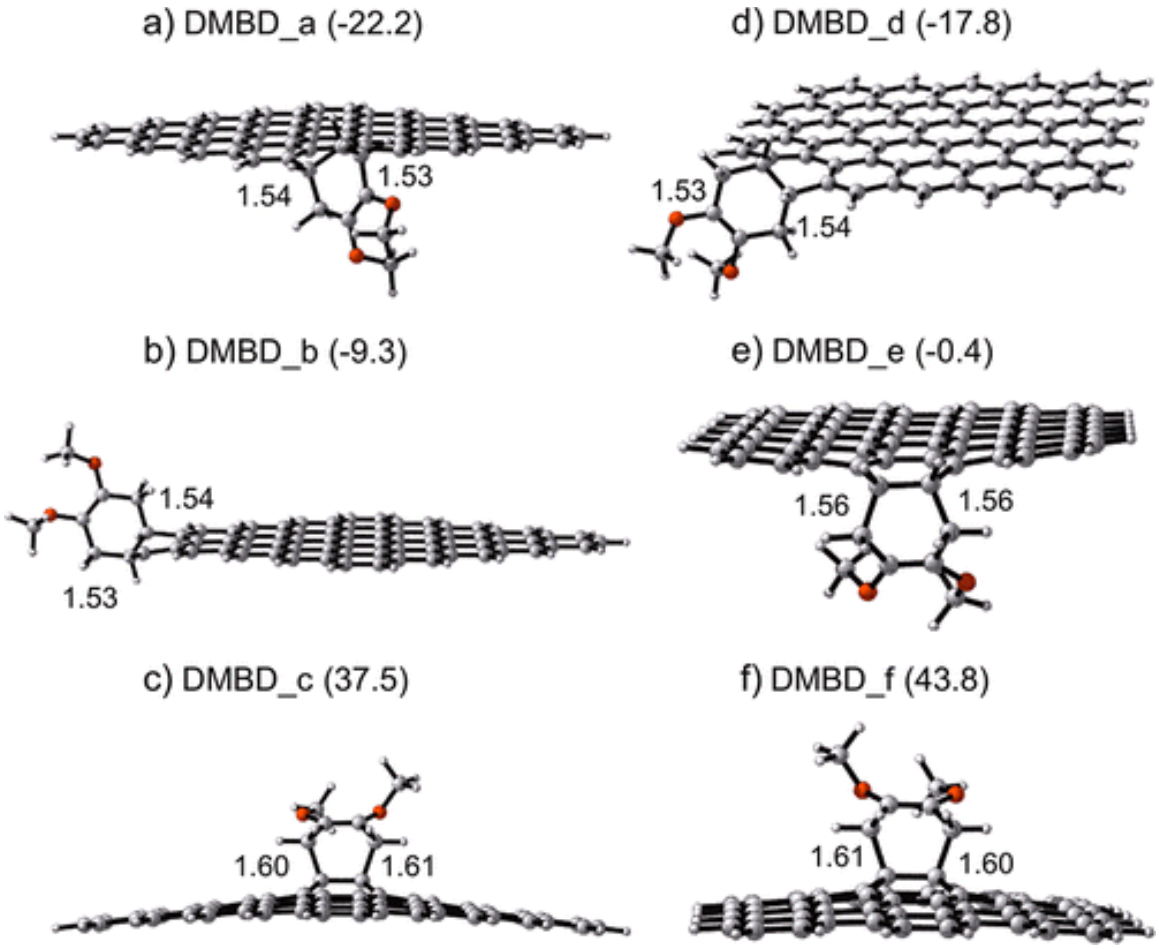

Figure 2.2 Diels-Alder adducts of DMBD with graphene on bonds a-c in Model 1 and d-f in Model 2, where graphene functions as a dienophile. Reaction enthalpies are given in kcal/mol. The C-C bond lengths are given in Å.

Figure 2.2 shows the product structures and reaction enthalpies for Diels-Alder reactions between DMBD and two graphene models, where graphene functions as a dienophile. The

peripheral bonds a and d are relatively reactive with comparable reaction enthalpies of -22.2 and -17.8 kcal/mol, respectively. The zigzag edge b and armchair edge e are slightly reactive with enthalpies of -9.3 and -0.4 kcal/mol. However, interior bonds c and f, are inert with highly endothermic reaction enthalpies of 37.5 and 43.8 kcal/mol. The DA reactions at interior bonds are highly endothermic due to the aromaticity breaking and curvature introduction. The reaction on the interior bond has a direct impact on four local benzene rings. Through comparing the product morphology shown in Figure 2.2, it is clearly seen that obvious curvature is introduced at the tetrahedral atoms where two new C-C bonds formed. This suggests that DMBD can functionalize graphene edges or defects through DA reactions, while the interior areas will not react at all. When DMBD reacts with graphene through the (4+4) cycloaddition on sites 1 to 3 in Model 1 and 4 to 6 in Model 2, these six reactions are all unfavorable with reaction enthalpies ranging from 12.8 to 57.1 kcal/mol. Overall, the (4+4) cycloaddition of DMBD with graphene is not feasible at edges or interior sites.

In addition to cycloaddition reactions, we also assessed the feasibility of the formation of DMBD-graphene complexes. Figure 2.3 shows the structures of DMBD-graphene complexes in two graphene models from two viewpoints (top and side). DMBD retains the *s-trans* conformation, and the distance between DMBD and graphene is about 3.2 Å. The binding enthalpies from the two models are very close, -14.9 and -15.7 kcal/mol, respectively. Recently, Otyepka and co-workers performed a combined experimental and theoretical exploration of the adsorption of seven small organic molecules onto graphene.[51] The experimental adsorption enthalpies of seven organic molecules on graphene were obtained from gas chromatography measurements and spanned from -5.9 (dichloromethane) to -13.5 kcal/mol (toluene). Quantum mechanical

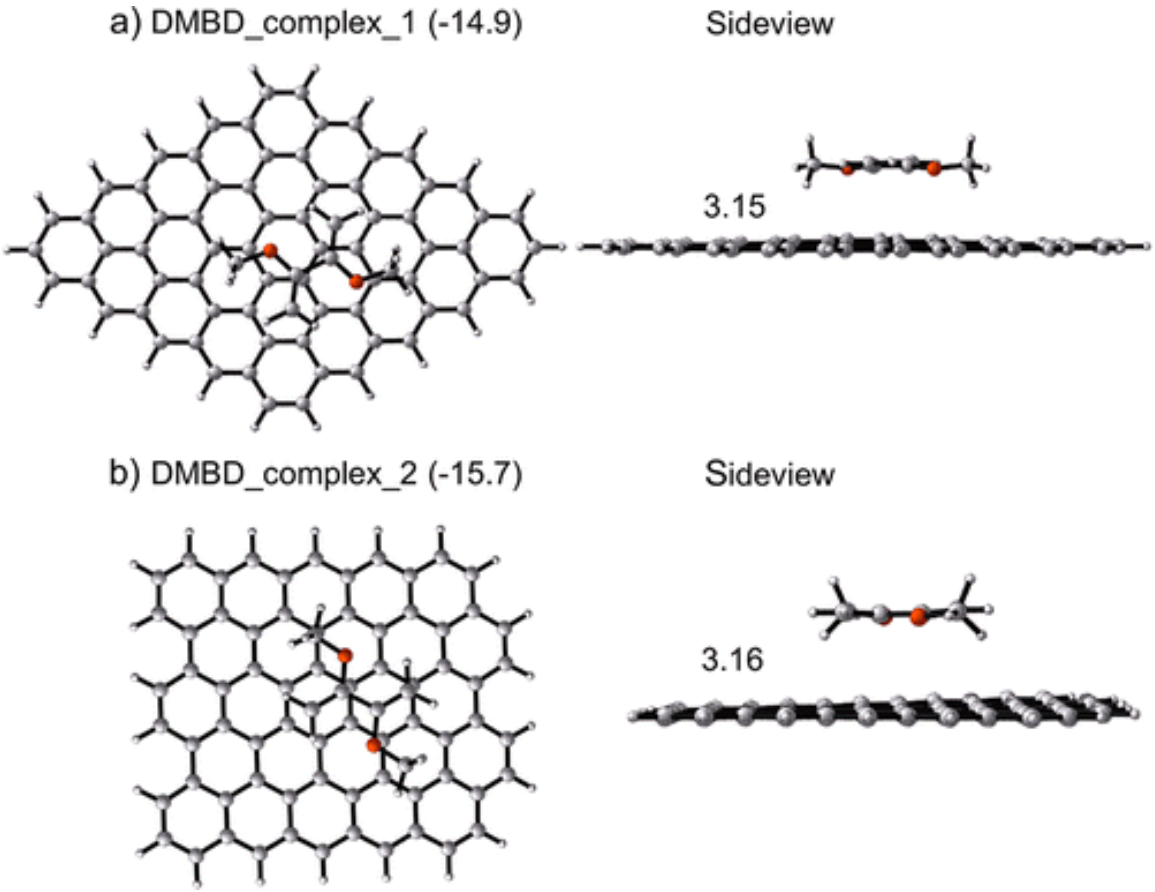

Figure 2.3 DMBD-graphene complex structures in both models from two viewpoints. The binding enthalpies are given in kcal/mol. The distances are given in Å.

calculations were conducted on coronene model to calculate theoretical interaction energies. M06-2X gives a mean error of 0.8 kcal/mol from the golden standard CCSD(T) method.[51] Therefore, our M06-2X calculations are believed to give reliable energetics for formation of complexes on graphene. In addition, it is found that noncovalent graphene complexes are predominately stablized by dispersion, which contributes more than 60% to the attractive energy, even in polar complexes.[51] Our calculations show that, for DMBD, noncovalent binding (Figure 2.3) is less exothermic than the DA functionalization on the edge bonds a/d (Figure 2.2). The

covalent functionalization on the graphene edges is preferred over the π complex. In contrast, the DA reaction at the interior, which consists of the majority of graphene bonds, is highly endothermic (around 40 kcal/mol; Figure 2.2). Formation of DMBD-graphene complex is exothermic by about 15 kcal/mol (Figure 2.3); therefore, the π complex is preferred over cycloaddition reactions on the interior of graphene surface.

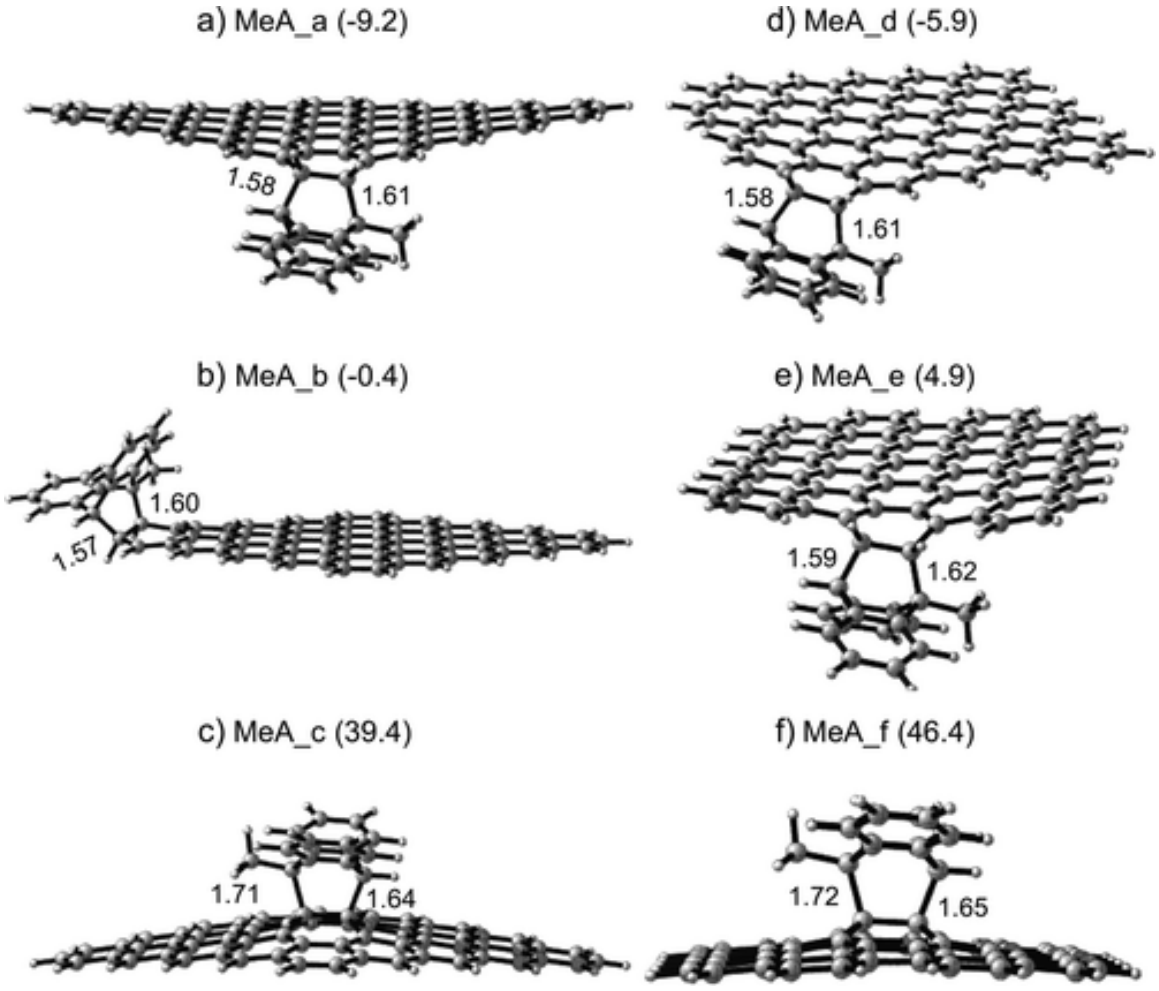

Figure 2.4 Diels-Alder adducts of MeA with graphene on bonds a-c in model 1 and d-f in model 2, where graphene functions as a dienophile. Reaction enthalpies are given in kcal/mol. The C-C bond lengths are given in Å.

The same calculations were performed on the MeA molecule. Figure 2.4 shows the product structures and reaction enthalpies for Diels-Alder reactions between MeA and graphene models, where graphene functions as a dienophile. In general, reactions of MeA are less exothermic than these of DMBD, because MeA forms strained bicyclo[2,2,2] octadiene addcuts. The edge bonds a, b, and d may react, as their reaction enthalpies are below 0 kcal/mol (Figure 2.4). The armchair edge e is barely reactive with an enthalpy of 4.9 kal/mol. Highly endothermic enthalpies (over 39 kcal/mol) in interior bonds c and f are obtained, indicating that MeA could not functionalize graphene surface through DA reactions. We also calculated the (4+4) reactions between MeA and graphene models. All the reaction enthalpies are highly endothermic, even on the edges. This suggests that the (4+4) cycloadditions are highly unfavorable.

The MeA-graphene non-covalent complex is much easier to form. Figure 2.5 shows the structure of MeA-graphene complexes in two graphene models from two viewpoints (top and side). The binding enthalpies from both models are quite large, around -24 kcal/mol, and are more favorable than the most reactive DA functionalization on bond a (-9.2 kcal/mol, Figure 2.4). MeA itself is an aromatic molecule, forming π-π stacking between graphene with a distance of 3.30 Å. The non-covalent interaction of graphene and anthracene was studied before. Lee and co-workers utilized the non-covalent interaction between 9-anthracene carboxylic acid and graphene to prepare stable aqueous graphene at room temprature.[52] The anthracene modified graphene material was found to have good electrochemical properties for supercapacitor application.[53] Such a stable π-π stacking interaction was also reported in other aromatic molecules on graphene.[26,54] Graphene functionalized by aromatic molecules is easily dispersible for solution processing. More importantly, the π-π stacking interaction is a promising method to control the electronic properties of graphene, such as opening the bandgap, optimizing the charge

carrier type, and so on.[26] Here our calculations indicate that, for the MeA molecule, the noncovalent interaction with graphene is significant, in agreement with the above experiments. Although the DA functionalization might occur on certain edges or defects, the noncovalent complex is preferred.

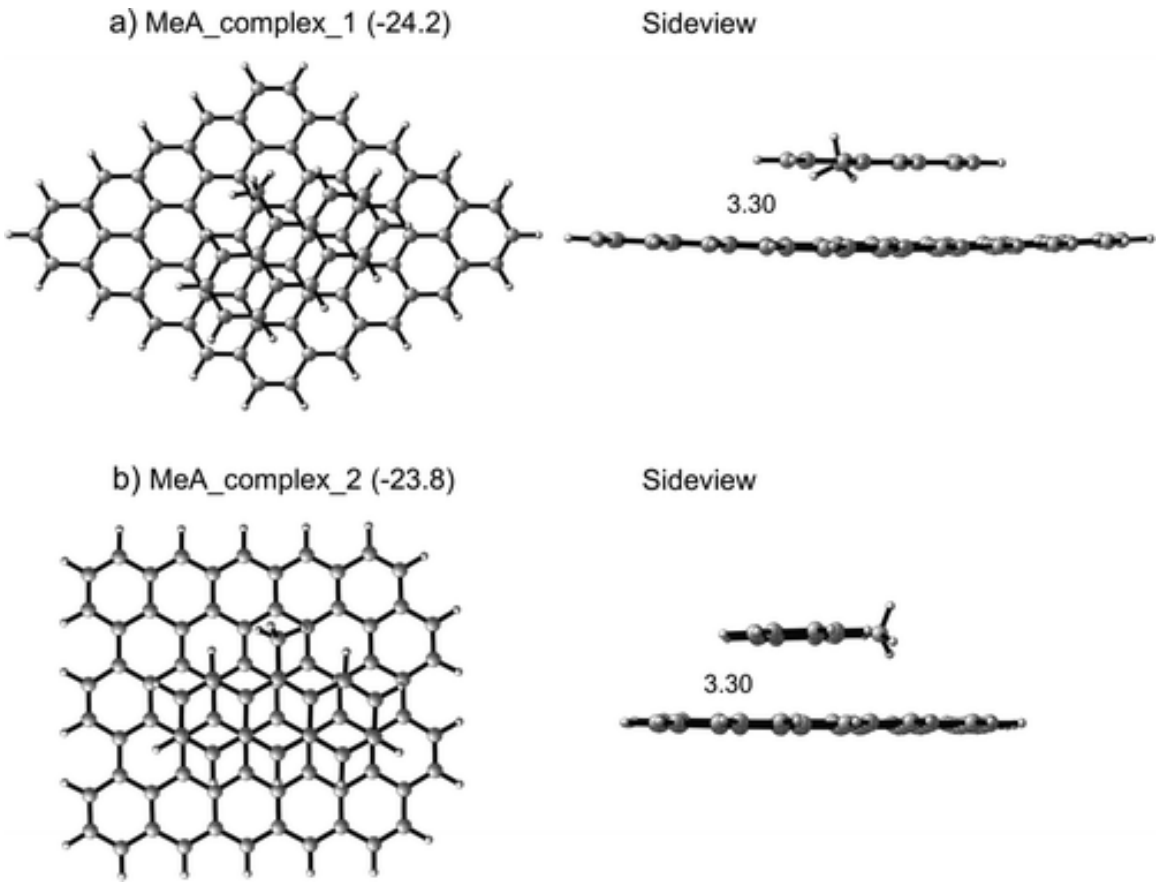

Figure 2.5 MeA−graphene complex structures in both models from two viewpoints. The binding enthalpies are given in kcal/mol. The distances are given in Å.

For graphene reactions with electron-deficient 2π components TCNE and maleic anhydride (MA), both (4+2) and (2+2) pathways were considered. Figure 2.6 shows the product structures and reaction enthalpies for Diels-Alder reactions between TCNE and two graphene

models. The DA reactions of dienes 1-3 in model 1 are all energetically unfavorable, with reaction enthalpies from 26.3 to 56.8 kcal/mol. The zigzag edges of graphene cannot function as a diene in this reaction. The armchair edge 5 resembles the bay region report by Scott.[38] The reaction of TCNE at this site has a slightly negative reaction enthalpy, -3.2 kcal/mol. The interior site 6 is unfeasible with an enthalpy of 42.5 kcal/mol.

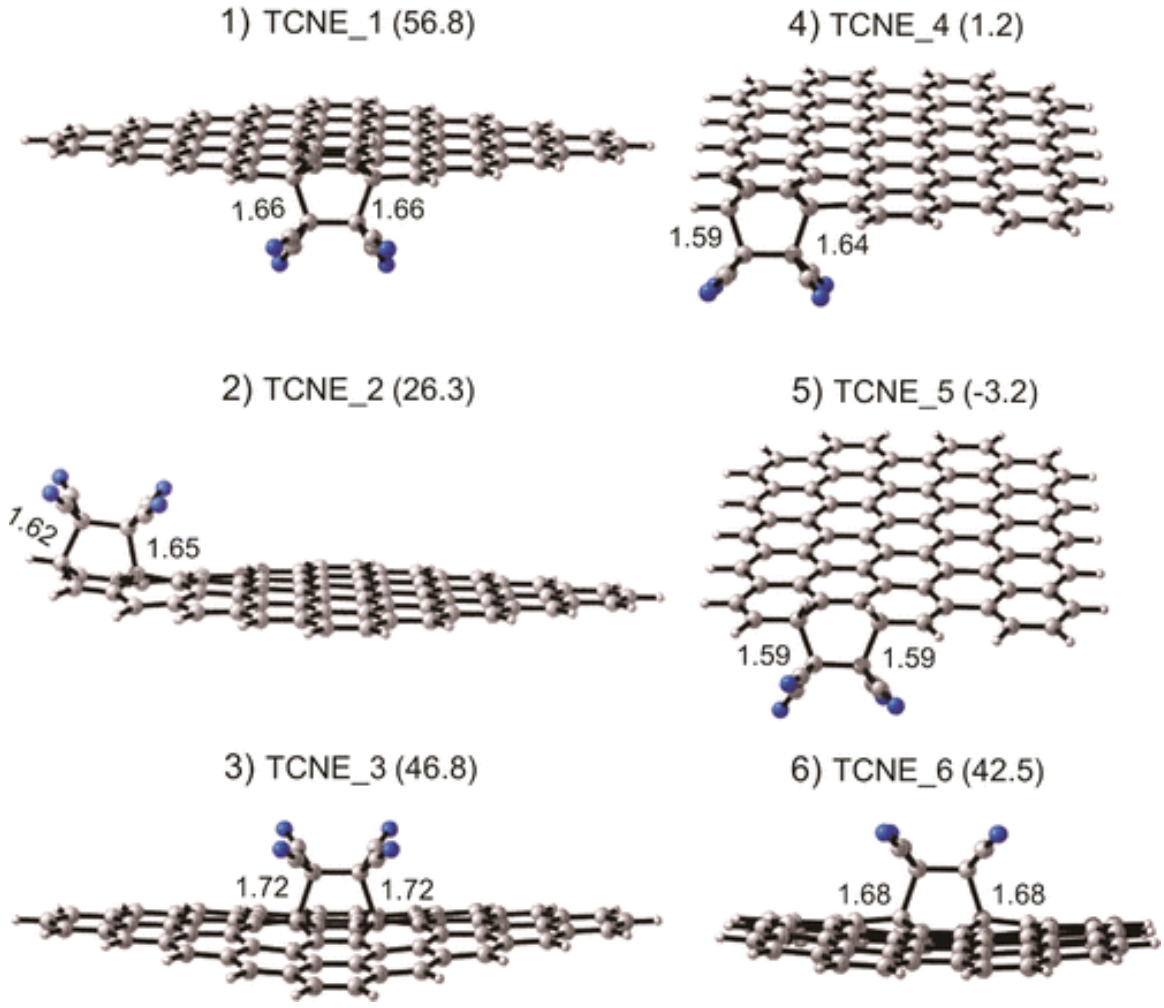

Figure 2.6 Diels-Alder adducts of TCNE with graphene on sites 1-3 in model 1 and 4-6 in model 2, where graphene functions as a diene. Reaction enthalpies are given in kcal/mol. The C-C bond lengths are given in Å.

TCNE is also known to react with electron-rich alkenes to give (2+2) adducts.[55] We tested the energetics of (2+2) adducts as shown in Figure 2.7. Six graphene bonds, a-f, were considered as 2π components in (2+2) reactions with TCNE. Only peripheral bonds a and d react favorably with enthalpies of -10.4 and -6.8 kcal/mol, respectively. The reaction on interior bonds c and f are endothermic by 38.9 and 45.1 kcal/mol. Therefore, TCNE could selectively functionalize graphene edges and defects through (2+2) or (4+2) reactions. However, interior areas will not react due to the highly unfavorable reaction energetics.

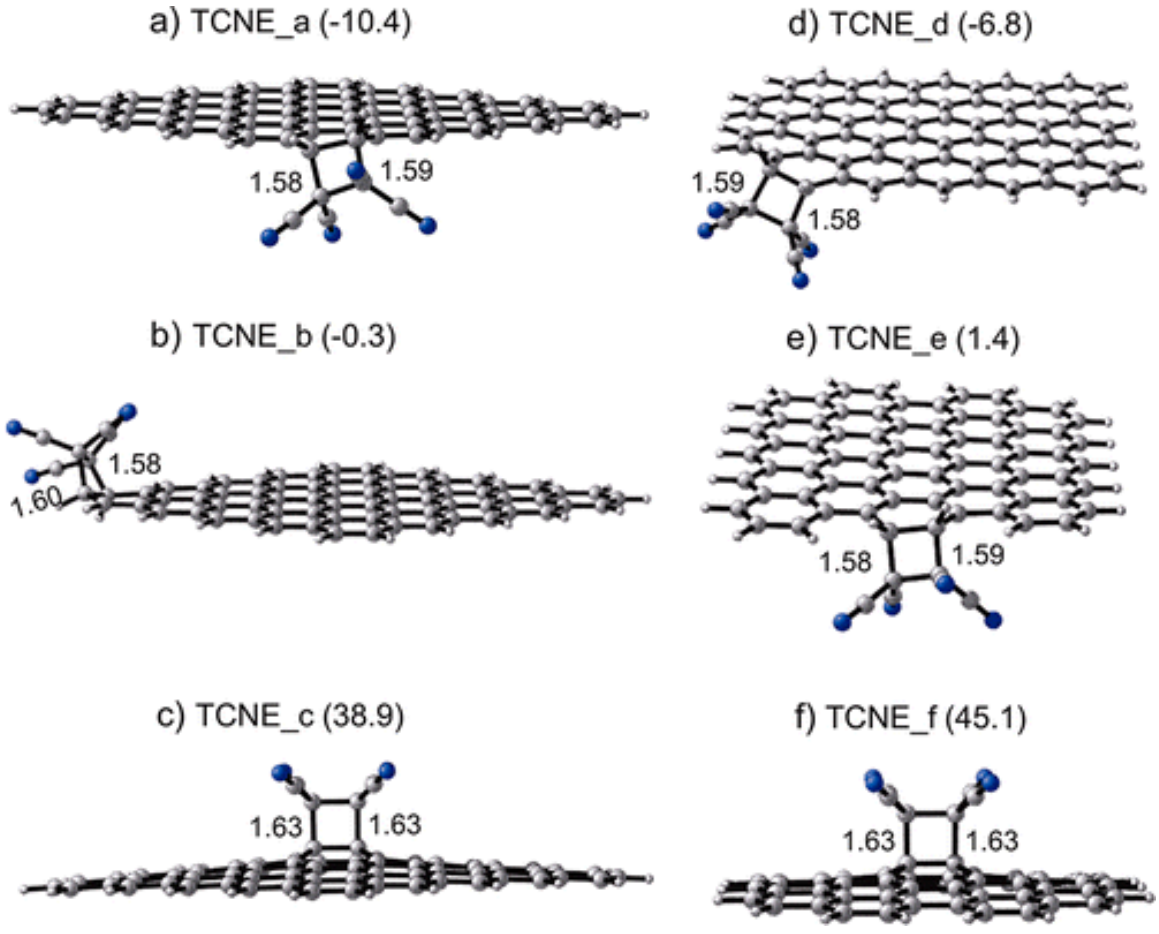

Figure 2.7 (2+2) adducts of TCNE with graphene on bonds a-c in model 1 and d-f in model 2, where graphene functions as a 2π component. Reaction enthalpies are given in kcal/mol. The C-C bond lengths are given in Å.

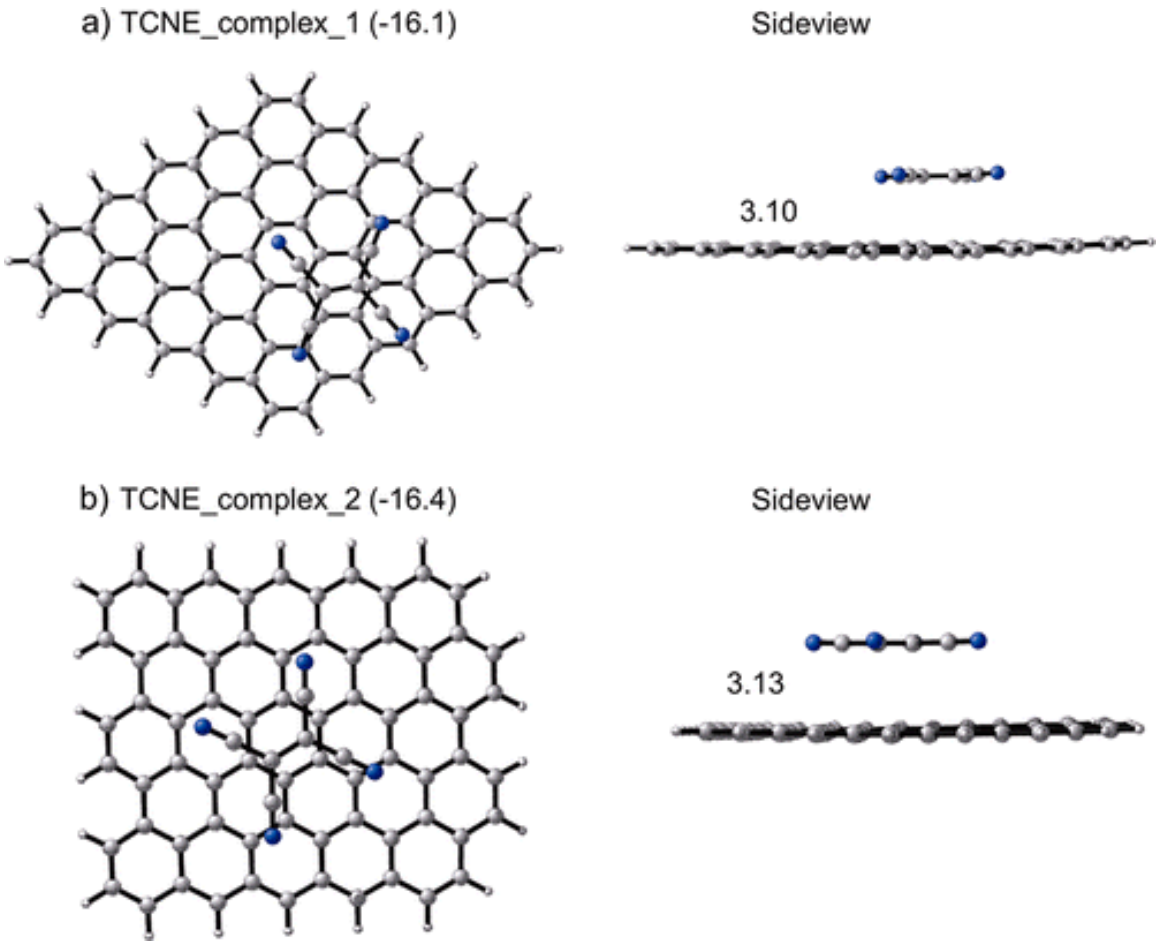

Figure 2.8 TCNE-graphene complex structures in both models from two viewpoints. The binding enthalpies are given in kcal/mol. The distances are given in Å.

Figure 2.8 shows TCNE-graphene complexes that are formed with a quite short distance of 3.10 Å. In addition, Mulliken change analysis shows that there is partial charge (0.05e) transfer from graphene to TCNE within their noncovalent complexes. The complexes from the two models have binding enthalpies of -16.1 and -16.4 kcal/mol, respectively. Rao's group has systematically studied the interaction of electron-donor and -acceptor molecules with graphene and single-walled carbon nanotubes. An experimental binding free energy has been measured to

be -5.7 kcal/mol for TCNE and graphene in solution from isothermal titration calorimetry (ITC) measurements.[29] This is in agreement with our DFT calculations, considering that the entropy contribution in solution is 5-10 kcal/mol. They found that the single-walled carbon nanotubes interacted reversibly with TCNE through charge transfer interaction. The noncovalent functionalization by TCNE has a significant impact on the electronic properties of metallic carbon nanotubes, with an opening in bandgap and changes in Raman spectral features.[29] A similar impact is expected on graphene. Both electron donors (tetrathiafulvalene) and electron acceptors (TCNE) establish charge transfer interactions with graphene, and the change in Raman spectral features of graphene were reported upon the noncovalent functionalization of TCNE.[28] These experimental observations support our computational results that the van der Waals complex is the dominant product of the reaction of TCNE with graphene.

The reactions of MA were also explored. For DA reactions, only armchair edges 4 and 5 in model 2 show exothermic enthalpies of -2.8 and -9.8 kcal/mol. The reaction enthalpies on two zigzag edges 1 and 2 are both more than 22 kcal/mol. The reactions on interior bonds in both models are about 40 kcal/mol. For the (2+2) cycloadditions, edge bonds a and d show slightly favorable enthalpies of -7.1 and -4.2 kcal/mol, respectively. Reactions of interior bonds c and f are endothermic by around 40 kcal/mol. Therefore, the interior bonds of graphene cannot be functionalized by MA through cycloadditions. Very recently, Baek and co-workers reported Diels-Alder reactions on graphite through dry ball-milling in the presence of MA, in which graphite functions as the diene and MA as the dienophile.[56] They found that the DA adducts are edge-selective. This is in agreement with our calculation results. The complex between MA and graphene is formed with a distance of 3.10 Å and exothermic by about -11 kcal/mol (Figure 2.9). This suggests that noncovalent complex formation is also dominant with MA.

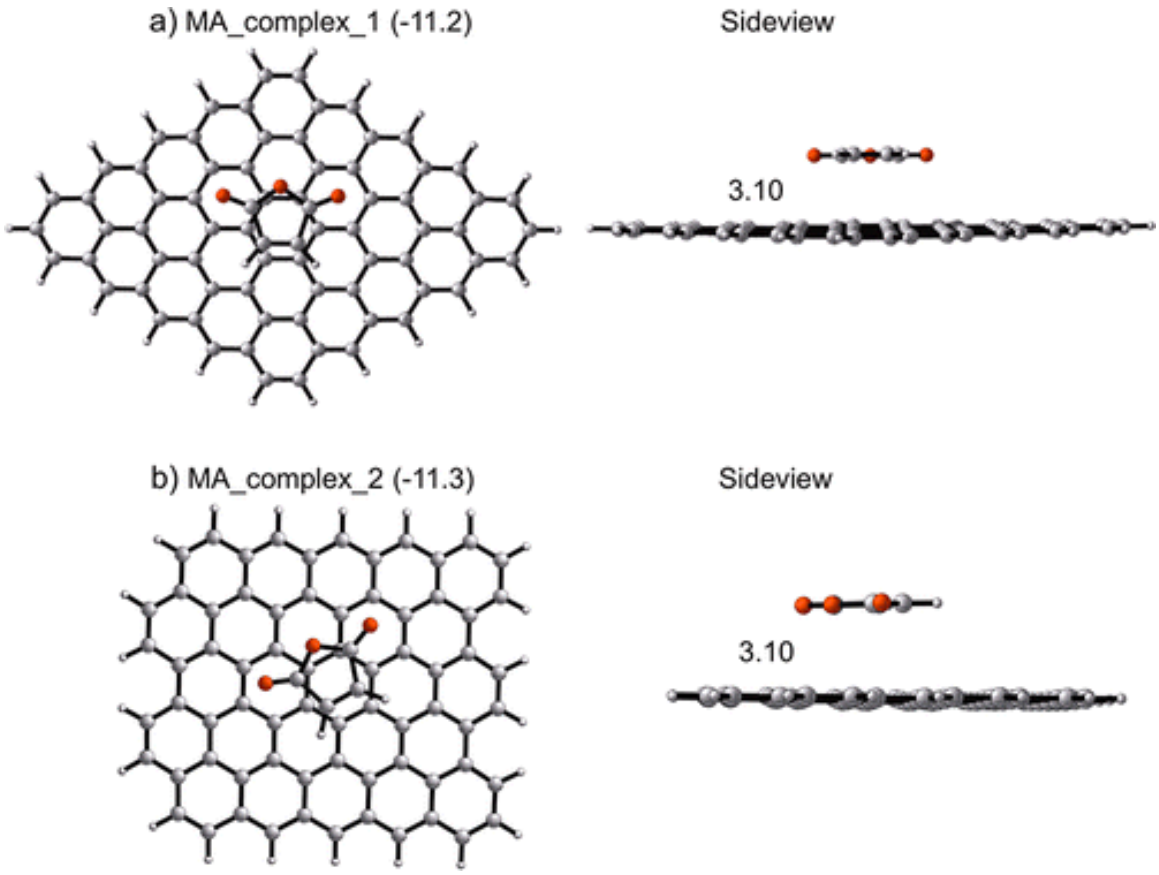

Figure 2.9 MA-graphene complex structures in both models from two viewpoints. The binding enthalpies are given in kcal/mol. The distances are given in Å.

Jiang and co-workers reported that, for graphene nanoribbons, the unpaired π electrons are distributed mainly on zigzag edges.[57] The partial radical character is related to the high chemical reactivity of zigzag edges. The partical radical character is related to the high chemical reactivity of zigzag edges in comparison to interior bonds and armchair edges of graphene.[58] Similar phenomena were reported by Lischka and co-workers.[37] We have calculated the spin density of two graphene models as shown in Figure 2.10, using unrestricted M06-2X calculations. The unpaired electron density is mainly distributed on the edges in both models. Model 2 has two

zigzag edges and two armchair edges. The unpaired π electron density is highest on zigzag edges. This is in agreement with previous studies and qualitatively explains why edges are generally much more reactive than interior regions.

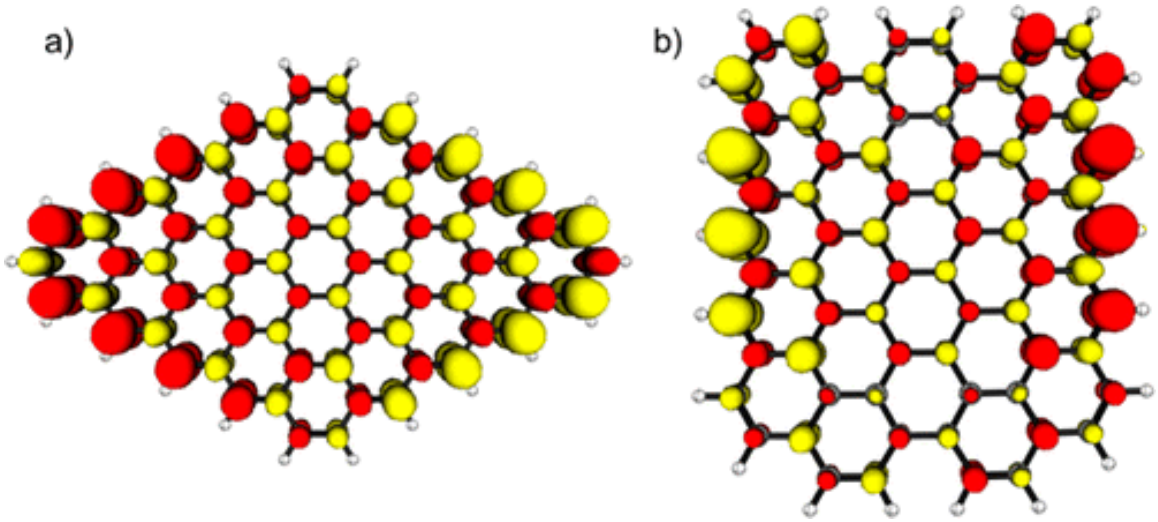

Figure 2.10 UM06-2X-computed spin densities for graphene model 1(a) and model 2(b).

We have also evaluated the reactivities of graphene using localization energies calculated by simple Hückel molecular orbital (HMO) theory. While very approximate, HMO does give a good account for reactivities of different aromatic hydrocarbons. The energy of π electrons is expressed in terms of α and β: $E = n\alpha + \lambda\beta$. The α is the Coulomb integral, and the β is the resonance integral. The localization energy (E_L) was recognized and developed by Wheland[59] and Brown[60] between 1940s-1950s. By definition, it is the energy difference between the residual molecule (E_r) and the original π system (E), $E_L = E_r - E$. Here, in our systems, the residual molecule is the remaining after the two reacting carbon atoms of the graphene are removed from model 1 and 2 (Figure 2.1). The localization energy qualitatively correlates with the reactivity of aromatic substitution reactions.[60] The most reactive position has the smallest localization energy.

We calculated the HMO energies using SHMO.[61] Table 2.1 summarizes the localization energies for our two graphene models. The 2α term is neglected, as it is the same for all reactions.

Table 2.1 HMO Localization Energies for Graphene Models Shown in Figure 2.1 (in units of |β|).

bond	E_L	site	E_L
a	3.0	1	5.5
b	3.3	2	4.6
c	4.4	3	5.1
d	3.1	4	4.2
e	3.3	5	3.9
f	4.6	6	4.9

When graphene functions as a 2π component, bonds a-c in model 1 and bonds d-f in model 2 are considered. Bond a is the most reactive with the smallest localization value of 3.0. Bond d with close reactivity to a has a value of 3.1. The interior bonds c and f are the most inert as indicated by their localization values of 4.4 and 4.6, respectively. In the case of graphene acting as a 4π component, sites 1-3 in model 1 and sites 4-6 in model 2 are considered. Although site 1 is in the edge, it is the least reactive with the largest value of 5.5. Site 5 with a value of 3.9 is the most reactive. In both models, interior regions of graphene are substantially more inert than active edges. These are all in agreement with the DFT calculations reported. This suggests that the reactivities of different graphene sites are largely determined by the loss of aromaticity

energies after functionalization. The HMO theory can quickly provide information for the prediction of the reaction sites on graphene fragments of any size.

2.4 Conclusion

We have calculated the cycloaddition reactions and noncovalent interactions of four reagents (DMBD, MeA, TCNE, and MA) on two graphene models. The interior bonds in both models, which resemble most of the bonds in graphene, cannot be directly functionalized through cycloaddition reactions by these four reagents, due to their highly unfavorable reaction enthalpies. DMBD and MeA could react with graphene edges through (4+2) cycloadditions. Both (4+2) and (2+2) reaction pathways are feasible between TCNE/MA and graphene edges. The enthalpies of non-covalent interactions of these four molecules range from -11.2 to -24.2 kcal/mol. Except for the DMBD molecule, the binding interactions of the other three molecules are all more favorable than their cycloaddition counterparts, even on reactive edge bonds. This suggests that the non-covalent interaction is dominant on graphene interior regions. We also performed the spin density and HMO calculations on our graphene models. The spin density diagram shows multi-radical character on edges, especially the zigzag edges. We found that Hückel molecular orbital (HMO) localization energies can be used to predict the relative reactivities of different sites in graphene.

2.5 Reference

1. Georgakilas, V.; Otyepka, M.; Bourlinos, A. B.; Chandra, V.; Kim, N.; Kemp, C. K.; Hobza, P.; Zboril, R.; Kim, K. S. *Chem. Rev.* **2012**, *112*, 6156–6214.
2. Loh, K. P.; Bao, Q.; Ang, P. K.; Yang, J. *J. Mater. Chem.* **2010**, *20*, 2277–2289.
3. Hummers, W. S.; Offenman, R. E. *J. Am. Chem. Soc.* **1958**, *80*, 1339-1339.

4. Chattopadhyay, J.; Mukherjee, A.; Hamilton, C. E.; Kang, J. H.; Chakraborty, S.; Guo, W.; Kelly, K. F.; Barron, A. R.; Billups, W. E. *J. Am. Chem. Soc.* **2008**, *130*, 5414–5415.

5. Cote, L. J.; Cruz-Silva, R.; Haung, J. *J. Am. Chem. Soc.* **2009**, *131*, 11027–11032.

6. Worsley, K. A.; Ramesh, P.; Mandal, S. K.; Niyogi, S.; Itkis, M. E.; Haddon, R. C. *Chem. Phys. Lett.* **2007**, *445*, 51–56.

7. Robinson, J. T.; Burgess, J. S.; Junkermeier, C. E.; Badescu, S. C.; Reinecke, T. L.; Perkins, F. K.; Zalalutdniov, M. K.; Baldwin, J. W.; Culbertson, J. C.; Sheehan, P. E. Snow, E. S. *Nano Lett.* **2010**, *10,* 3001–3005.

8. Bon, S. B.; Valentini, L.; Verdejo, R.; Fierro, J. L. G.; Peponi, L.; Lopez-Manchado, M. A.; Kenny, J. M. *Chem. Mater.* **2009**, *21*, 3433–3438.

9. Ryu, S.; Han, M. Y.; Maultzsch, J.; Heinz, T. F.; Kim, P.; Steigerwald, M. L.; Brus, L. E. *Nano Lett.* **2008**, *8*, 4597–4602.

10. Balog, R.; Jørgensen, B.; Nilsson, L.; Andersen, M.; Rienks, E.; Bianchi, M.; Fanetti, M.; Lægsgaard, E.; Baraldi, A.; Lizzit, S.; Sljivancanin, Z.; Besenbacher, F.; Hammer, B.; Pedersen, T. G.; Hofmann, P.; Hornekær, L. *Nat. Mater.* **2010**, *9*, 315–319.

11. Yang, Z.; Sun, Y.; Alemany, L. B.; Narayanan, T. N.; Billups, W. E. J. *Am. Chem. Soc.* **2012**, *134*, 18689–18694.

12. Lomeda, J. R.; Doyle, C. D.; Kosynkin, D. V.; Hwang, W. F.; Tour, J. M. *J. Am. Chem. Soc.* **2008**, *130*, 16201–16206.

13. Bekyarova, E.; Itkis, M. E.; Ramesh, P.; Berger, C.; Sprinkle, M.; de Heer, W. A.; Haddon, R. C. *J. Am. Chem. Soc.* **2009**, *131*, 1336–1337.

14. Liu, L.-H.; Yan, M. *Nano Lett.* **2009**, *9*, 3375–3378.

15. Strom, T. A.; Dillon, E. P.; Hamilton, C. E.; Barron, A. R. *Chem. Commun.* **2010**, *46*, 4097–4099.

16. Zhong, X.; Jin, J.; Li, S.; Niu, Z.; Hu, W.; Li, R.; Ma, J. *Chem. Commun.* **2010**, *46*, 7340-7342.

17. Denis, P. A.; Iribarne, F. *J. Mater. Chem.* **2012**, *22*, 5470-5477.

18. Quintana, M.; Spyrou, K.; Grzelczak, M.; Browne, W. R.; Rudolf, P.; Prato, M. *ACS Nano*, **2010**, *4*, 3527–3533.

19. Georgakilas, V.; Bourlinos, A. B.; Zboril, R.; Steriotis, T. A.; Dallas, P.; Stubos, A. K.; Trapalis, C. *Chem. Commun.* **2010**, *46*, 1766–1768.

20. Sarkar, S.; Bekyarova, E.; Niyogi, S.; Haddon, R. C. *J. Am. Chem. Soc.* **2011**, 133, 3324–3327.

21. Sarkar, S.; Bekyarov, E.; Haddon, R. C. *Acc. Chem. Res.* **2012**, *45*, 673–682.

22. Lu, C. H.; Yang, H. H.; Zhu, C. L.; Chen, X.; Chen, G. N. *Angew. Chem., Int. Ed.* **2009**, *48*, 4785– 4787.

23. Shan, C. S.; Yang, H. F.; Song, J. F.; Han, D. X.; Ivaska, A.; Niu, L. *Anal. Chem.* **2009**, *81*, 2378– 2382.

24. Baby, T. T.; Aravind, S. S. J.; Arockiadoss, T.; Rakhi, R. B.; Ramaprabhu, S. *Sens. Actuators B* **2010**, *145*, 71– 77.

25. Haldar, S.; Kolar, M.; Sedlak, R.; Hobza, P. *J. Phys. Chem. C.* **2012**, *116*, 25328-25336.

26. Zhang, Z.; Huang, H.; Yang, X.; Zhang, L. *J. Phys. Chem. Lett.* **2011**, *2*, 2897– 2905.

27. Ishikawa, R.; Bando, M.; Morimoto, Y.; Sandhu, A. *Nanoscale Res. Lett.* **2011**, 6, 111.

28. Voggu, R.; Das, B.; Rout, C. S.; Rao, C. N. R. *J. Phys.: Condens. Matter* **2008**, *20*, 472204.

29. Varghese, N.; Ghosh, A.; Voggu, R.; Rao, C. N . R. *J. Phys. Chem. C*. **2009**, *113*, 16855-16859.

30. Choudhury, D.; Das, B.; Sarma, D. D.; Rao, C. N. R. *Chem. Phys. Lett*. **2010**, *497*, 66-69.

31. Rao, C. N. R.; Voggu, R. *Mater. Today* **2010**, *13*, 34-40.

32. Denis, P. A. *Chem. Eur. J*. **2013**, DOI: 10.1002/chem.201302622.

33. Geim, A. K.; Novoselov, K. S. *Nature Mater*. **2007**, *6*, 183–191.

34. Heyrovska, R. *arXiv.org Physics* **2008**, DOI: arxiv.org/abs/0804.4086.

35. Ritter, K. A.; Lyding, J. W. *Nanotechnology* **2008**, *19*, 015704.

36. Jia, X.; Campos-Delgado, J.; Terrones, M.; Meunier, V.; Dresselhaus, M. S. *Nanoscale*, **2011**, *3*, 86-95.

37. Plasser, F.; Pasalic, H.; Gerzabek, M. H.; Libisch, F.; Reiter, R.; Burgdorfer, J.; Müller, T.; Shepard, R.; Lischka, H. *Angew. Chem., Int. Ed*. **2013**, *52*, 2581 –2584.

38. Fort, E. H.; Jeffreys, M. S.; Scott, L. T. *Chem. Commun*. **2012**, *48*, 8102-8104.

39. Strout, D. L.; Scuseria, G. E. *J. Chem. Phys*. **1995**, *102*, 8448-8452.

40. Pérez-Jordá, J. M.; Yang, W. *J. Chem. Phys*. **1997**, *107*, 1218-1226.

41. Krukau, A. V.; Scuseria, G. E.; Perdew, J. P.; Savin, A. *J. Chem. Phys*. **2008**, *129*, 124103.

42. Cao, Y.; Houk, K. N. *J. Mater. Chem*., **2011**, *21*, 1503-1508.

43. Bendikov, M.; Duong, H. M.; Starkey, K.; Houk, K. N.; Carter, E. A.; Wudl, F. *J. Am. Chem. Soc*. **2004**, *126*, 7416–7417.

44. Bian, S.; Scott, A. M.; Cao, Y.; Liang, Y.; Osuna, S.; Houk, K. N.; Braunschweig, A. B. *J. Am. Chem*. Soc. **2013**, *135*, 9240-9243.

45. Frisch, M. J.; Trucks, G. W.; Schlegel, H. B.; Scuseria, G. E.; Robb, M. A.; Cheeseman, J. R.; Scalmani, G.; Barone, V.; Mennucci, B.; Petersson, G. A.; Nakatsuji, H.; Caricato, M.;

Li, X.; Hratchian, H. P.; Izmaylov, A. F.; Bloino, J.; Zheng, G.; Sonnenberg, J. L.; Hada, M.; Ehara, M.; Toyota, K.; Fukuda, R.; Hasegawa, J.; Ishida, M.; Nakajima, T.; Honda, Y.; Kitao, O.; Nakai, H.; Vreven, T.; Montgomery, J. A., Jr.; Peralta, J. E.; Ogliaro, F.; Bearpark, M.; Heyd, J. J.; Brothers, E.; Kudin, K. N.; Staroverov, V. N.; Kobayashi, R.; Normand, J.; Raghavachari, K.; Rendell, A.; Burant, J. C.; Iyengar, S. S.; Tomasi, J.; Cossi, M.; Rega, N.; Millam, J. M.; Klene, M.; Knox, J. E.; Cross, J. B.; Bakken, V.; Adamo, C.; Jaramillo, J.; Gomperts, R.; Stratmann, R. E.; Yazyev, O.; Austin, A. J.; Cammi, R.; Pomelli, C.; Ochterski, J. W.; Martin, R. L.; Morokuma, K.; Zakrzewski, V. G.; Voth, G. A.; Salvador, P.; Dannenberg, J. J.; Dapprich, S.; Daniels, A. D.; Farkas, O.; Foresman, J. B.; Ortiz, J. V.; Cioslowski, J.; Fox, D. J.; Gaussian 09, revision C.01; Gaussian Inc.: Wallingford, CT, 2010.

46. Zhao, Y.; Truhlar, D. G. *Theor. Chem. Acc.* **2008**, *120*, 215-241.

47. Zhao, Y.; Truhlar, D. G. *Acc. Chem. Res.* **2008**, *41*, 157-167.

48. Hehre, W. J.; Radom, L.; Schleyer, P. v. R.; Pople, J. A. *Ab Initio Molecular Orbital Theory*, Wiley: New York, 1986.

49. Chai, J.-D.; Head-Gordon, M. *Phys. Chem. Chem. Phys.* **2008**, *10*, 6615-6620.

50. Lan, Y.; Zou, L.-F.; Cao, Y.; Houk, K. N. *J.* Phys. *Chem. A.* **2011**, *115*, 13906-13920.

51. Lazar, P.; Karlický, F.; Jurečka, P.; Kocman, M.; Otyepková, E.; Šafářová, K.; Otyepka, M. *J. Am. Chem. Soc.* **2013**, *135*, 6372-6377.

52. Bose, S.; Kuila, T.; Mishra, A. K.; Kim, N. H.; Lee, J. H. *Nanotechnology*, **2011**, 22, 405603.

53. Khanra, P.; Kuila, T.; Bae, S. H.; Kim, N. H.; Lee, J. H. *J. Mater. Chem.* **2012**, *22*, 24403-24410.

54. Mann, J. A.; Dichtel, W. R. *ACS Nano* **2013**, *7*, 7193-7199.

55. Kivala, M.; Diederich, F. *Acc. Chem. Res.* **2009**, *42*, 235 –248.

56. Seo, J. M.; Jeon, I. Y.; Baek, J. B. *Chem. Sci.* **2013**, *4*, 4273-4277..

57. Jiang, D.; Sumpter, B. G.; Dai, S. *J. Chem. Phys.* **2007**, *126*, 134701.

58. Tang, Q.; Zhou, Z.; Chen, Z. F. *Nanoscale*, **2013**, *5*, 4541-4583.

59. Wheland, G. W. *J. Am. Chem. Soc.* **1942**, *64*, 900–908.

60. Brown, R. D. *Q. Rev. Chem. Soc.* **1952**, *6*, 63-99.

61. http://www.chem.ucalgary.ca/SHMO/

Chapter 3 Covalently Patterned Graphene Surfaces by a Forced Accelerated Diels-Alder Reaction

3.1 Abstract

Cyclopentadienes (CPs) with Raman and electrochemically active tags were patterned covalently onto graphene surfaces using force-accelerated Diels-Alder (DA) reactions that were induced by an array of elastomeric tips mounted onto the piezoelectric actuators of an atomic force microscope. These force-accelerated cycloadditions are a feasible route to locally alter the chemical composition of graphene defects and edge sites under ambient atmosphere and temperature over large areas (~1 cm^2)

3.2 Results and discussion

Graphene has become the focus of considerable research attention because of its high conductivity, 2D structure, and superior mechanical properties.[1] Patterning onto the basal plane of graphene may increase the bandgap of graphene, a boon for integrated optics and electronics, or for the fabrication of graphene-based sensors.[2] However, a consequence of the stabilizing π-conjugation of graphene is that the basal plane is resistant towards chemical functionalization, so carrying out organic chemistry on graphene site-specifically is particularly challenging. Scalable methods to covalently pattern organic molecules onto graphene have not, to the best of our knowledge, been demonstrated. Functional molecules have been anchored to graphene using noncovalent interactions[3] or bonding to oxidized defect sites and edges.[2d,4] Alternatively, photochemical,[5] dipolar-cycloadditions,[6] and diazonium salt[2b,7] reactions couple organics directly with the basal plane of graphene, albeit not in patterns and with an input of energy that would denature or destroy soft matter. The recent report by Haddon *et al*. proposing that single layer

graphene (SLG) participates in DA reactions as a dienophile at temperatures as low as 50 ºC over 3 h[8] suggested to us conditions that could be used to scalably pattern graphene at ambient temperatures and atmosphere. Because of their negative activation volumes,[9] cycloaddition reactions are significantly accelerated in pressurized reaction vessels, and the Reinhoudt and Ravoo groups have covalently micropatterned various surfaces by inducing Cu^{I}-free Huisgen and DA reactions through applied force between inked elastomeric stamps and surfaces.[10] Thus, we reasoned that a localized force exerted between SLG and a diene would accelerate the DA reactions and thereby immobilize molecules into patterns onto the basal plane of graphene through the formation of two new C–C bonds (Figure 3.1a).

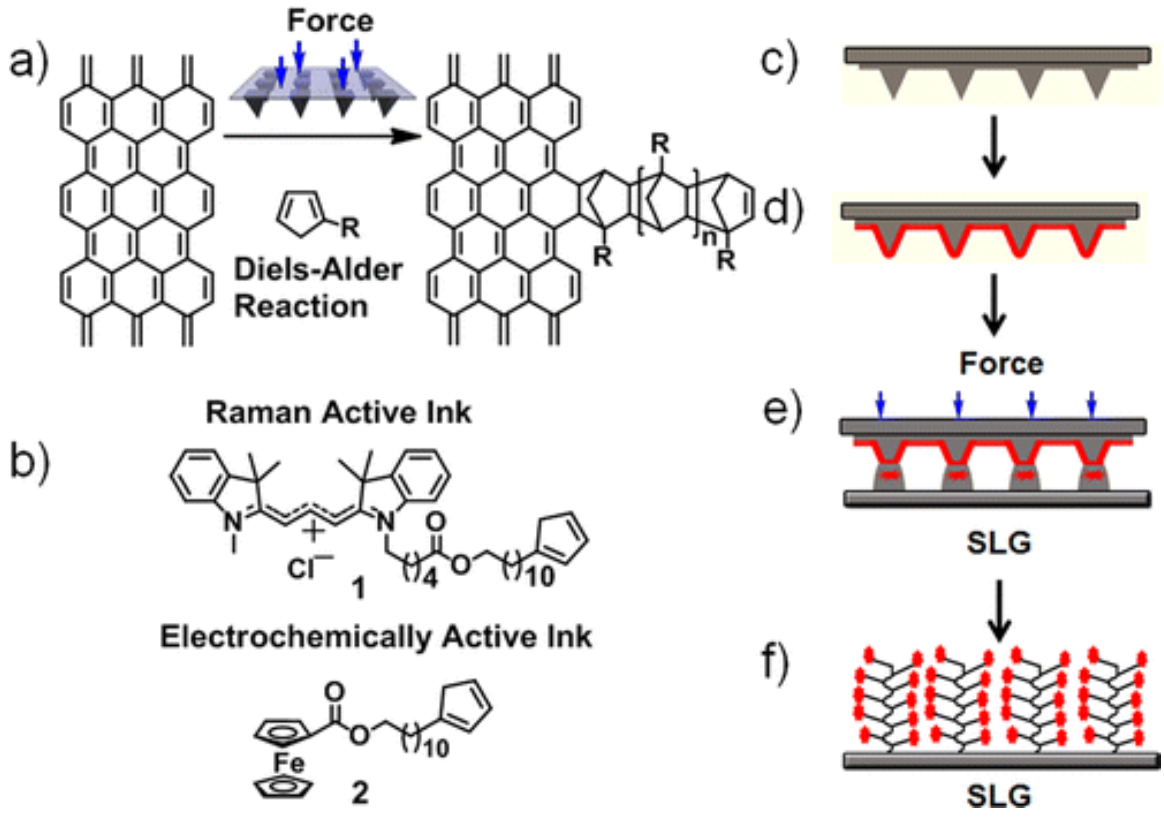

Figure 3.1 a) DA oligomerization reaction between functionalized CP and a single layer graphene (SLG) surface. b) Cy3-containing Raman active 1 and ferrocene-containing

electrochemically active 2 ink molecules used to confirm force-accelerated patterning. c) An elastomeric tip-array. d) The tip-array coated with an ink mixture (red) consisting of a CP and poly(ethylene glycol) (PEG). e) The inked tip array is pushed into the SLG surface. f) Following rinsing of the surface to remove the PEG and excess CP, only the covalently immobilized molecules remain on the surface.

To demonstrate that force accelerated cycloadditions could covalently pattern large areas (~1 cm^2) of SLG sheets, we used an elastomeric tip array mounted onto the piezoelectric actuators of an atomic force microscope (AFM) to exert a localized force between functionalized CPs and SLG sheets. These tip arrays are commonly used for polymer pen lithography,[11] where patterns are formed by ink transfer from the tips to the surface through an aqueous meniscus. Moreover, their large areas (>1 cm^2) and the computer-controlled movement of the piezoactuators that hold the array provide high throughput and flexible pattern design. We have recently induced both the Cu^I-catalyzed azide-alkyne click reaction[12] and the Staudinger ligation[13] on Au and SiO_2 surfaces with these tip arrays under ambient temperatures and pressures, confirming the suitability of these tip-arrays for covalently immobilizing soft matter nondestructively through selective organic transformations. Because the elastomeric tips also compress upon contact with surfaces, they can apply a predictable force between molecular inks and a surface,[14] so that in this experiment, the position, force, and reaction time can all be controlled precisely to pattern surfaces over cm^2 areas with micrometer-scale features.

Raman-active cyanine 3 (Cy3) containing CP **1** and electrochemically-active ferrocene CP **2** (Figure 3.1b) were designed to characterize the bonding upon cycloaddition between the SLG surface and the CPs. CPs react quickly in DA reactions because of their geometric

preorganization, and as a result, they have been utilized already in the context of surface patterning.[15] The Haddon group[8a] used Raman spectroscopy to follow a DA reaction on graphene and found that the D band at 1324 cm^{-1} that corresponds to the A_{1g} breathing vibration of sp^2 carbon rings, which is suppressed in pure graphene, increases significantly because the introduction of defects or covalently adsorbed molecules reduces the symmetry of the graphene lattice. The ratio of the D- and G-band integrations (I_D/I_G) is a measure of the degree of functionalization of graphene.[16] Alternatively, electrochemistry can confirm the immobilization of the ink onto the surface and quantify the density of surface-bound molecules.[12,17]

Molecules **1** and **2** were synthesized and characterized by ^{1}H NMR, ^{13}C NMR, and high-resolution mass spectrometry, and all analytical data were consistent with the proposed structures.[18] The 8500 tip PDMS arrays with a tip-to-tip spacing of 80 or 160 μm were prepared following previously published literature protocols.[11] To induce the DA reaction between **1** and the SLG surface, **1** (0.8 mg, 1.2 mmol) and poly(ethylene glycol) (PEG) (2000 g mol^{-1}, 10 mg ml^{-1}) in 0.8 mL 60 : 20 THF/H_2O, which was sonicated to ensure solution homogeneity, were spin coated (2000 rpm, 2 min) onto a tip array. The PEG matrix that encapsulates the CPs ensures even distribution of ink across the tip array and that ink transport from the tips to a surface is predictable and reproducible.[12] The tips were mounted onto the z-piezo of an AFM that was specially equipped with an apparatus to hold the tip arrays, an environmental chamber to regulate the humidity, and customized lithography software to control the position, force, and dwell-time of the tips (Figure 3.1c).[18] A 2x3 dot pattern of **1** with feature-to-feature spacing of 20 μm was produced by each tip in the array by pushing the tips into the SLG surface (SLG on 285 nm SiO_2) at times ranging from 15-30 min and a force of ~100 mN at each spot.[14] The transfer of

the **1**/PEG mixture into 2x3 patterns and an approach dot to level the arrays on the surface was confirmed by light microscopy (Figure 3.2a).

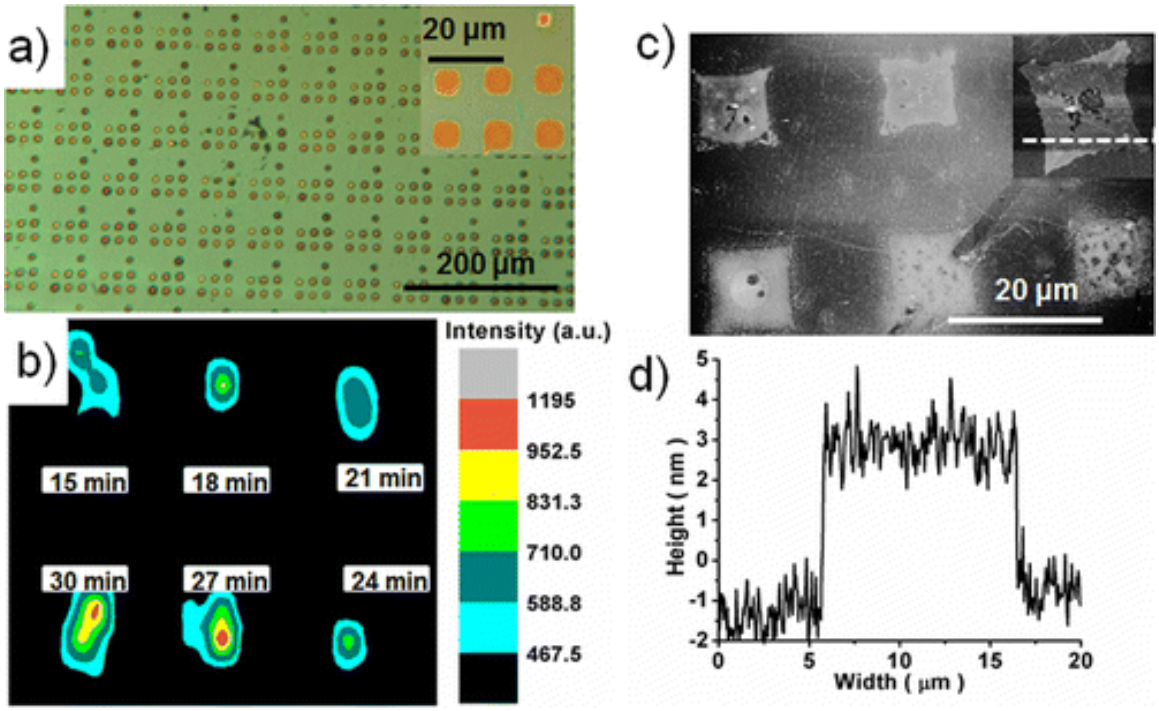

Figure 3.2 a) Light microscopy image (10x magnification) of 2 x 3 dot arrays of a mixture containing 1 and PEG, with varying dwell times (30, 27, 24, 21, 18, 15 min), that were patterned by each pen in the tip array. Scale bar is 200 µm. Inset is a magnified image of one array. Scale bar is 20 µm. b) Raman mapping image (1324 cm^{-1}, D band) of 2 x 3 dot arrays of 1 covalently immobilized onto the SLG. Scale bar is 20 µm. c) AFM image of a single feature printed onto the SLG. d) Height profile of a single feature of 1 patterned onto SLG.

After washing the surfaces with EtOH and H_2O to remove unreacted **1** and PEG, the surface bonding was analyzed by Raman microscopy (WITec, 633 nm excitation). A Raman map of the surface that was obtained following force accelerated printing of **1** revealed a 2 x 3 pattern of features where I_D was elevated significantly compared to surrounding areas (Figure 3.2b). The

20 μm spacing between features in the 2 x 3 patterns observed in the Raman map matched with the pattern of features printed by the pen array.[18] The elevated I_D was observed at all points where the tips were pressed into the surface for all dwell times above 15 min, but poor signal was obtained for dwell times below 12 min. Importantly, control experiments where **1** was not present in the ink mixture or where **1** was present, but force was not applied to the surface upon ink transfer, did not produce similar patterns or significantly elevated I_D/I_G, confirming that the diene and force are both necessary for changes in bonding to occur. AFM height images show the presence of elevated surfaces where the dienes had been printed (Figure 3.2c and 3.2d), with a height of ~3.5 nm, which is too high for a monolayer of **1**.

Spectra associated with different points on the Raman map further confirmed that the changes in bonding were produced because of localized DA reactions (Figure 3.3). A Raman spectrum taken at a point where the inked tips were pressed into the surface had peaks of **1** as well as an increased I_D/I_G value of 0.56, compared to 0.14 for the unaltered surface, 0.17 where the tips had been pressed into the surface in the absence of **1**, and 0.16 for the original SLG surface.[19] Changes in the I_D/I_G indicate that the force-induced reaction of **1** with SLG converts some C–C bonds in the SLG from sp^2 to sp^3, consistent with previous observations for DA reactions on SLG surfaces.[8]

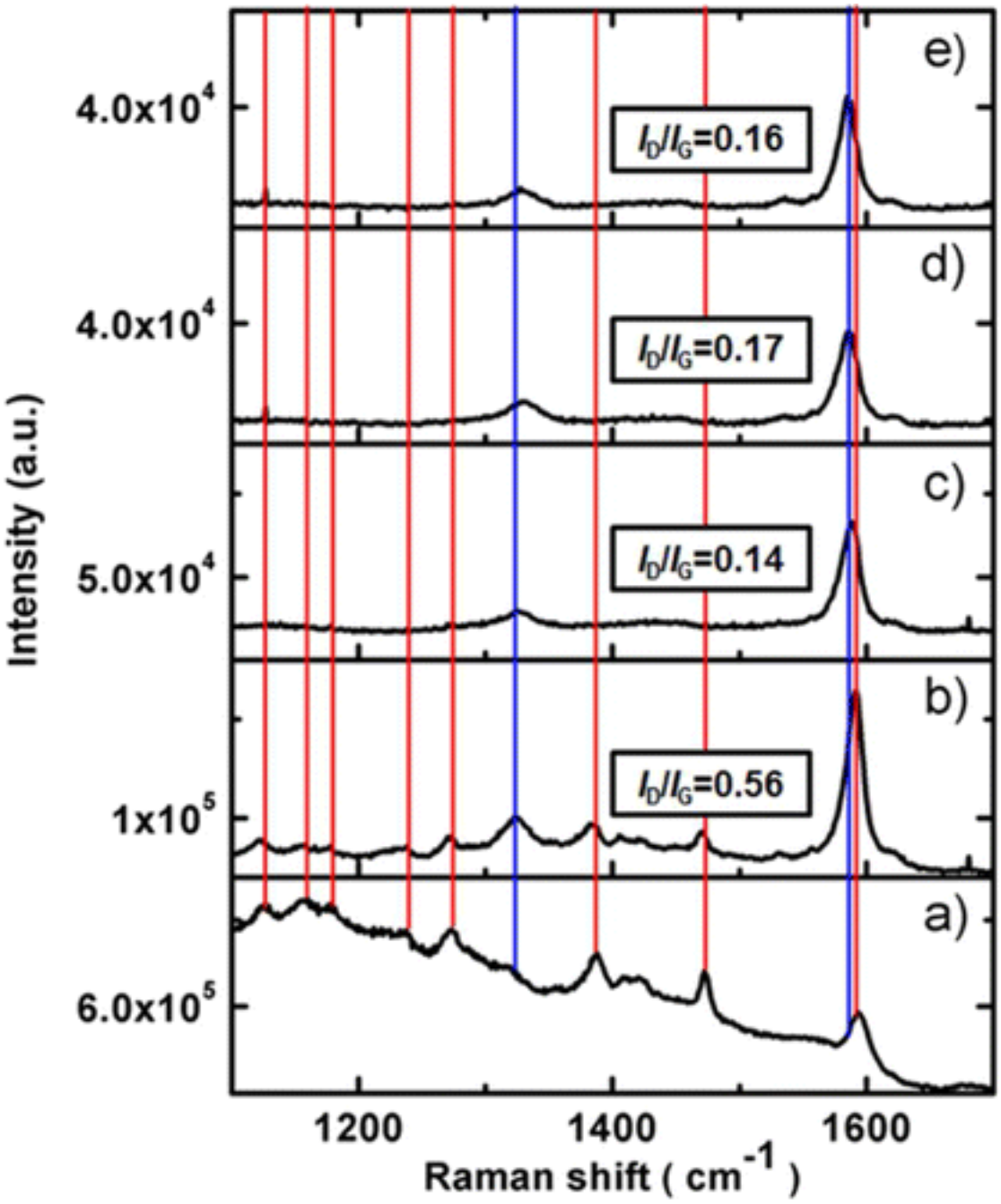

Figure 3.3 a) Raman spectrum of 1 on a SiO_2 surface. b) Raman spectrum from a map with force accelerated printing of 1 (Figure 3.2b) taken at a position with increased D-band intensity (I_D) compared to unreacted SLG also has peaks corresponding to 1. c) Raman spectrum from the map of the same printed surface taken at a position without increased I_D. d) Raman spectrum of

control experiment where PEG and force were applied to the SLG surface without 1, taken at a point where the tips were pushed into the SLG surface. e) Raman spectrum of pure SLG. Red lines mark peaks of 1 (11124, 1157, 1178, 1272, 1387, 1594 cm^{-1}). Blue lines mark SLG peaks (1324, 1584 cm^{-1}).

Electrochemically active CP **2** was patterned onto SLG following a similar protocol described above, and the immobilization density of **2** on the SLG surface was analyzed by cyclic voltammetry (CV). Each tip in the pen array produced a 2 x 3 dot pattern over the 1 cm^2 area with an average feature edge length of 7.1 μm and area of 50.4 μm^2. Following washing of the surface with EtOH and H_2O to remove the PEG and unreacted **2**, CV was carried using a Ag/AgCl reference electrode, a Pt counter electrode, and the patterned SLG as the working electrode. A strong redox peak at E^o = 590 mV (vs Ag/AgCl) confirmed the presence of the ferrocene (fc)/ferrocenium (fc^+) reversible redox couple from **2** (Figure 3.4), which is shifted anodically compared to fc because of the ester linking the fc to the CP. Control experiments where **2** was deposited without force did not result in any observable current corresponding to the fc/fc^+ redox couple after washing, confirming that force is necessary to induce the DA reaction under these conditions. The linear relationship between peak current and scan rate confirmed **2** is immobilized on the SLG surface[17,19] but that the localized changes in bonding from sp^2 to sp^3 do not prevent conduction through the SLG. Interestingly, the increase in ΔE with scan rate ($\partial V/\partial t$) as well as the slope of 0.7 in the ln ($\partial V/\partial t$) vs ln (I), indicates complexity in the charge transfer from the fc to the SLG. From integraton of the CV, a charge density (Γ_{fc}) of (5.34 ± 0.76) x 10^{14} cm^{-2} was obtained,[18] which is significantly higher than would be expected from the increase in the D-band intensity of the Raman spectrum.

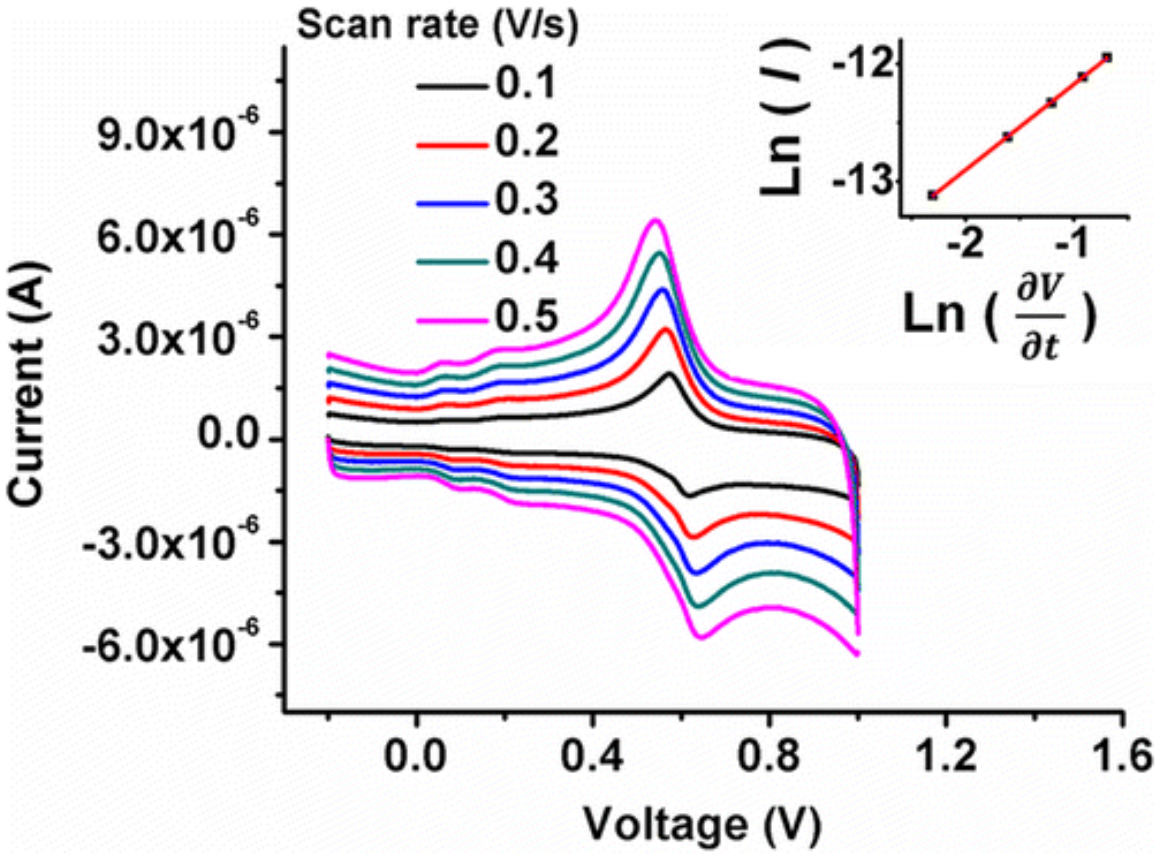

Figure 3.4 Cyclic voltammetry (CV) of 2 on SLG using a Pt counter electrode and Ag/AgCl reference electrode in 0.1 M $HClO_4$ electrolyte. (Inset) Relationship between ln(scan rate) and ln(current).

To further study the reaction between CP and SLG as well as explain the CV and AFM results, DFT calculations were conducted for DA reactions of CP on three representative bonds in a 5x5 graphene model (Figure 3.5a). Hydrogen-substituted edges were used, although the nature of the edge is likely complex.[2d,4] The corner bond "a" can be viewed as the joint part of zigzag and armchair edges of graphene. Another periphery bond "b" represents the edges, and the center bond "c" most resembles the pristine graphene interior. All structures were optimized at (U)M06-2X/6-31G(d) level, and single point energy calculations were carried on the

optimized structures at the (U)M06-2X/6-311G(d,p) level.[18] We report here only the situation of graphene acting as dienophile, and CP as diene. Two more reaction pathways were also calculated but found to be unfavorable.[18]

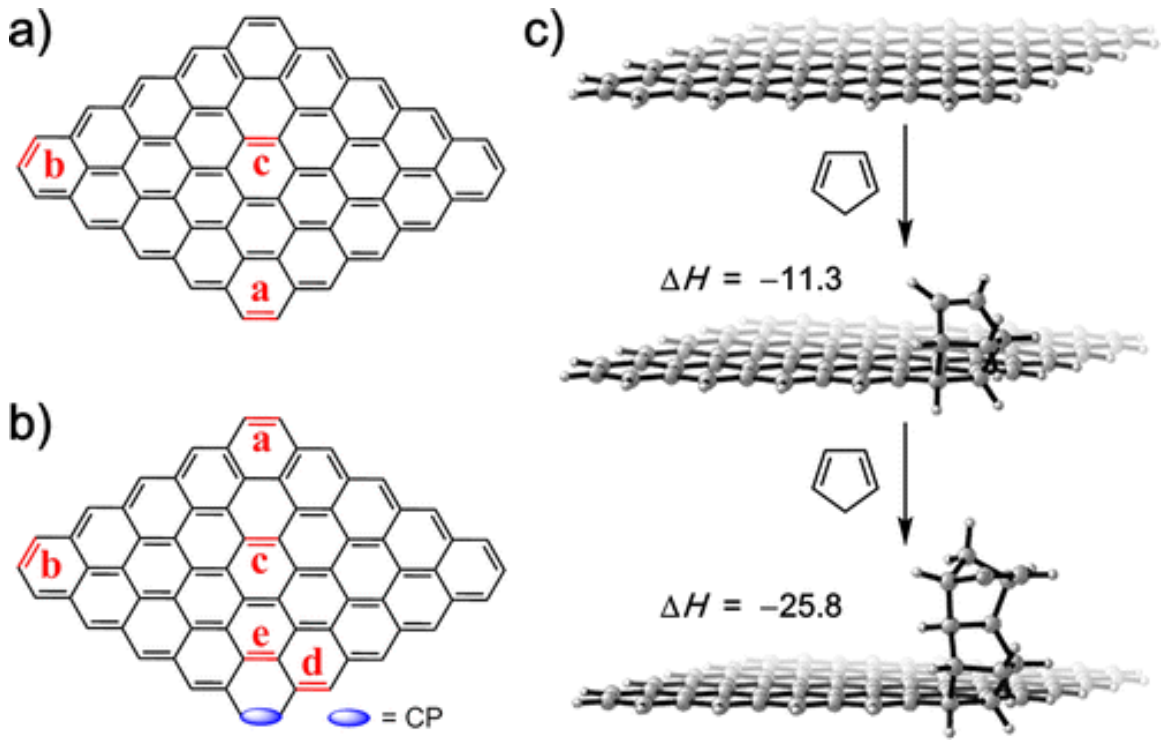

Figure 3.5 a) The 5x5 graphene model with the representative addition sites in red. b) DA reaction sites of the second CP on graphene-CP cycloadduct. c) Structures of graphene, graphene-CP cycloadduct, and the following CP dimerization product, reaction enthalpies in kcal/mol.

Computational results show that the Diels-Alder cycloadditions at bonds "a" and "b" have reaction enthalpies of –11.3 and –1.4 kcal/mol, respectively. However, bond "c" involves unfavorable, endothermic enthalpy (36.6 kcal/mol) under standard conditions. The bond "c" most resembles the interior of pristine graphene. The thermochemical calculations of single CP

on graphene demonstrate that center bonds cannot be functionalized through DA reactions with CPs, and only some special edges, comparable to defect sites, will be reactive. However, once the CP has been attached to the edge positions, it might either activate nearby bonds or itself react. The DA reaction of a second CP on the graphene-CP cycloadduct (functionalized on bond "a") was also calculated (Figure 3.5b). Five additional bonds were evaluated ("a", "b", "c", "d", and "e", Figure 3.5b). The new reaction enthalpies for the CP addition on bonds "a", "b", and "c" of the graphene-CP cycloadduct are practically unchanged. This clearly indicates that the functionalization at the edge bond "a" does not favor the subsequent CP addition on the graphene lattice. The reaction enthalpies on neighboring bonds "d" and "e" are 1.6 and 37.4 kcal/mol, respectively. Cycloaddition on bond "e" is impossible because of high endothermicity. Bond "d" can be viewed as the edge bond on a 4x4 graphene model and thus possesses a reactivity comparable to bond "a". The enthalpy of 1.6 kcal/mol on bond "d" indicates that the CP group has in fact deactivated its nearby bonds by steric hindrance.

From CV data, we determine that approximately 1 fc is present on the surface for every 5 graphene double bonds, while calculations indicate that such a high coverage is not attainable because most of the graphene double bonds are unreactive with CP. How can the differences between experiment and computation be explained? Inspired by recent report of the functionalization of graphene by polymerization,[20] we postulate that CP also oligomerizes through DA reactions. Figure 3.5c shows structures of the graphene-CP cycloadduct and its CP dimerization product. The double bond of the graphene-CP cycloadduct resembles that of norbornene. The reaction enthalpy for the cycloaddition of a second CP is –25.8 kcal/mol. This is significantly more exothermic than any of the reactions of graphene calculated above (the most reactive site on graphene model is bond "a" with ΔH of –11.3 kcal/mol). Once one CP reacts

with a reactive edge or defect on graphene, the second CP can react with the norbornene double bond. This can be repeated because CP is well known to dimerize and polymerize through DA reactions.[21] Oligomerization of CP induced by initial Diels-Alder reaction at a graphene defect is preferred over multi-site functionalization. On the basis of the CV characterization and feature height of 3.5 nm, which would correspond to a degree of CP oligomerization of 15,[18] the functionalization degree of graphene is about 1.3%. Finally, the dependence of ΔE with scan rate of the CV and the slope of 0.7 in the inset of Figure 3.4 can be attributed to hopping of electrons through the fc chains appended to the CP oligomers.

In conclusion, SLG sheets on SiO_2 substrates have been patterned covalently with oligomers of organic small molecules through a force-accelerated DA reaction induced on graphene defect and edge sites by an array of pyramidal elastomeric tips. The changes in bonding were characterized by Raman microscopy, cyclic voltammetry, and electronic structure calculations, and the results are consistent with micrometer scale features composed of covalently immobilized molecules patterned over large (cm^2) areas. Importantly, these reactions occur at ambient temperature and atmosphere, while accessing one of the most versatile reactions in organic chemistry. Future studies will extend this method to other reactions that are accelerated by force, and elucidate the role of force on reaction rate, reversibility, and regioselectivity. This method for functionalizing the basal plane of graphene, while maintaining the conductivity of the surface, could find utility in sensors, electronics, and optical devices.

3.3 Reference

(1) Novoselov, K. S.; Geim, A. K.; Morozov, S. V.; Jiang, D.; Zhang, Y.; Dubonos, S. V.; Grigorieva, I. V.; Firsov, A. A. *Science* **2004**, *306*, 666.

(2) a) Lin, Y. M.; Dimitrakopoulos, C.; Jenkins, K. A.; Farmer, D. B.; Chiu, H. Y.; Grill, A.; Avouris, P. *Science* **2010**, *327*, 662; b) Wang, Q. H.; Jin, Z.; Kim, K. K.; Hilmer, A. J.; Paulus, G. L. C.; Shih, C. J.; Ham, M. H.; Sanchez-Yamagishi, J. D.; Watanabe, K.; Taniguchi, T.; Kong, J.; Jarillo-Herrero, P.; Strano, M. S. *Nat. Chem.* **2012**, *4*, 724; c) Rodriguez-Lopez, J.; Ritzert, N. L.; Mann, J. A.; Tan, C.; Dichtel, W. R.; Abruna, H. D. *J. Am. Chem. Soc.* **2012**, *134*, 6224; d) Kim, S. N.; Kuang, Z. F.; Slocik, J. M.; Jones, S. E.; Cui, Y.; Farmer, B. L.; McAlpine, M. C.; Naik, R. R. *J. Am. Chem. Soc.* **2011**, *133*, 14480; e) Ragoussi, M. E.; Malig, J.; Katsukis, G.; Butz, B.; Spiecker, E.; de la Torre, G.; Torres, T.; Guldi, D. M. *Angew. Chem. Int. Ed.* **2012**, *51*, 6421; f) Liu, M.; Yin, X. B.; Ulin-Avila, E.; Geng, B. S.; Zentgraf, T.; Ju, L.; Wang, F.; Zhang, X. *Nature* **2011**, *474*, 64.

(3) a) Lee, B.; Chen, Y.; Duerr, F.; Mastrogiovanni, D.; Garfunkel, E.; Andrei, E. Y.; Podzorov, V. *Nano Lett.* **2010**, *10*, 2427; b) Zhou, X.; He, S.; Brown, K. A.; Mendez-Arroyo, J.; Boey, F.; Mirkin, C. A. *Nano Lett.* **2013**, *13*, 1616.

(4) Steenackers, M.; Gigler, A. M.; Zhang, N.; Deubel, F.; Seifert, M.; Hess, L. H.; Lim, C. H. Y. X.; Loh, K. P.; Garrido, J. A.; Jordan, R.; Stutzmann, M.; Sharp, I. D. *J. Am. Chem. Soc.* **2011**, *133*, 10490.

(5) Liu, H. T.; Ryu, S. M.; Chen, Z. Y.; Steigerwald, M. L.; Nuckolls, C.; Brus, L. E. *J. Am. Chem. Soc.* **2009**, *131*, 17099.

(6) Quintana, M.; Spyrou, K.; Grzelczak, M.; Browne, W. R.; Rudolf, P.; Prato, M. *ACS Nano* **2010**, *4*, 3527.

(7) a) Bekyarova, E.; Itkis, M. E.; Ramesh, P.; Berger, C.; Sprinkle, M.; de Heer, W. A.; Haddon, R. C. *J. Am. Chem. Soc.* **2009**, *131*, 1336; b) Georgakilas, V.; Bourlinos, A. B.; Zboril, R.; Steriotis, T. A.; Dallas, P.; Stubos, A. K.; Trapalis, C. *Chem. Commun.* **2010**, *46*, 1766; c)

Lomeda, J. R.; Doyle, C. D.; Kosynkin, D. V.; Hwang, W. F.; Tour, J. M. *J. Am. Chem. Soc.* **2008**, *130*, 16201; d) Hossain, M. Z.; Walsh, M. A.; Hersam, M. C. *J. Am. Chem. Soc.* **2010**, *132*, 15399.

(8) a) Sarkar, S.; Bekyarova, E.; Niyogi, S.; Haddon, R. C. *J. Am. Chem. Soc.* **2011**, *133*, 3324; b) Sarkar, S.; Bekyarova, E.; Haddon, R. C. *Acc. Chem. Res.* **2012**, *45*, 673.

(9) a) van Eldik, R.; Asano, T.; le Noble, W. J. *Chem. Rev.* **1989**, *89*, 549; b) Kuster, C. J. T.; Scheeren, H. W. In *High Pressure Chemistry*; van Eldik, R., Klaerner, F.-G., Eds.; Wiley-VCH: Weinheim, 2007; pp284-304.

(10) a) Rozkiewicz, D. I.; Janczewski, D.; Verboom, W.; Ravoo, B. J.; Reinhoudt, D. N. *Angew. Chem. Int. Ed.* **2006**, *45*, 5292; b) Mehlich, J.; Ravoo, B. J. *Org. Biomol. Chem.* **2011**, *9*, 4108.

(11) Huo, F.; Zheng, Z.; Zheng, G.; Giam, L. R.; Zhang, H.; Mirkin, C. A. *Science* **2008**, *321*, 1658.

(12) Bian, S.; He, J.; Schesing, K. B.; Braunschweig, A. B. *Small* **2012**, *8*, 2000.

(13) Bian, S. D.; Schesing, K. B.; Braunschweig, A. B. *Chem. Commun.* **2012**, *48*, 4995.

(14) Liao, X.; Braunschweig, A. B.; Zheng, Z. J.; Mirkin, C. A. *Small* **2010**, *6*, 1082.

(15) Yousaf, M. N.; Mrksich, M. *J. Am. Chem. Soc.* **1999**, *121*, 4286.

(16) Cancado, L. G.; Jorio, A.; Ferreira, E. H. M.; Stavale, F.; Achete, C. A.; Capaz, R. B.; Moutinho, M. V. O.; Lombardo, A.; Kulmala, T. S.; Ferrari, A. C. *Nano Lett.* **2011**, *11*, 3190.

(17) Bard, A. J.; Faulkner, L. R. *Electrochemical methods: fundamentals and applications*, 2nd ed.; Wiley: New York, 2001.

(18) See Supporting Information for details.

(19) Chidsey, C. E. D.; Bertozzi, C. R.; Putvinski, T. M.; Mujsce, A. M. *J. Am. Chem. Soc.* **1990**, *112*, 4301.

(20) Ma, X.; Li, F.; Wang, Y.; Hu, A. *Chem. Asian J.* **2012**, *7*, 2547.

(21) Alder, K.; Stein, G. *Justus Liebigs Ann. Chem.* **1933**, *504*, 216.

Chapter 4 Why Bistetracenes Are Much Less Reactive than Pentacenes in Diels-Alder Reactions with Fullerenes

4.1 Abstract

The Diels-Alder (DA) reactions of pentacene (PT), 6,13-bis(2-trimethylsilylethynyl)pentacene (TMS-PT), bistetracene (BT), and 8,17-bis(2-trimethylsilylethynyl)bistetracene (TMS-BT) with the [6,6] double bond of [60]fullerene have been investigated by density functional theory (DFT) calculations. Reaction barriers and free energies have been obtained to assess the effects of frameworks and substituent groups on the Diels-Alder reactivity and product stability. Calculations indicate that TMS-BT is about 5 orders of magnitude less reactive than TMS-PT in the reactions with [60]fullerene. This accounts for the observed much higher stability of TIPS-BT than TIPS-PT when mixed with PCBM. Surprisingly, calculations predict that the bulky silylethynyl substituents of TMS-PT and TMS-BT have only a small influence on reaction barriers. However, the silylethynyl substituents significantly destabilize the corresponding products due to steric repulsions in the adducts. This is confirmed by experimental results here. Architectures of the polycyclic aromatic hydrocarbons (PAHs) play a crucial role in determining both the Diels-Alder barrier and the adduct stability. The reactivities of different sites in various PAHs are related to the loss of aromaticity, which can be predicted using the simple Hückel molecular orbital localization energy calculations.

4.2 Introduction

Polycyclic aromatic hydrocarbons (PAHs) composed of linearly fused benzene rings have been widely explored as organic semiconductor materials for their unique electronic properties.[1] Pentacene (PT) is among the most well-studied molecules and has emerged as a promising donor

material for organic photovoltaic (OPV) devices due to its significantly large exciton diffusion length[2] and high hole mobility.[3] PT is also studied as the model system for calculating exciton dissociation and charge-recombination processes.[4] More recently, the quantum efficiency of pentacene/fullerene based OPVs was significantly improved by singlet exciton fission effect.[5] Despite great progress, there is a fundamental problem regarding the chemical stability of pentacene systems that requires further investigation. Pentacene is unstable in air or visible light, suffering from oxidation and rapid conversion to transannular peroxides.[6] It has extremely poor solubility in organic solvents,[7] which makes it impossible for large-area, solution-based applications. Pentacene has been found to be highly reactive as a diene in Diels-Alder (DA) reactions with [60]fullerene. Miller and co-workers reported that the DA reaction of fullerene with pentacene in solution yields the C_{2v} symmetric monoadduct across the central 6,13-carbons of pentacene.[8] They also found that when the reactive 6,13-positions on pentacene are substituted, C_{60} reacts with pentacene at 5,14- and 7,12-positions to generate bis- and mono-fullerene adducts.[9] One example is 6,13-bis(2-trimethylsilylethynyl)pentacene (TMS-PT, Figure 4.1).[9b] The reaction of TMS-PT with excess fullerene in CS_2 leads to monoadduct across 5,14-carbons after 24 hours. Bisfullerene-pentacene adducts also form after longer reaction times (2-3 days). In fact, the DA reactions between pentacene and its derivatives with fullerene are so efficient that they have been applied as methods to synthesize functional fullerene materials.[9c,d]

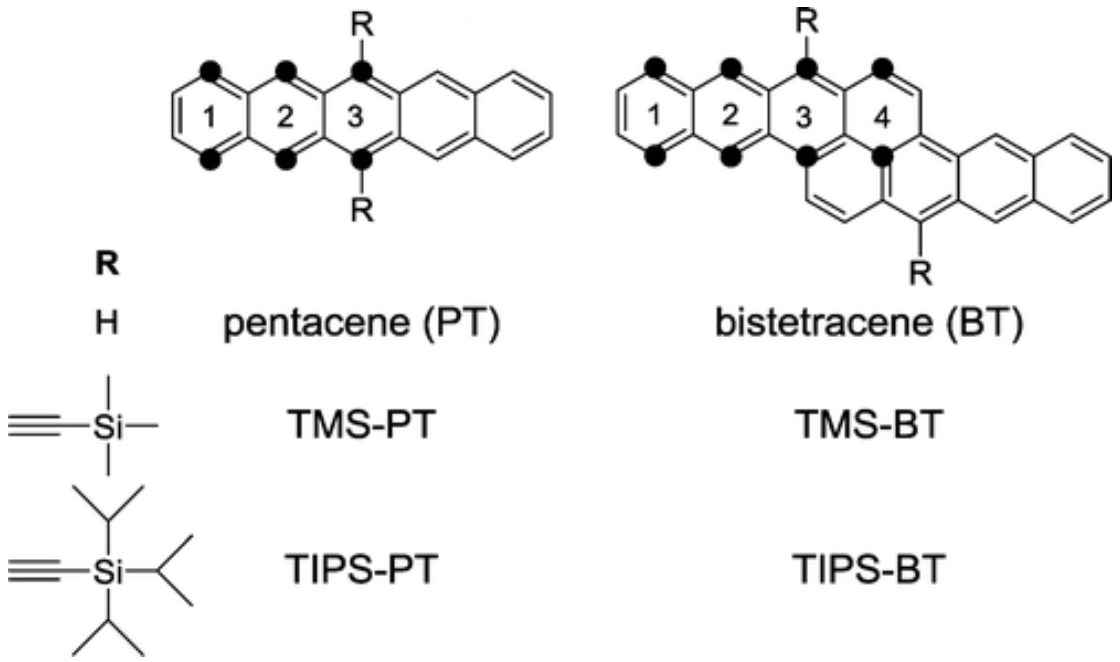

Figure 4.1 Structures of pentacene, bistetracene, and their derivatives with their reaction sites as dienes in DA reactions.

In the search for alternative air stable, solution processable, highly crystalline organic materials for electronic device applications, substituent groups such as silylethynyl, aryl, and alkyl groups have been introduced on pentacene backbones.[1,10] In general, the substituted pentacenes are more stable and more soluble than the parent compound, but many have the disadvantages of minimal π-stacking and poorer device performance.[11] Other polycyclic aromatic hydrocarbons have been designed to achieve desirable electronic properties and chemical stability.[12] Recently, the Briseno group synthesized and characterized bistetracene (BT) and its derivative, triisopropylsilylethynyl-substituted bistetracene (TIPS-BT, Figure 4.1).[13] TIPS-BT is reported to have a half-life of four days under UV/vis irradiation in chloroform, which is about 200 times longer than the half-life of pentacene. Further investigation showed that the

bistetracene derivative has promising properties, such as small band-gap and high carrier mobilities up to 6 $cm^2/(V \cdot s)$.[13]

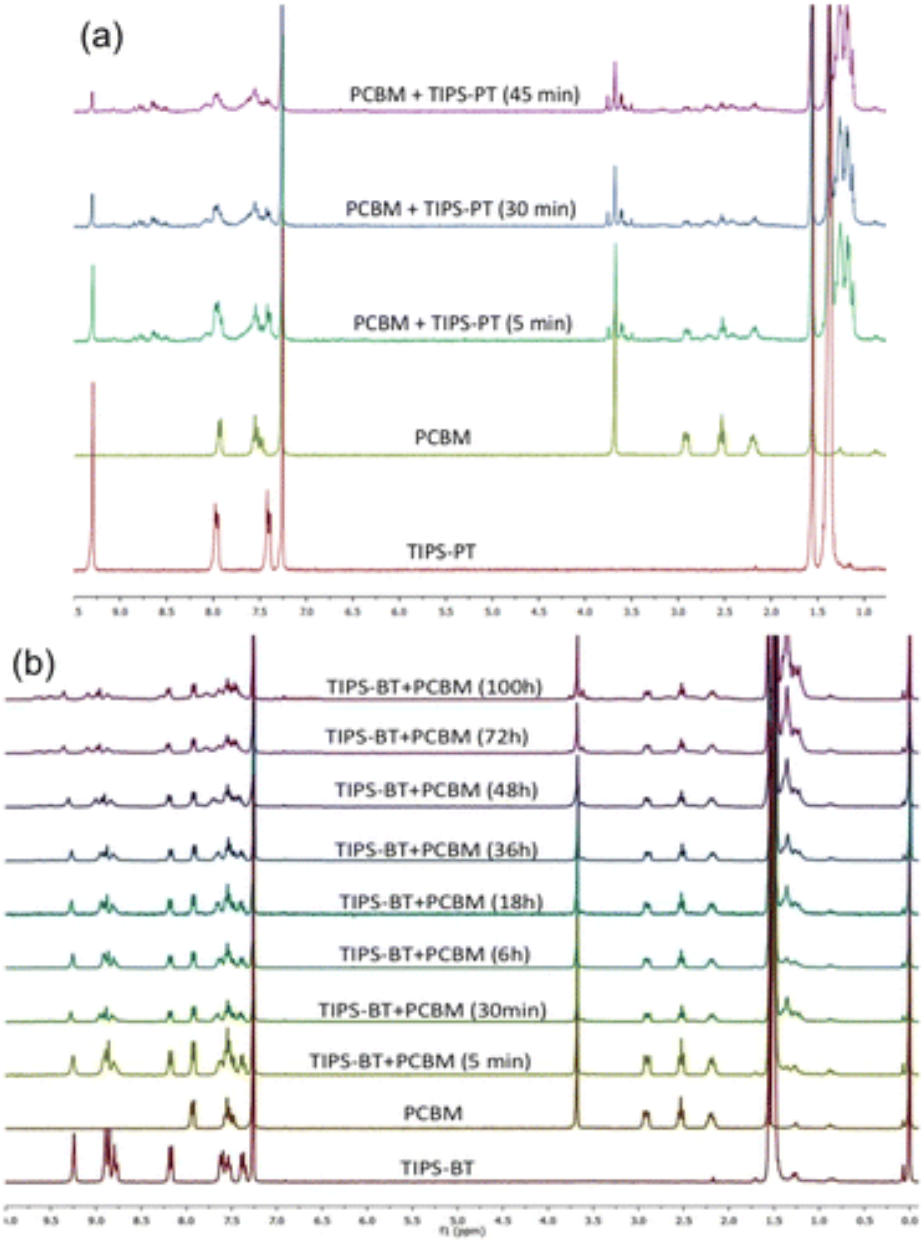

Figure 4.2 ^{1}H-NMR spectra at various time intervals of TIPS-PT (a) and TIPS-BT (b) mixed with PCBM in $CDCl_3$ at room temperature.

To compare the stability between TIPS-PT and TIPS-BT (Figure 4.1) in the fullerene system, the reactions of these compounds with [6,6]-phenyl-C_{61}-butyric acid methyl ester (PCBM) were carried out in $CDCl_3$ under ambient conditions and monitored by ^{1}H-NMR (for details, see the Supporting Information). As shown in Figure 4.2a, the DA reaction between TIPS-PT and PCBM is very fast, and several new signals can be observed within a few minutes. This is consistent with previous reports regarding the propensity of pentacene derivatives to undergo DA reactions with fullerene derivatives.[8,9] By contrast, the NMR spectra of mixed TIPS-BT and PCBM show almost no observable change in the first 36 hours (Figure 4.2b). There are a few signal changes after longer reaction time (>48 hours). This indicates that the DA reaction of TIPS-BT with PCBM is much slower than that of TIPS-PT.

These promising results stimulated the Briseno group to investigate other conjugated polycyclic aromatic hydrocarbon derivatives that have appropriate properties with sufficient chemical inertness to be used in organic photovoltaic devices.[12] To enable rational design of new molecules, there is the need to improve the understanding of the influence of both substituent groups and frameworks on stabilities of potential organic electronic materials.

These factors have been analyzed here by density functional theory (DFT) and Hückel molecular orbital (HMO) calculations. We show here that the bistetracene system is significantly less reactive than pentacene, since it is more difficult to interrupt the aromatic conjugation of the more highly condensed benzene rings of BT. The rate of the Diels-Alder reaction between the fullerene and TMS-BT is predicted to be 70,000 times slower than that of TMS-PT molecule at 25 ºC. The introduction of bulky silylethynyl groups on site 3 (Figure 1) in PT and BT molecules is surprisingly found to only slightly influence the DA barriers on site 3, but to destabilize the corresponding products substantially. The localization energies obtained from HMO methods are

found to correlate with the activation free energies and reaction free energies from DFT calculations on the DA reactions of fullerene with PT and BT. As has been described for other DA reactions of polyacenes,[14] the HMO localization energies of different sites in various PAHs can be used to estimate the reactivities of PAHs.

4.3 Computational methods

The DFT calculations were all performed with the Gaussian 09 programs.[15] Recently, DFT calculations of cycloaddition reactions on carbon nanotubes were reported,[16] where optimizations were performed at the B3LYP/3-21G* level.[17,18] We started our geometry optimizations with the same method and basis set, followed by single point calculations at the B3LYP/6-31G(d) level. However, the B3LYP results significantly underestimate observed reactivities. For pentacene, the DA reaction between site 3 (Figure 1) and the [6,6] bond of [60]fullerene was reported to rapidly occur.[8] However, the B3LYP calculations gave an activation free energy of over 32 kcal/mol and an endergonic product with a reaction energy of 5.8 kcal/mol. This experimental and theoretical difference is consistent with previous discoveries that B3LYP failed to give reliable energetics for medium- to long-range electron correlations and dispersion effects.[19,20] The M06-2X method[21] was demonstrated to yield more accurate energetics for such systems and cycloaddition reactions.[22] The performance of M06-2X has been verified on graphene chemistry.[23] Consequently, we have performed optimizations at the M06-2X/3-21G* level. The vibrational frequencies were computed at the same level to ensure each optimized structure is an energy minimum or a transition state and to evaluate zero-point vibrational energies (ZPVE) and thermal corrections at 298 K. Single point energy calculations in $CHCl_3$ using the CPCM model[24] were carried out subsequently on the optimized structures at the M06-2X with a larger basis set 6-31G(d). We tested optimizations at the M06-2X/6-31G(d) level for

the [60]fullerene-pentacene system. The differences in both activation free energies and reaction free energies are less than 1.0 kcal/mol. In addition, we tested single point energy calculations at the B3LYP-D3/6-31G(d) or BP86-D3/6-31G(d) level for all the investigated system. Their results are shown in Table 4.1. As shown in Table 4.1, B3LYP-D3 and BP86-D3 show the same trends in both activation free energies and reaction free energies as M06-2X. However, B3LYP-D3 shows a systematic increase in reaction energies by about 8 kcal/mol as compared to M06-2X. For example, B3LYP-D3 predicts that the formation of the adduct on TMS-PT site 3 is endergonic by 1.1 kcal/mol. This is inconsistent with the experimental result, which will be discussed later. BP86-D3 significantly underestimates the activation barriers, inconsistent with experiments as well. Therefore, the following discussions only based on M06-2X results.

Table 4.1 M06-2X, B3LYP-D3, and BP86-D3-Computed Activation and Reaction Free Energies for All the Investigated Systems

ΔG (kcal/mol)	M06-2X/6-31G(d)//M06-2X/3-21G*	B3LYP-D3/6-31G(d) //M06-2X/3-21G*	BP86-D3/6-31G(d) //M06-2X/3-21G*
PT_TS1	29.9	29.2	19.9
PT_TS2	19.1	16.5	8.0
PT_TS3	17.6	14.2	6.1
PT_P1	4.3	12.8	7.8
PT_P2	-14.3	-5.7	-9.7
PT_P3	-18.6	-9.7	-13.2
TMS-PT_TS1	29.6	27.6	18.3
TMS-PT_TS2	19.8	13.0	2.6
TMS-PT_TS3	16.8	13.1	2.1
TMS-PT_P1	4.8	12.7	7.7
TMS-PT_P2	-13.0	-8.6	-13.6
TMS-PT_P3	-8.7	1.1	-3.4
BT_TS1	31.4	30.7	21.3
BT_TS2	22.1	19.2	10.1

BT_TS3	23.1	20.6	10.7
BT_TS4	37.1	36.3	24.2
BT_P1	7.0	15.1	9.7
BT_P2	-8.3	-1.2	-5.9
BT_P3	2.2	10.6	5.6
BT_P4	27.4	34.3	26.2
TMS-BT_TS1	33.6	30.2	20.3
TMS-BT_TS2	23.4	19.1	8.7
TMS-BT_TS3	25.9	23.8	12.6
TMS-BT_TS4	39.8	35.9	21.9
TMS-BT_P1	7.9	15.5	10.3
TMS-BT_P2	-7.3	-2.7	-8.0
TMS-BT_P3	8.4	17.2	11.7
TMS-BT_P4	29.5	33.2	24.0

We calculated the DA reactions of [60]fullerene with polycyclic aromatics, PT, TMS-PT, BT, and TMS-BT. Their structures and DA reaction sites are shown in Figure 4.1, and the structures of transition states and products are given in Figures 4.4-4.5 and 4.7-4.8. Substituent effects were assessed by comparing PT/BT and TMS-PT/TMS-BT systems. The effects of additional fused aromatic rings were evaluated through the comparison of PT and BT systems.

Solà and co-workers reported the enthalpies of DA reactions involving C_{60}.[19a] The optimized reactant complexes were local minima and were stabilized by 4-12 kcal/mol in enthalpy with respect to separated reactants. We also considered the complexes between C_{60} and four PAHs and observed the same stabilization effect of 8-12 kcal/mol in enthalpy, due primarily to dispersion interactions.[25] Here we report energy profiles in terms of Gibbs free energy. In the free energy ($\Delta G = \Delta H - T\Delta S$), the entropy term ($-T\Delta S$ is positive), causes the free energies of these four complexes to actually be higher than those of separated reactants. As a result, the energies discussed in the text are all given relative to separated fullerene and PAHs.

We also analyzed the activation barriers using the distortion/interaction model.[26,27] This model relates the activation energy (E_{act}) to the distortion energy (E_{dist}) required for the geometrical deformation of the reactants to achieve their transition-state conformations and the interaction energy (E_{int}) arising from the interactions between two distorted reactants in the transition state.[28] Fragment distortion and interaction energies were computed at the M06-2X/6-31G(d) level in the gas phase. In all cases, the distortion energies of PAHs are predominant, around 75% of the total distortion energies.

4.4 Results and Discussion

There are two types of C=C bonds in [60]fullerene. The [5,6] bond is located between the fused 5- and 6-membered rings, and the [6,6] bond is located between two fused 6-membered rings. It is well established both experimentally and computationally that the DA reaction of fullerene occurs on a [6,6] double bond.[28g,29] For the Diels-Alder reactions of C_{60} and pentacene, our calculations indicate that the reaction barriers on the [5,6] bond are about 14 kcal/mol higher than those on the [6,6] bond, and that the adducts on the [5,6] bond are less stable by about 21 kcal/mol (Figure 4.3). Therefore, we only discuss the DA reactions on a [6,6] bond of fullerene here.

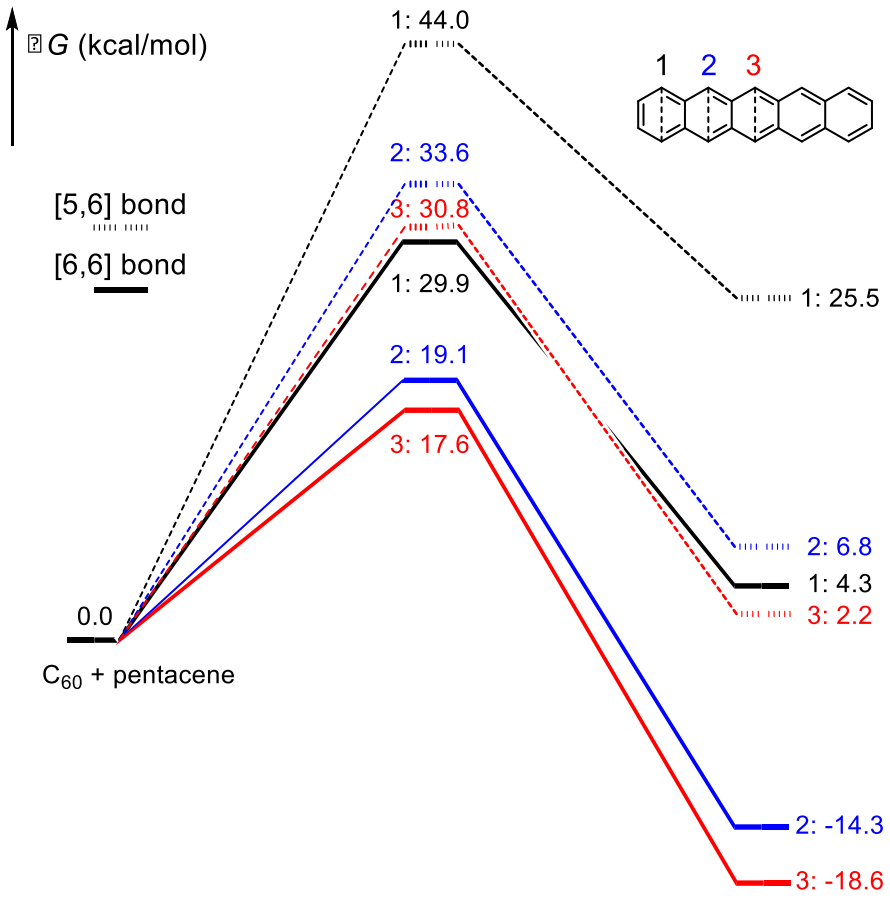

Figure 4.3 DFT-computed activation and reaction free energies for the Diels-Alder reactions involving the [5,6] and [6,6] bonds of C_{60} and the diene sites 1-3 of pentacene.

Figure 4.4 shows the DA transition states and products involving pentacene (PT) and the [6,6] bond of fullerene. Site 3 is the most reactive site of PT as the diene, where the DA barrier is only 17.6 kcal/mol. The free energy barrier on site 2 is slightly higher (19.1 kcal/mol). Site 1 has the highest reaction barrier of 29.9 kcal/mol. According to the distortion/interaction analysis, the interaction energies (E_{int}) for three transition states are very close, between -5.0 and -5.9 kcal/mol. The distortion energies (E_{dist}), are related to the position of transition states, measured as the partially formed C-C bond length. The distortion energies control activation barriers.

Smaller distortion energies lead to lower activation energies. It is easiest to interrupt the aromatic system of pentacene on site 3. This corresponds to the earliest transition state (**PT_TS3**) with longest forming C-C bonds (2.39 Å) and thus the smallest transition state distortion energy (E_{dist}) of 9.0 kcal/mol. Site 1 has the highest reaction barrier, and formation of the DA adduct is endergonic. Its transition state has the shortest forming C-C bonds (2.22 Å) and the largest distortion energy (20.4 kcal/mol). The C-C bond lengths on site 2 are intermediate, with a distortion energy of 10.6 kcal/mol. The adduct on site 3 (**PT_P3**) is the most stable one with a reaction free energy of -18.6 kcal/mol. The adduct on site 2 (**PT_P2**) is less exergonic, with a free energy of -14.3 kcal/mol. The DA reaction on site 1 is endergonic by 4.3 kcal/mol. Therefore, the DA reaction on site 3 is preferred kinetically, with the earliest transition state, and thermodynamically, with the most exergonic product.[30] This result is in agreement with the experiment that pentacene reacts rapidly with C_{60} through the DA reaction across the central 6,13-carbons.[8]

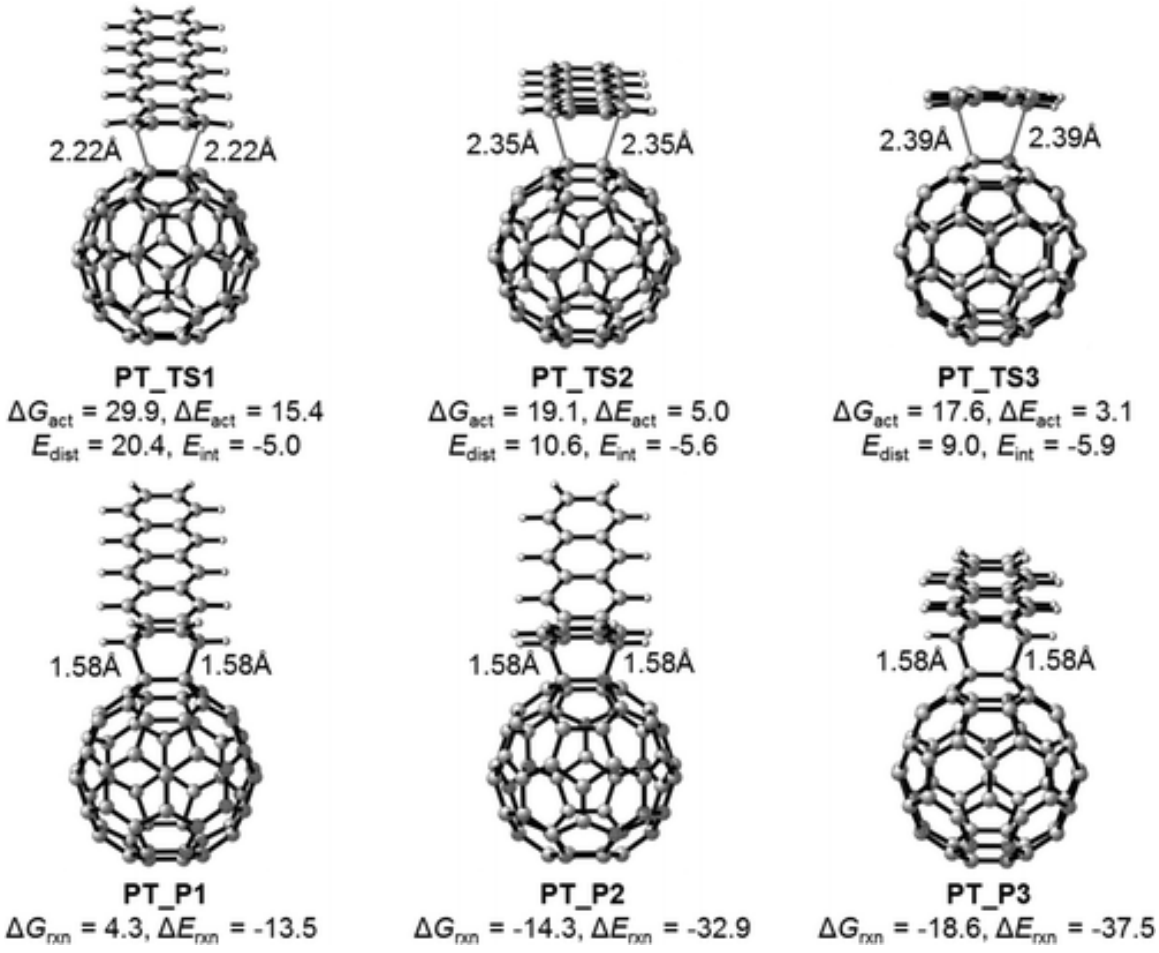

Figure 4.4 Free energy diagram and distortion/interaction analysis for the C_{60}-PT system (energies in kcal/mol).

Figure 4.5 shows the DA transition states and products from reactions of TMS-PT and [60]fullerene. The introduction of the trimethylsilylethynyl substituent groups does not have a significant effect on the DA reactivity. The barriers for reactions on sites 1-3 of TMS-PT are very close to those of PT. Site 3 in TMS-PT is the most reactive one among the three sites with an activation free energy of 16.8 kcal/mol. This barrier is even slightly lower than that for pentacene via transition state **PT_TS3** (17.6 kcal/mol, Figure 3). This indicates that the reaction

of TMS-PT with C_{60} will be quite fast at room temperature. The reaction on site 2 via **TMS-PT_TS2** requires an activation free energy of 19.8 kcal/mol, which is 3.0 kcal/mol higher than that on site 3 via **TMS-PT_TS3**. The reaction on site 1 has the highest barrier of 29.6 kcal/mol. The distortion/interaction analysis shows that both interaction energies (E_{int}) and distortion energies (E_{dist}) vary with the length of the forming C-C bonds. The longer the C-C bonds, the lower the distortion energies. Similar to pentacene, site 3 has the earliest transition state with the longest C-C bonds (2.35 Å). The distortion energy of transition state **TMS-PT_TS3** is 12.1 kcal/mol. The transition state on site 2 is intermediate with slightly shorter C-C bonds of 2.34 Å. Site 1 has the latest transition state with the shortest C-C bonds (2.22 Å), which leads to more severe distortion energy of 20.7 kcal/mol. The interaction energies become more favorable as bond length elongates. It ranges from -5.1 kcal/mol on site 1 to -10.7 kcal/mol on site 2 to -14.1 kcal/mol on site 3. The stabilizing dispersion interactions between TMS-PT and fullerene mainly contribute to the interaction energies. There is a better alignment in **TMS-PT_TS3**, and thus it has an enhanced stabilizing dispersion between TMS-PT and fullerene.

Similar to PT, the DA reaction of TMS-PT on site 1 is endergonic by 4.8 kcal/mol. However, the stability of the products on sites 2 and 3 is reversed by the bulky side groups (Figures 4.4 and 4.5). The reaction free energy of adduct **TMS-PT_P2** is -13.0 kcal/mol, 4.3 kcal/mol more favorable than that of adduct **TMS-PT_P3** on site 3 (-8.7 kcal/mol, Figure 4.5). As shown in Figures 4.4 and 4.5, five out of six DA adducts have formed C-C bonds of 1.58 Å. To avoid the large steric repulsions between the bulky silylethynyl groups of TMS-PT and fullerene, the adduct on site 3 has to stretch the formed C-C bonds to 1.60 Å. This significantly destabilizes the product **TMS-PT_P3**.

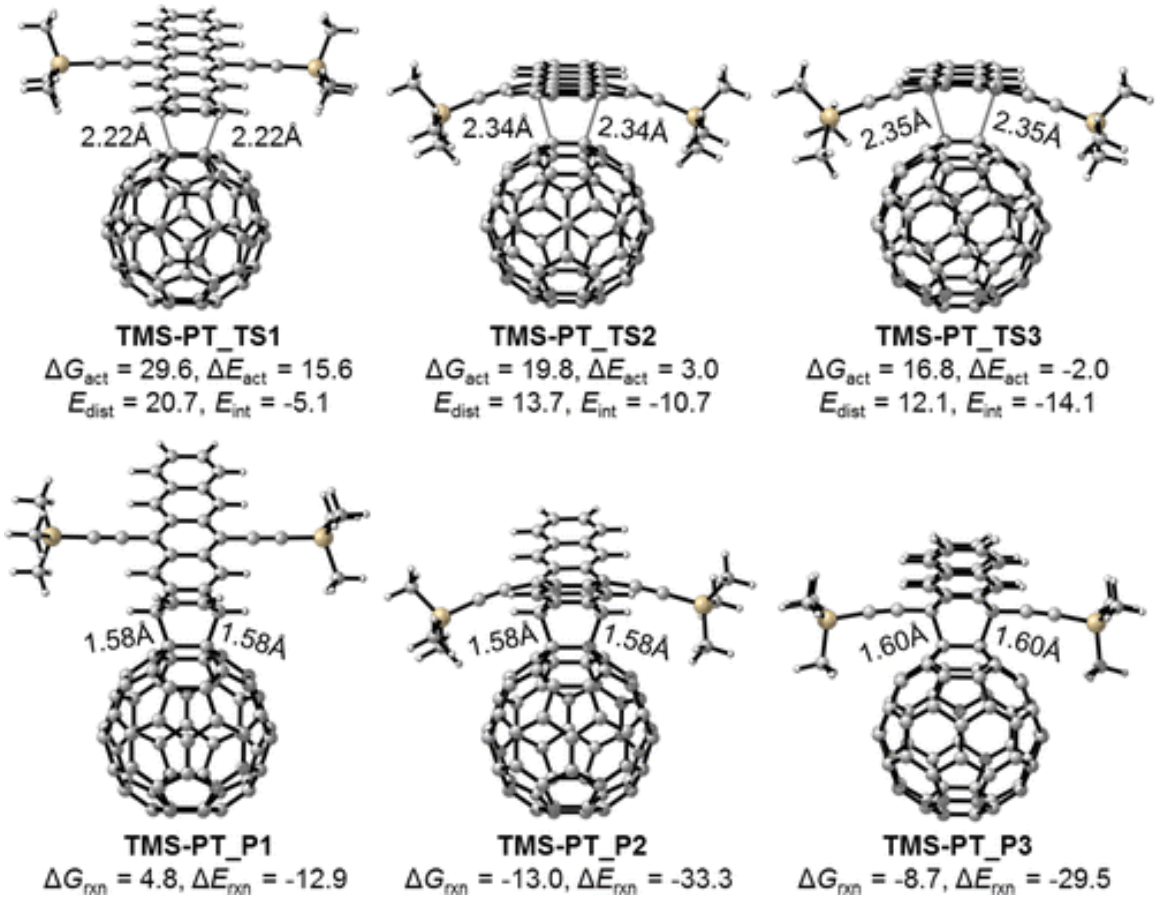

Figure 4.5 Free energy diagram and distortion/interaction analysis for the C60-TMS-PT system (energies in kcal/mol).

The DA reaction between TMS-PT and C_{60} was reported by Miller's group.[9b] The monoadduct across the site 2 (TMS-PT_P2) was obtained in a yield of 75% after refluxing in CS_2 for 24 hours, while the adduct across the site 3 (**TMS-PT_P3**) was not isolated. This is consistent with the computational result that the DA reaction on site 2 is thermodynamically much more favorable. However, calculations indicate that the formation of adduct on site 3 is preferred kinetically. To test this prediction, we conducted the reaction of TIPS-PT with C_{60} in a $CDCl_3/CS_2$ mixed solution at room temperature and monitored it by ^{1}H-NMR (Figure 4.6). As

expected, it was found that about half of TIPS-PT was converted into the fullerene monoadduct on site 3 (**TIPS-PT_P3**) in 5 minutes with almost no signals of the adduct on site 2 (**TIPS-PT_P2**, Figure 4.6). This shows that the DA reaction of fullerene on site 3 of silylethynyl substituted pentacene is still much faster than that on site 2, although the adduct on site 3 is less stable.

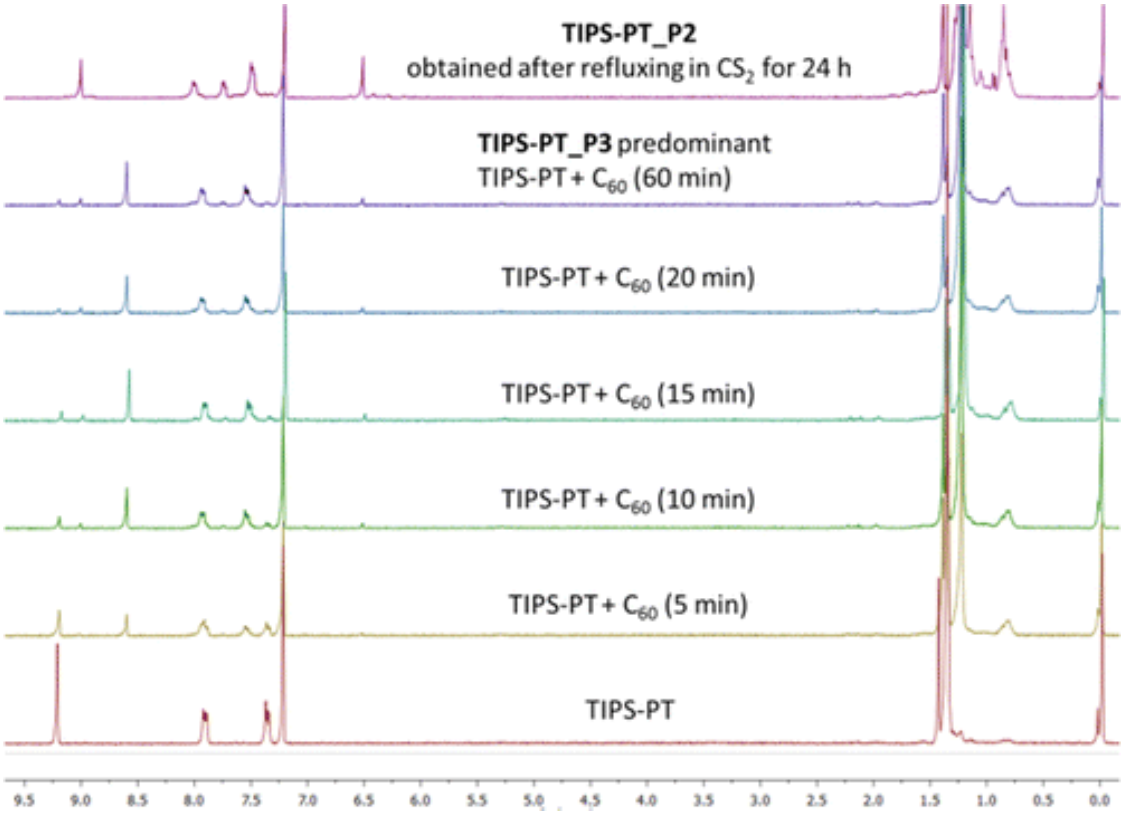

Figure 4.6 ^{1}H-NMR spectra at various time intervals of TIPS-PT mixed with C_{60} in $CDCl_3/CS_2$ at room temperature.

As shown in Figure 4.7, for BT molecule, the DA barriers are substantially higher than those with PT molecule. The two-row fused aromatic ring framework deactivates the whole system. Site 2 is the most reactive one among four possible reaction sites (Figure 4.1), requiring

an activation free energy of 22.1 kcal/mol. The reaction on site 3 has a similar barrier of 23.1 kcal/mol. The reaction barriers on sites 1 and 4 are much higher, 31.4 and 37.1 kcal/mol, respectively. Site 2 has the earliest transition state with lowest distortion energy of 13.4 kcal/mol. For products, only the adduct on site 2 is formed exergonically, with a free energy of -8.3 kcal/mol. The formation of the product on site 3 is endergonic by 2.2 kcal/mol. This implies that retro-DA reaction on site 3 is faster than the forward DA reaction. Even with a surmountable transition barrier, **BT_P3** is highly unstable and easily decomposes. The reaction free energies on sites 1 and 4 are even more endergonic.

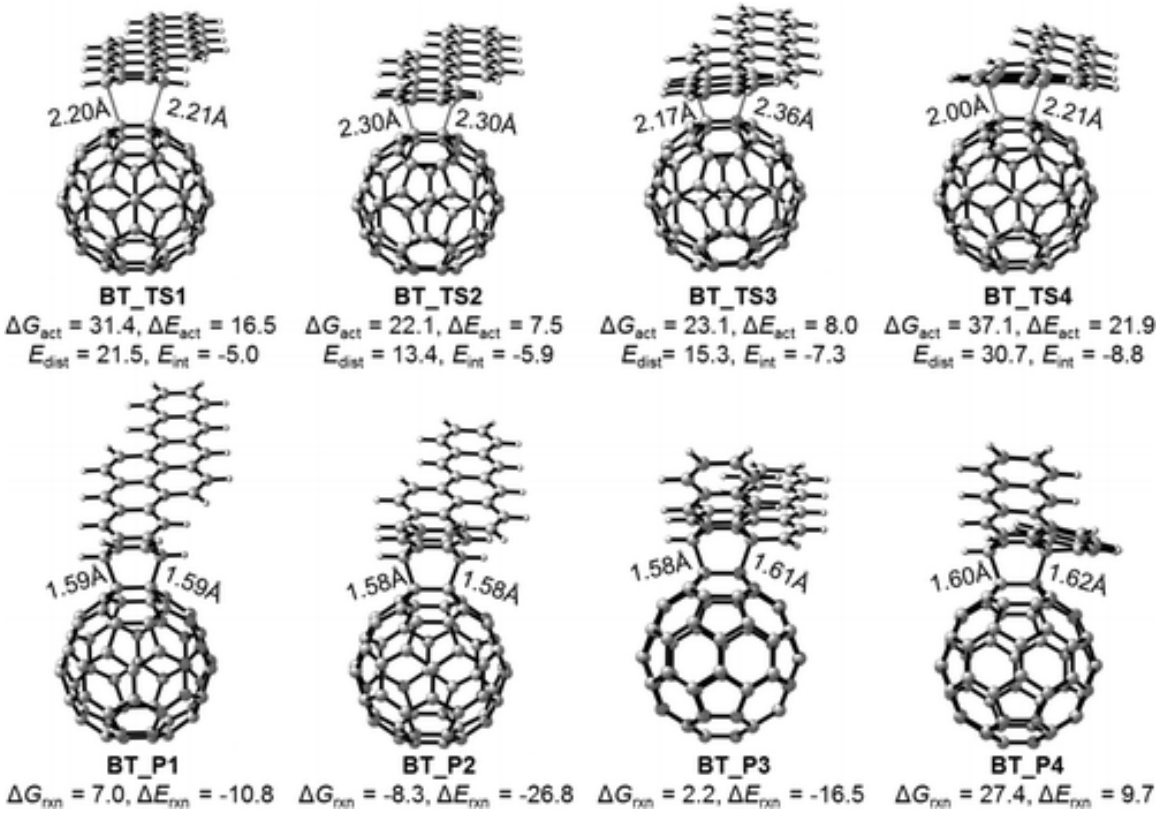

Figure 4.7 Free energy diagram and distortion/interaction analysis for the C_{60}-BT system (energies in kcal/mol).

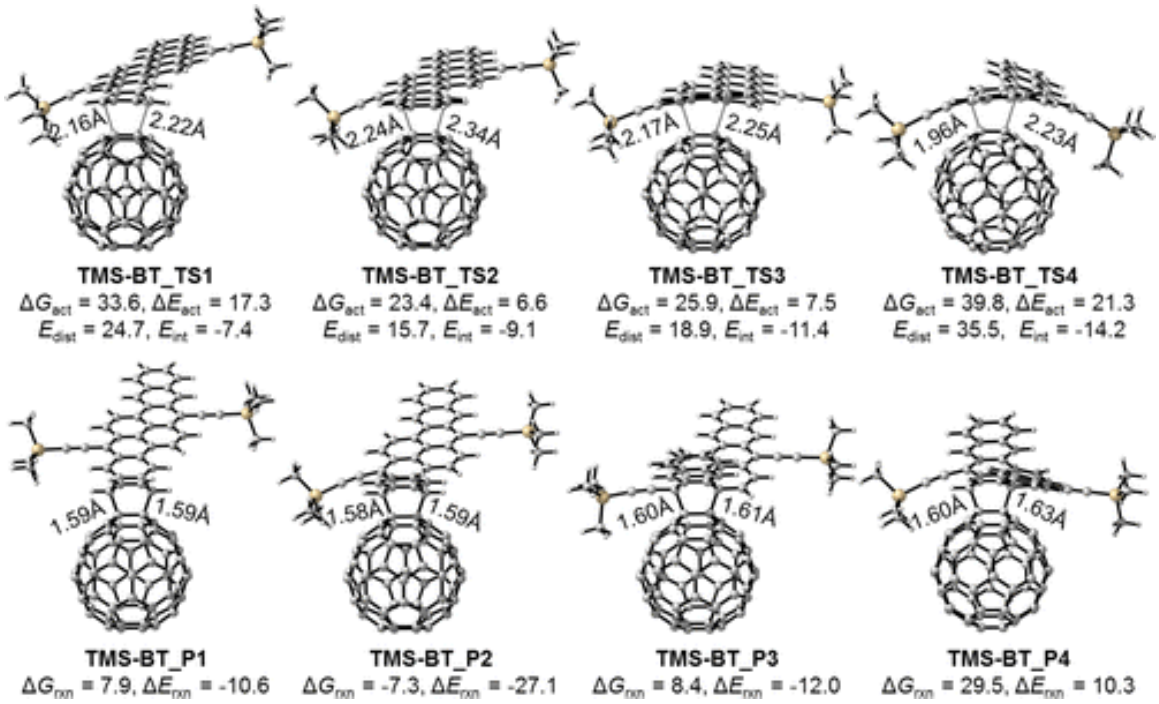

Figure 4.8 Free energy diagram and distortion/interaction analysis for the C_{60}-TMS-BT system (energies in kcal/mol).

Figure 4.8 shows the DA transition states and adducts involving four reaction sites of TMS-BT and fullerene. Very similar to the BT molecule, the reaction on site 2 has the lowest free energy barrier of 23.4 kcal/mol. The final adduct can only be formed on site 2 with a reaction free energy of -7.3 kcal/mol. The trimethylsilylethynyl groups make the DA adduct on site 3 (**TMS-BT_P3)** much more unfavorable with a free energy of 8.4 kcal/mol above reactants. Comparing the free energy of **TMS-BT_P3** and **BT_P3**, an additional side group destabilizes the product by 6.2 kcal/mol (8.4 versus 2.2 kcal/mol, Figures 4.8 and 4.7). Therefore, the DA reaction on site 2 of TMS-BT is preferred both kinetically and thermodynamically.

In summary, for pentacene, the reaction across central 6,13-carbons is preferred both kinetically and thermodynamically. Adding bulky substituent groups on these two carbons does

little to the transition state energy but decreases the product stability by about 10 kcal/mol. This is confirmed by experimental results here (Figure 4.6). Similarly, for bistetracene, one side group on site 3 reduces the stability of the corresponding product by about 6 kcal/mol. Therefore, the introduction of each bulky group decreases the stability of adduct on the substituted carbon site by approximately 5 kcal/mol. The lowest DA transition states for TMS-PT and TMS-BT molecules are **TMS-PT_TS3** (Figure 4.5) and **TMS-BT_TS2** (Figure 4.8), requiring activation free energies of 16.8 and 23.4 kcal/mol, respectively. On the basis of the free energy difference of 6.6 kcal/mol, we predict that TMS-BT is 70,000 times less reactive than TMS-PT in reactions with fullerene. This accounts for the experimental results shown in Figure 4.2: the mixed TIPS-BT and PCBM shows almost no signal change until about 2 days, while the reaction between TIPS-PT and PCBM readily occurs within a few minutes.

The concept of localization energy was developed by Wheland[31] and Brown[32] in 1940s. By definition, the localization energy (E_L) is the energy difference between the initial π system (E) and that remaining (Er) after removal of one or more p orbital and electron from the π system: $E_L = E\text{r} - E$. The localization energies were found to correlate with the reactivities in some types of aromatic substitution reactions[32] and Diels-Alder reactions.[14,33] For different reaction sites in one molecule, the larger E_L is, the more stable the site is and the more difficult the cycloaddition reaction is. The most reactive position has the smallest localization energy. The properties and stabilities of large polycyclic aromatic hydrocarbons (PAHs) depend upon the number and the spatial arrangement of benzene rings in their conjugated systems, which are usually, associated with their resonance energies. Developed in 1930s, the Hückel molecular orbital (HMO) theory can be applied to calculations of the energies of π electrons in such planar

conjugated systems. Schleyer *et al*. have also explored the relationship between other aromaticity indices and the reactivities of polyacenes in Diels-Alder reactions.[34]

We recently applied HMO calculations on graphene models and found that the HMO localization energies could predict the reactivities of different graphene sites.[23b] The HMO energies were calculated using the online Hückel program SHMO developed by Arvi Rauk.[35] In the HMO theory, the energy of π electrons is expressed in terms of α and β: $E = n\alpha + \lambda\beta$, where α is the Coulomb integral and β is the resonance integral. Here the localization energies on seven reaction sites within PT and BT molecules (Figure 4.1) were calculated by HMO theory. Because all seven sites have the same loss in α term, the α term is neglected. The computed localization energies (in units of –β) for PT, BT, and other PAHs are summarized in Figure 4.9.

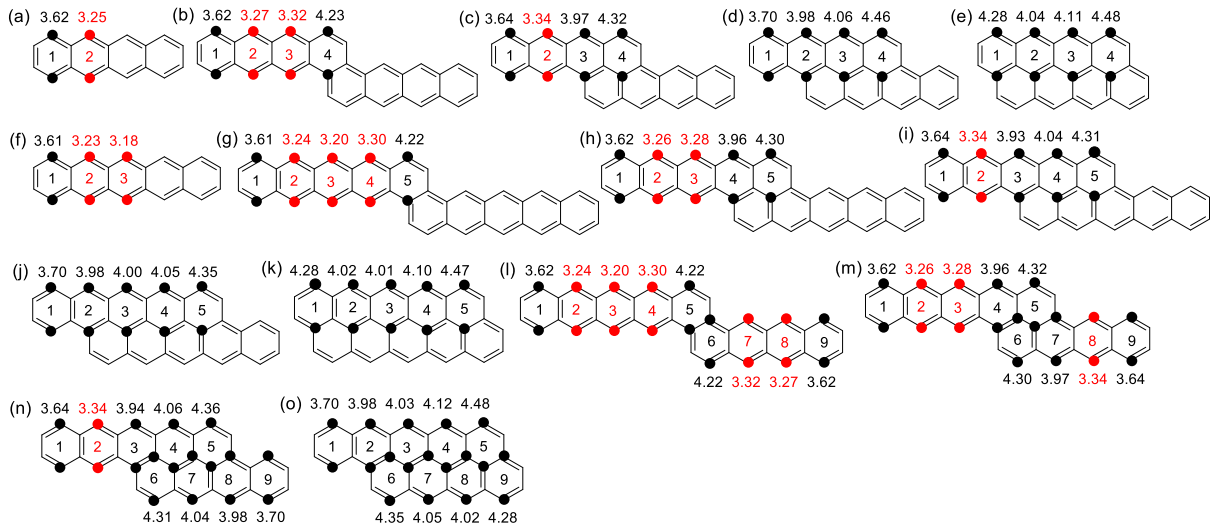

Figure 4.9 HMO localization energies for different PAHs (in units of -β).

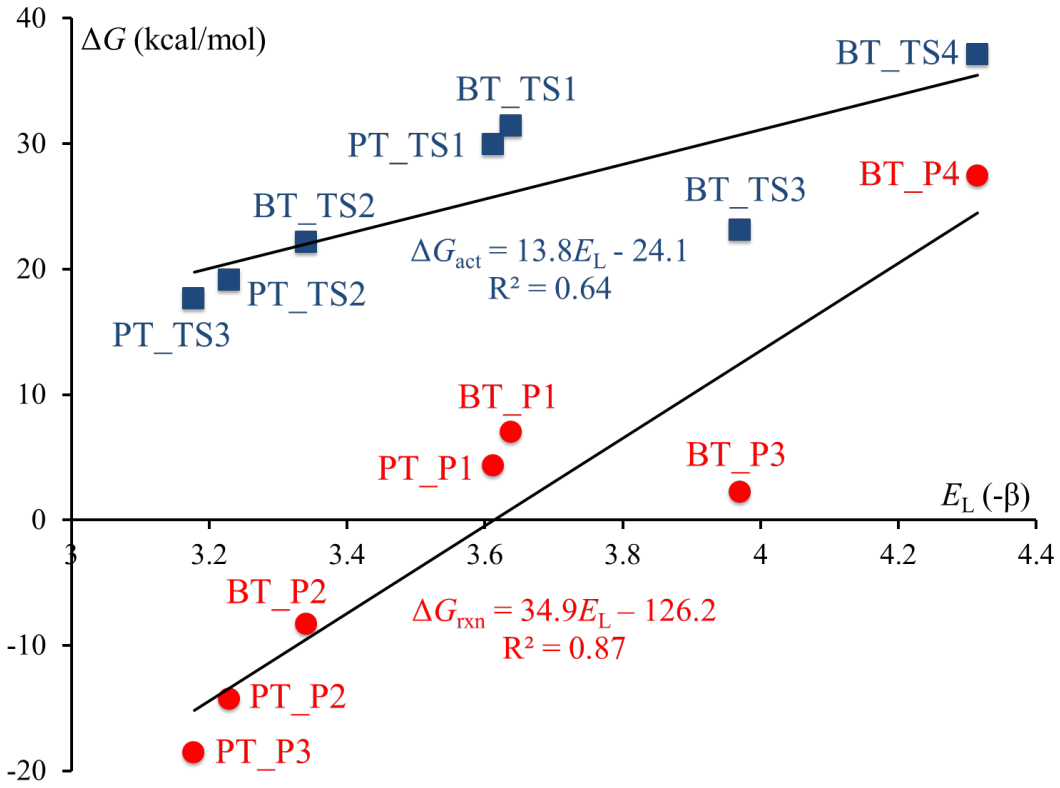

Figure 4.10 Correlation between HMO localization energies and DFT activation free energies (in blue) or reaction free energies (in red) of DA reactions on seven reaction sites in PT and BT.

As shown in Figure 4.10, the localization energies from HMO method correlate with DFT activation free energies and reaction free energies of the DA reactions on seven reaction sites in PT and BT molecules, although some points, such as **BT_TS3** and **BT_P3**, have large deviations from the lines. This shows that the reactivities of different sites in PAHs are mainly determined by the loss of the resonance energies after reactions. Although highly simplified, the HMO localization energy can be used as a tool to estimate the reactivities of various PAH molecules for experimental guidance. According to the linear equation in red (Figure 4.10), the HMO localization energy of 3.6 corresponds to a reaction free energy of about 0 kcal/mol. We

set the localization energy of 3.6 as the critical value. Only reaction sites with localization energies lower than 3.6 are able to undergo DA reactions with fullerene. We further explored other aromatic molecules composed of one or two rows of pentacene or tetracene with all the possible arrangements. Their chemical structures and HMO localization energies of different diene sites are listed in Figure 4.9. The reaction sites with localization energies lower than 3.6 are highlighted in red.

To test the applicability of two linear equations shown in Figure 4.10, we applied them on five reactive sites (E_L < 3.6) of another three PAHs (b, h, and i) shown in Figure 8. Based on their HMO localization energies, the derived activation free energies (ΔG_{act}-D) and reaction free energies (ΔG_{rxn}-D) in cycloadditions with [60]fullerene are obtained (Table 4.2). For comparison, the corresponding values from DFT calculations are listed as ΔG_{act} and ΔG_{rxn} in Table 4.2. For activation free energies, the differences between the HMO method and the M06-2X method are in the range of 2.5 to -1.0 kcal/mol. Similarly, the differences of reaction free energies are in the range of 3.8 to -2.4 kcal/mol. These results demonstrate that the simple HMO method can be of considerable value in estimating reaction barriers and thermodynamics.

Table 4.2 Comparison of Activation Free Energies and Reaction Free Energies Derived (ΔG_{act}-D and ΔG_{rxn}-D, in kcal/mol) from Linear Equations (Figure 9) and those (ΔG_{act} and ΔG_{rxn}, in kcal/mol) from DFT Calculations

PAH_site	E_L (-β)	ΔG_{act}-D	ΔG_{act}	ΔG_{rxn}-D	ΔG_{rxn}
b_2	3.27	21.0	22.0	-12.1	-9.7
b_3	3.32	21.7	22.2	-10.3	-9.2

h_2	3.26	20.9	20.9	-12.4	-12.2
h_3	3.28	21.2	18.7	-11.7	-15.5
i_2	3.34	22.0	21.3	-9.6	-10.5

4.4 Conclusion

The Diels-Alder reactions of C_{60} with pentacene, bistetracene, and their bis(2-trimethylsilylethynyl)-substituted derivatives have been studied by DFT calculations. For pentacene, the reaction on the central diene site 3 is favorable both kinetically and thermodynamically. For TMS-PT, the substituent groups on site 3 only have strong influence on the stability of product TMS-PT_P3. The formation of TMS-PT_P3 is still kinetically favored, which is validated by NMR experiments at room temperature. Under thermodynamically controlled conditions (refluxing in CS_2 for 24 hours), the most stable adduct on site 2 (**TMS-PT_P2**) is obtained as the major product. For bistetracene, the two-row fused aromatic ring framework deactivates the molecule toward DA reactions. The DA barriers are significantly higher than those with pentacene. Site 2 in BT is the most reactive one among four reaction sites, and only the reaction on site 2 is exergonic. The additional side groups slightly affect the reaction barriers with TMS-BT, which are quite close to those with BT. One silylethynyl substituent on site 3 can further destabilize the stability of the corresponding adduct (**TMS-BT_P3**) by about 6 kcal/mol. In addition, calculations show that TMS-BT is about 5 orders of magnitude less reactive than TMS-PT in the reactions with fullerene. This accounts for the chemical inertness of the TIPS-BT molecule. We also investigated the localization energies of different sites in a series of PAHs based on the HMO method. We found that the HMO localization energies can be used to estimate the reactivities of various PAH molecules in

cycloadditions with fullerenes. Our study provides valuable insight into the design of stable unconventional linear PAHs for organic electronic applications.

4.5 References

1. Anthony, J. E. *Angew. Chem., Int. Ed.* **2008**, *47*, 452.
2. Yoo, S.; Domercq, B.; Kippelen, B. *Appl. Phys. Lett.* **2004**, *85*, 5427.
3. Jurchescu, O.D.; Baas, J.; Palstra, T.T.M. *Appl. Phys. Lett.* **2004**, *84*, 3061.
4. Yi, Y.; Coropceanu, V.; Brédas, J.-L. *J. Am. Chem. Soc.* **2009**, *131*, 15777.
5. Congreve, D. N.; Lee, J.; Thompson, N. J.; Hontz, E.; Yost, S. R.; Reusswig, P. D.; Bahlke, M. E.; Reineke, S.; Van Voorhis, T.; Baldo, M. A. *Science* **2013**, *340*, 334.
6. Yamada, M.; Ikemote, I.; Kuroda, H. *Bull. Chem. Soc. Jpn.* **1988**, *61*, 1057.
7. Takahashi, T.; Kitamura, M.; Shen, B. J.; Nakajima, K. *J. Am. Chem. Soc.* **2000**, *122*, 12876.
8. Mack, J.; Miller, G. P. *Fullerene Sci., Technol.* **1997**, *5*, 607.
9. (a) Miller, G. P.; Mack, J. *Org. Lett.* **2000**, *2*, 3979. (b) Miller, G. P.; Mack, J.; Briggs, J. B. *Org. Lett.* **2000**, *2*, 3983. (c) Miller, G. P.; Briggs, J. B. *C. R. Chimie* **2006**, *9*, 916. (d) Kaur, I.; Miller, G. P. *New. J. Chem.* **2008**, *32*, 459.
10. (a) Kaur, I.; Jia, W.; Kopreski, R.; Selvarasah, S.; Dokmeci, M. R.; Pramanik, C.; McGruer, N.; Miller, G. P. *J. Am. Chem. Soc.* **2008**, *130*, 16274. (b) Fudickar, W.; Linker, T. *J. Am. Chem. Soc.* **2012**, *134*, 15071.
11. (a) Payne, M. M.; Parkin, S. R.; Anthony, J. E. *J. Am. Chem. Soc.* **2005**, *127*, 8028. (b) Chun, D.; Cheng, Y.; Wudl, F. *Angew. Chem., Int. Ed.* **2008**, *47*, 8380. (c) Xiao, J. C.; Duong, H. M.; Liu, Y.; Shi, W. X.; Li, G.; Li, S. Z.; Liu, X. W.; Ma, J.; Wudl, F.; Zhang, Q. C. *Angew. Chem., Int. Ed.* **2012**, *51*, 6094.

12. (a) Zhang, L.; Fonari, A.; Zhang, Y.; Zhao, G.; Coropceanu, V.; Hu, W.; Parkin, S.; Brédas, J.–L.; Briseno, A. L. *Chem. Eur. J.* **2013**, *19*, 17907. (b) Zhang, L.; Walker, B.; Liu, F.; Colella, N. S.; Mannsfeld, S. C. B.; Watkins, J. J.; Nguyen, T.-Q.; Briseno, A. L. *J. Mater. Chem.* **2012**, *22*, 4266.

13. Zhang, L.; Fonari, A., Liu, Y.; Hoyt, A.-L. M.; Lee, H.; Granger, D.; Parkin, S.; Russell, T. P.; Anthony, J. E.; Brédas, J.-L.; Coropceanu, V.; Briseno, A. L. *J. Am. Chem. Soc.* **2014**, *136*, DOI: 10.1021/ja503643s.

14. Biermann, D.; Schmidt, W. *J. Am. Chem. Soc.* **1980**, *102*, 3173.

15. Frisch, M. J.; Trucks, G. W.; Schlegel, H. B.; Scuseria, G. E.; Robb, M. A.; Cheeseman, J. R.; Scalmani, G.; Barone, V.; Mennucci, B.; Petersson, G. A.; Nakatsuji, H.; Caricato, M.; Li, X.; Hratchian, H. P.; Izmaylov, A. F.; Bloino, J.; Zheng, G.; Sonnenberg, J. L.; Hada, M.; Ehara, M.; Toyota, K.; Fukuda, R.; Hasegawa, J.; Ishida, M.; Nakajima, T.; Honda, Y.; Kitao, O.; Nakai, H.; Vreven, T.; Montgomery, J. A., Jr.; Peralta, J. E.; Ogliaro, F.; Bearpark, M.; Heyd, J. J.; Brothers, E.; Kudin, K. N.; Staroverov, V. N.; Keith, T.; Kobayashi, R.; Normand, J.; Raghavachari, K.; Rendell, A.; Burant, J. C.; Iyengar, S. S.; Tomasi, J.; Cossi, M.; Rega, N.; Millam, J. M.; Klene, M.; Knox, J. E.; Cross, J. B.; Bakken, V.; Adamo, C.; Jaramillo, J.; Gomperts, R.; Stratmann, R. E.; Yazyev, O.; Austin, A. J.; Cammi, R.; Pomelli, C.; Ochterski, J. W.; Martin, R. L.; Morokuma, K.; Zakrzewski, V. G.; Voth, G. A.; Salvador, P.; Dannenberg, J. J.; Dapprich, S.; Daniels, A. D.; Farkas, O.; Foresman, J. B.; Ortiz, J. V.; Cioslowski, J.; Fox, D. J.; *Gaussian 09, revision D.01*; Gaussian Inc.: Wallingford, CT, 2013.

16. Yang, T.; Zhao, X.; Nagase, S. *Org. Lett.* **2013**, *15*, 5960.

17. (a) Becke, A. D. *Phys. Rev. A* **1988**, *38*, 3098. (b) Becke, A. D. *J. Chem. Phys.* **1993**, *98*, 5648. (c) Lee, C.; Yang, W.; Parr, R. G. *Phys. Rev. B* **1988**, *37*, 785.

18. (a) Hariharan, P. C.; Pople, J. A. *Theor. Chim. Acta* **1973**, *28*, 213. (b) Hehre, W. J.; Ditchfield, R.; Pople, J. A. *J. Chem. Phys.* **1972**, *56*, 2257.

19. (a) Osuna, S.; Swart, M.; Solà, M. *J. Phys. Chem. A* **2011**, *115*, 3491. (b) Garcia-Borràs, M.; Osuna, S.; Swart, M.; Luis, J. M.; Solà, M. *Chem. Commun.* **2013**, *49*, 1220.

20. (a) Chai, J.-D.; Head-Gordon, M. *Phys. Chem. Chem. Phys.* **2008**, *10*, 6615. (b) Fokin, A. A.; Chernish, L. V.; Gunchenko, P. A.; Tikhonchuk, E. Y.; Hausmann, H.; Serafin, M.; Dahl, J. E.; Carlson, R. M.; Schreiner, P. R. *J. Am. Chem. Soc.* **2012**, *134*, 13641.

21. (a) Zhao, Y.; Truhlar, D. G. *Theor. Chem. Acc.* **2008**, *120*, 215. (b) Zhao, Y.; Truhlar, D. G. *Acc. Chem. Res.* **2008**, *41*, 157.

22. (a) Paton, R. S.; Mackey, J. L.; Kim, W. H.; Lee, J. H.; Danishefsky, S. J.; Houk, K. N. *J. Am. Chem. Soc.* **2010**, *132*, 9335. (b) Lan, Y.; Zou, L.-F.; Cao, Y.; Houk, K. N. *J. Phys. Chem. A.* **2011**, *115*, 13906.

23. (a) Bian, S.; Scott, A. M.; Cao, Y.; Liang, Y.; Osuna, S.; Houk, K. N.; Braunschweig, A. B. *J. Am. Chem. Soc.* **2013**, *135*, 9240. (b) Cao, Y.; Osuna, S.; Liang, Y.; Haddon, R. C.; Houk, K. N. *J. Am. Chem. Soc.* **2013**, *135*, 17643. (c) Lazar, P.; Karlický, F.; Jurečka, P.; Kocman, M.; Otyepková, E.; Šafářová, K.; Otyepka, M. *J. Am. Chem. Soc.* **2013**, *135*, 6372.

24. (a) Barone, V.; Cossi, M. *J. Phys. Chem. A* **1998**, *102*, 1995. (b) Cossi, M.; Rega, N.; Scalmani, G.; Barone, V. *J. Comput. Chem.* **2003**, *24*, 669. (c) Takano, Y.; Houk, K. N. *J. Chem. Theory Comput.* **2005**, *1*, 70.

25. Grimme, S. *WIREs Comput. Mol. Sci.* **2011**, *1*, 211.

26. (a) Ess, D. H.; Houk, K. N. *J. Am. Chem. Soc.* **2007**, *129*, 10646. (b) Legault, C. Y.; Garcia, Y.; Merlic, G. A.; Houk, K. N. *J. Am. Chem. Soc.* **2007**, *129*, 12664. (c) Ess, D. H.; Houk, K. N. *J. Am. Chem. Soc.* **2008**, *130*, 10187.

27. For reviews, see: (a) van Zeist, W.-J.; Bickelhaupt, F. M. *Org. Biomol. Chem.* **2010**, *8*, 3118. (b) Fernández, I. *Phys. Chem. Chem. Phys.* **2014**, *16*, 7662.

28. (a) Fernández, I.; Bickelhaupt, F. M. *J. Comput. Chem.* **2012***, 33,* 509. (b) Gordon, C. G.; Mackey, J. L.; Jewett, J. C.; Sletten, E. M.; Houk, K. N.; Bertozzi, C. R. *J. Am. Chem. Soc.* **2012**, *134*, 9199. (c) Liang, Y.; Mackey, J. L.; Lopez, S. A.; Liu, F.; Houk, K. N. *J. Am. Chem. Soc.* **2012**, *134*, 17904. (d) Fernández, I.; Bickelhaupt, F. M.; Cossío, F. P. *Chem. Eur. J.* **2012**, *18*, 12395. (e) Lopez, S. A.; Houk, K. N. *J. Org. Chem.* **2013**, *78*, 1778. (f) Zou, L.; Paton, R. S.; Eschenmoser, A.; Newhouse, T. R.; Baran, P. S.; Houk, K. N. *J. Org. Chem.* **2013**, *78*, 4037. (g) Fernández, I.; Solà, M.; Bickelhaupt, F. M. *Chem. Eur. J.* **2013**, *19*, 7416. (h) Kamber, D. N.; Nazarova, L. A.; Liang, Y.; Lopez, S. A.; Patterson, D. M.; Shih, H.-W.; Houk, K. N.; Prescher, J. A. *J. Am. Chem. Soc.* **2013**, *135*, 13680. (i) Liu, F.; Paton, R. S.; Kim, S.; Liang, Y.; Houk, K. N. *J. Am. Chem. Soc.* **2013**, *135*, 15642. (j) Usharani, D.; Lacy, D. C.; Borovik, A. S.; Shaik, S. *J. Am. Chem. Soc.* **2013**, *135*, 17090. (k) Hong, X.; Liang, Y.; Griffith, A. K.; Lambert, T. H.; Houk, K. N. *Chem. Sci.* **2014**, *5*, 471. (l) Yang, Y.-F.; Cheng, G.-J.; Liu, P.; Leow, D.; Sun, T.-Y.; Chen, P.; Zhang, X.; Yu, J.-Q.; Wu, Y.-D.; Houk, K. N. *J. Am. Chem. Soc.* **2014**, *136*, 344. (m) Hong, X.; Liang, Y.; Houk, K. N. *J. Am. Chem. Soc.* **2014**, *136*, 2017. (n) Fernández, I.; Bickelhaupt, F. M. *J. Comput. Chem.* **2014***, 35,* 371. (o) Yang, J.; Liang, Y.; Šečkutė, J.; Houk, K. N.; Devaraj, N. K. *Chem. Eur. J.* **2014**, *20*, 3365. (p) Liu, S.; Lei, Y.; Qi, X.; Lan, Y. *J. Phys. Chem. A.* **2014**, *118*, 2638.

29. Hirsch, A.; Brettreich, M. *Fullerenes: Chemistry and Reactions*; WILEY-VCH: Weinheim, 2004.

30. Slanina, Z.; Stobinski, L.; Tomasik, P.; Lin, H.-M.; Adamowicz, L. *J. Nanosci. Nanotech.* **2003**, *3*, 193.

31. Wheland, G. W. *J. Am. Chem. Soc.* **1942**, *64*, 900.

32. Brown, R. D. *Q. Rev. Chem. Soc.* **1952**, *6*, 63.

33. For the relationship between distortion energies and the DA reactivities of PAHs, see: Hayden, A. E.; Houk, K. N. *J. Am. Chem. Soc.* **2009**, *131*, 4084.

34. Schleyer, P. v. R.; Manoharan, M.; Jiao, H.; Stahl, F. *Org. Lett.* **2001**, *3*, 3643.

35. http://www.chem.ucalgary.ca/SHMO/

Chapter 5 Computational Assessment of (1+2) Cycloadditions to Fullerene, Carbon Nanotube and Graphene

5.1 Introduction

A variety of cycloaddition reactions on graphene have been studied in Chapter 1-3, including the 1,3 dipolar cycloadditions, DA reactions, (2+2) and (4+4) cycloadditions. Chapter 4 reached out to the DA reactions between acenes and fullerenes. Our early goal of these studies was mainly to predict effective and tunable functionalization methods on carbon materials, especially graphene. However, cycloaddition reactions we studied so far are not ideal. They mainly attack the peripheral of graphene with strong preference to form non-covalent interactions. The (1+2) cycloaddition reactions through carbene, nitrene and oxene are well known to enable modifications on carbon materials. Much progress has been made in this type of reactions. In this chapter, we investigated this type of reactions on fullerene, carbon nanotube and graphene models

5.2 Computational methods and models

All calculations were performed with Gaussian 09.[1] The geometry optimizations of all the minima were carried out at the (U)M06-2X level of theory[2-3] with the 6-31G(d) basis set.[4] The electronic energy (ΔE) is used to evaluate the feasibility of reactions. Figure 5.1 shows carbon allotrope models with representative addition sites.

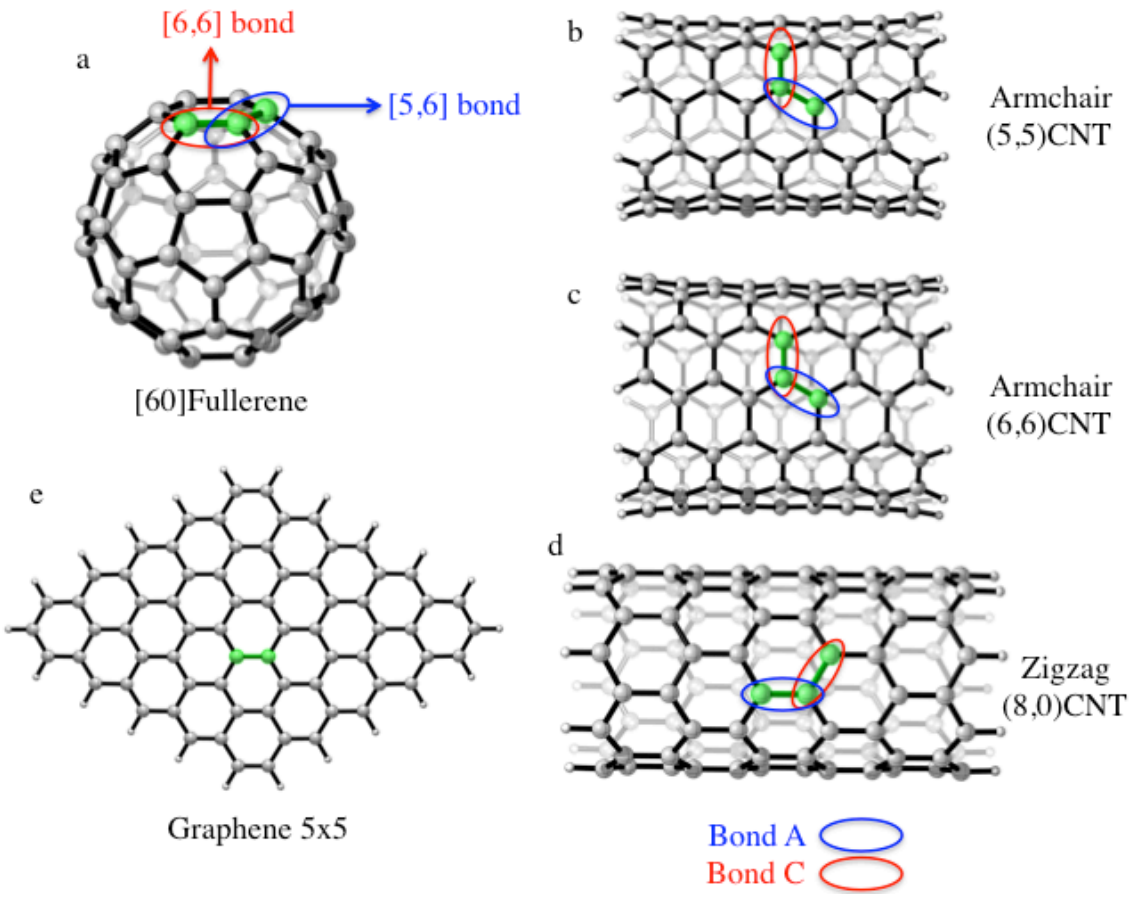

Figure 5.1 (a) [60]fullerene model with the [5,6] bond in blue and the [6,6] bond in red. Carbon nanotube models of (b) armchair (5,5)CNT, (c) armchair (6,6)CNT, and (d) zigzag (8,0)CNT with the bond A in blue and the bond C in red. (e) The 5x5 graphene model with the center addition bond.

5.3 The (1+2) cycloaddition to fullerene

The (1+2) cycloaddition to fullerene has been thoroughly studied in the past twenty years both experimentally and computationally. The addition of dichlorocarbene to [60]fullerene was first reported in 1993.[5] The resulting adducts were isolated and characterized by mass spectroscopy and ^{13}C NMR spectroscopy. There are two types of C=C bonds in [60]fullerene

(Figure 5.1a). The [5,6] bond is located between the fused 5- and 6-membered rings, and the [6,6] bond is located between two fused 6-membered rings. In a 1993 report, the monoadduct was found to occur at the [6,6] bond, giving a cyclopropane or methanofullerene structure.[5] Later computational studies supported their experimental results.[6] DFT calculations showed that the CCl_2 insertion to the [6,6] bond would form the closed cyclopropane three-membered ring adduct with the bridged C-C bond length of 1.6 Å, while the carbene addition to the [5,6] bond would lead to the opened ring structure, or homofullerene, with the C-C distance of 2.2 Å. The closed-ring [6,6] monoadduct is more favorable than the opened-ring [5,6] product kinetically and thermodynamically.[6]

Here, we have performed similar calculations on carbene additions to the [5,6] and [6,6] bonds of fullerene at M06-2X/6-31G(d) level. For carbene addition to the [5,6] bond, full optimization leads to the opened-ring structure as shown in Figure 5.2(a), with a C-C bond distance of 2.19 Å. The full optimization on the adduct of the [6,6] bond results in the closed-ring structure as shown in Figure 5.2(d), with a C-C bridge of 1.60 Å. To estimate the energy difference between opened- and closed-ring structures, the carbene-fullerene addition on the [5,6] bond with a fixed C-C bond at 1.60 Å (Figure 5.2(b)), the same bond length in the [6,6] adduct closed structure, was also considered. The closed-ring [5,6] adduct is 12.7 kcal/mol less stable than the opened-ring counterparts. Similarly, we fixed the C-C bond of the [6,6] adduct at 2.19 Å (Figure 5.2(c)). The opened-ring [6,6] adduct is 11.9 kcal/mol less stable than its closed-ring counterparts.

The nitrene addition and oxene addition to fullerene were also explored (Figure 5.2(e)-(l)). For [5,6] bond adducts, opened structures are all preferred by 17-18 kcal/mol over the closed

structures. For [6,6] bridged adducts, closed structures are more stable by 13-15 kcal/mol than opened-bond counterparts.

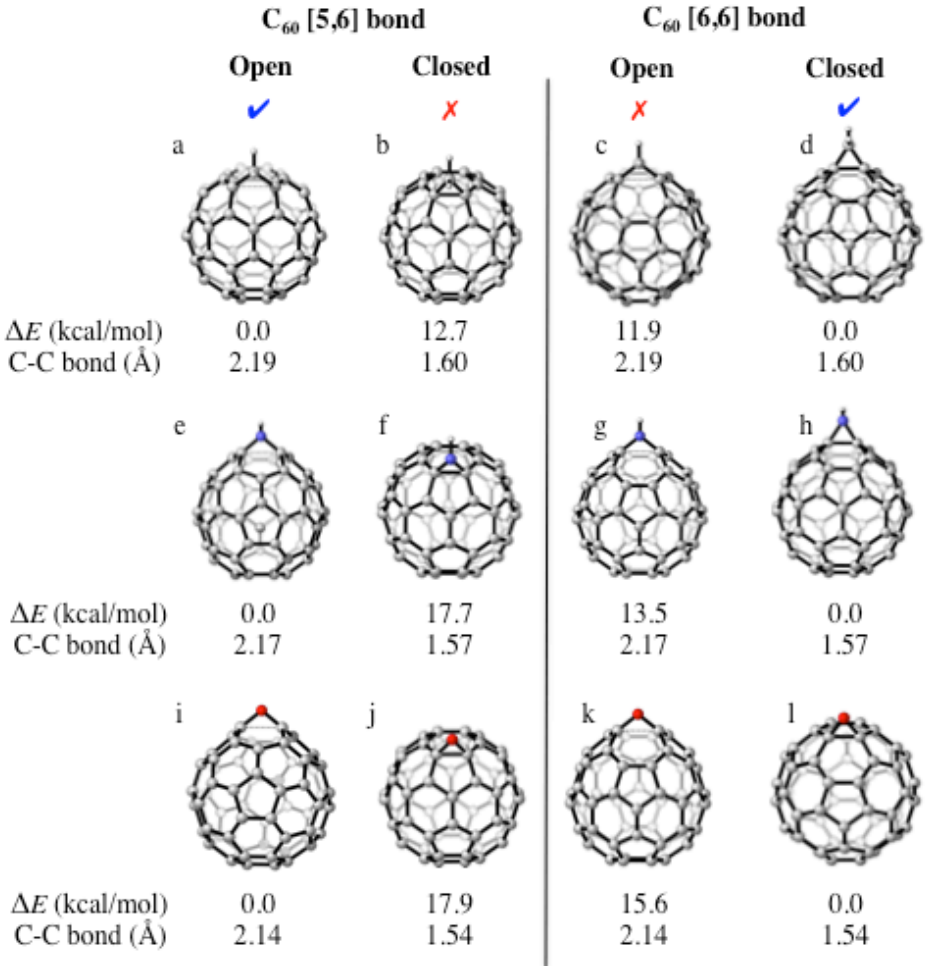

Figure 5.2 The (a) opened and (b) closed adduct structures formed by the (1+2) cycloaddition of carbene, CH_2, with the [5,6] bond of fullerene. The (c) opened and (d) closed adduct structures formed by the (1+2) cycloaddition of carbene with the [6,6] bond of fullerene. The (e) opened and (f) closed adduct structures formed by the (1+2) cycloaddition of nitrene, NH, with the [5,6] bond of fullerene. The (g) opened and (h) closed adduct structures formed by the (1+2) cycloaddition of nitrene with the [6,6] bond of fullerene. The (i) opened and (j) closed adduct structures formed by the (1+2) cycloaddition of oxene, O, with the [5,6] bond of fullerene. The

(k) opened and (l) closed adduct structures formed by the (1+2) cycloaddition of oxene with the [6,6] bond of fullerene. Reaction electronic energies are given in kcal/mol. The C-C bond lengths are given in Å.

5.4 The (1+2) cycloaddition to carbon nanotubes

We have studied additions to two types of bonds, the axial bond (bond a) and the circumferential bond (bond c), on three carbon nanotube (CNT) models.[6] Figure 5.1(b)-(d) shows structures of the three models: the (5,5)CNT model and (6,6)CNT model with armchair edges; the (8,0)CNT model with a zigzag edge. They are all terminated with hydrogen atoms.

For (1+2) cycloadditions with carbon nanotubes, carbene, nitrene and oxene additions were considered. Figure 5.3 to 5.5 show the product structures for three CNT models. For the bond a of armchair-edged carbon nanotubes, the adducts of (1+2) cycloadditions clearly favor closed bond structures. As shown in Figure 5.3 and 5.4, closed structures on bond a are all preferred by 15-18 kcal/mol than opened structures. The situation for bond c is more ambiguous as energy differences between closed and opened structures are very small, within 3 kcal/mol. For (5,5)CNT models, full optimization of the nitreene additions on bond c can lead to both closed and opened structures, depending on starting geometries. Such close energetic profiles leave an open question for further investigations in our group. The conclusion for the zigzag-edge carbon nanotube, (8,0)CNT, is clear (Figure 5.5). For its bond a, closed structures are all preferred by 15-17 kcal/mol than opened structures, while opened structures on bond c are more stable by 8-11 kcal/mol than closed structures.

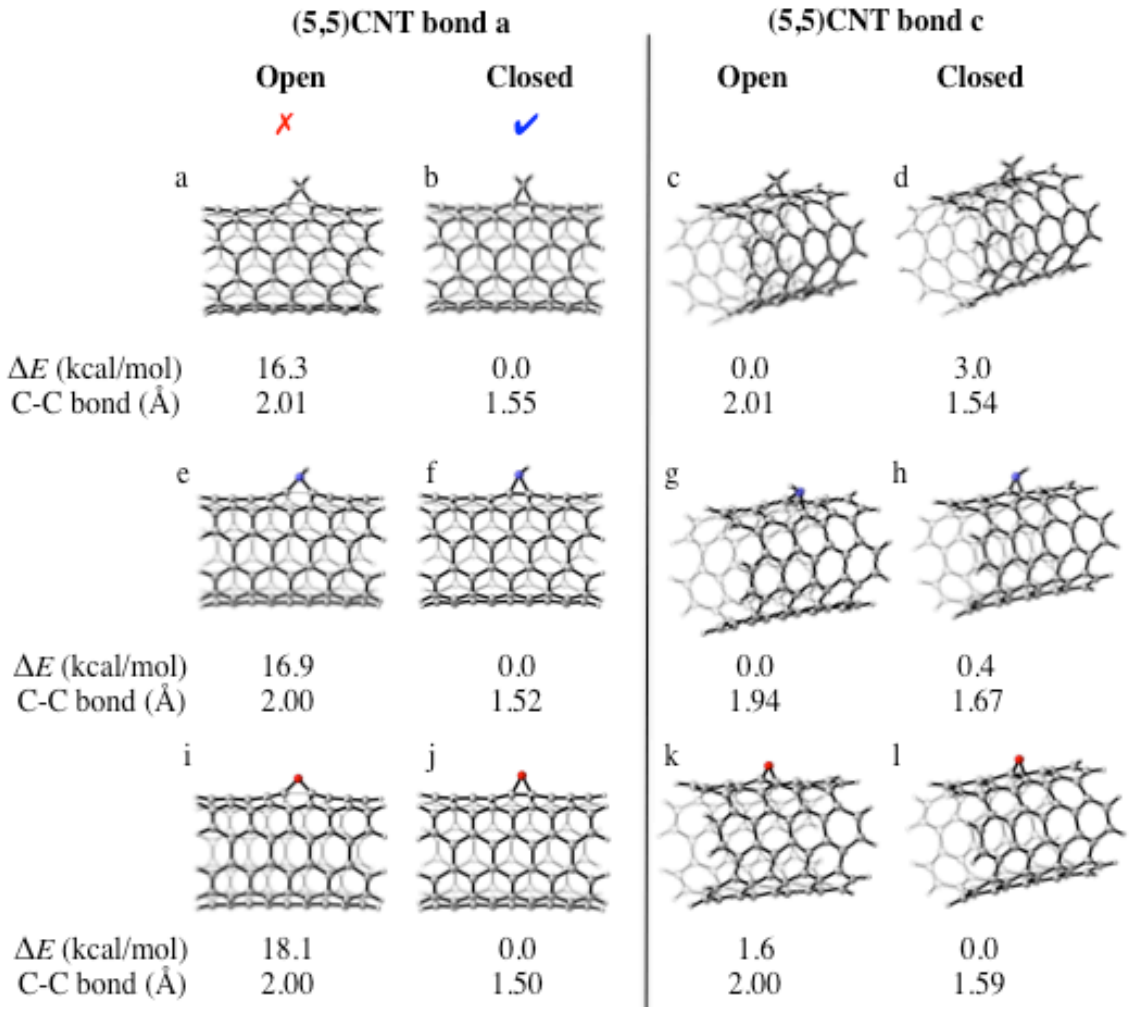

Figure 5.3 The (a) opened and (b) closed adduct structures formed by the (1+2) cycloaddition of carbene with bond a of (5,5)CNT. The (c) opened and (d) closed adduct structures formed by the (1+2) cycloaddition of carbene with bond c of (5,5)CNT. The (e) opened and (f) closed adduct structures formed by the (1+2) cycloaddition of nitrene with bond a of (5,5)CNT. The (g) opened and (h) closed adduct structures formed by the (1+2) cycloaddition of nitrene with bond c of (5,5)CNT. The (i) opened and (j) closed adduct structures formed by the (1+2) cycloaddition of oxene with bond a of (5,5)CNT. The (k) opened and (l) closed adduct structures formed by the (1+2) cycloaddition of oxene with bond c of (5,5)CNT. Reaction electronic energies are given in kcal/mol. The C-C bond lengths are given in Å.

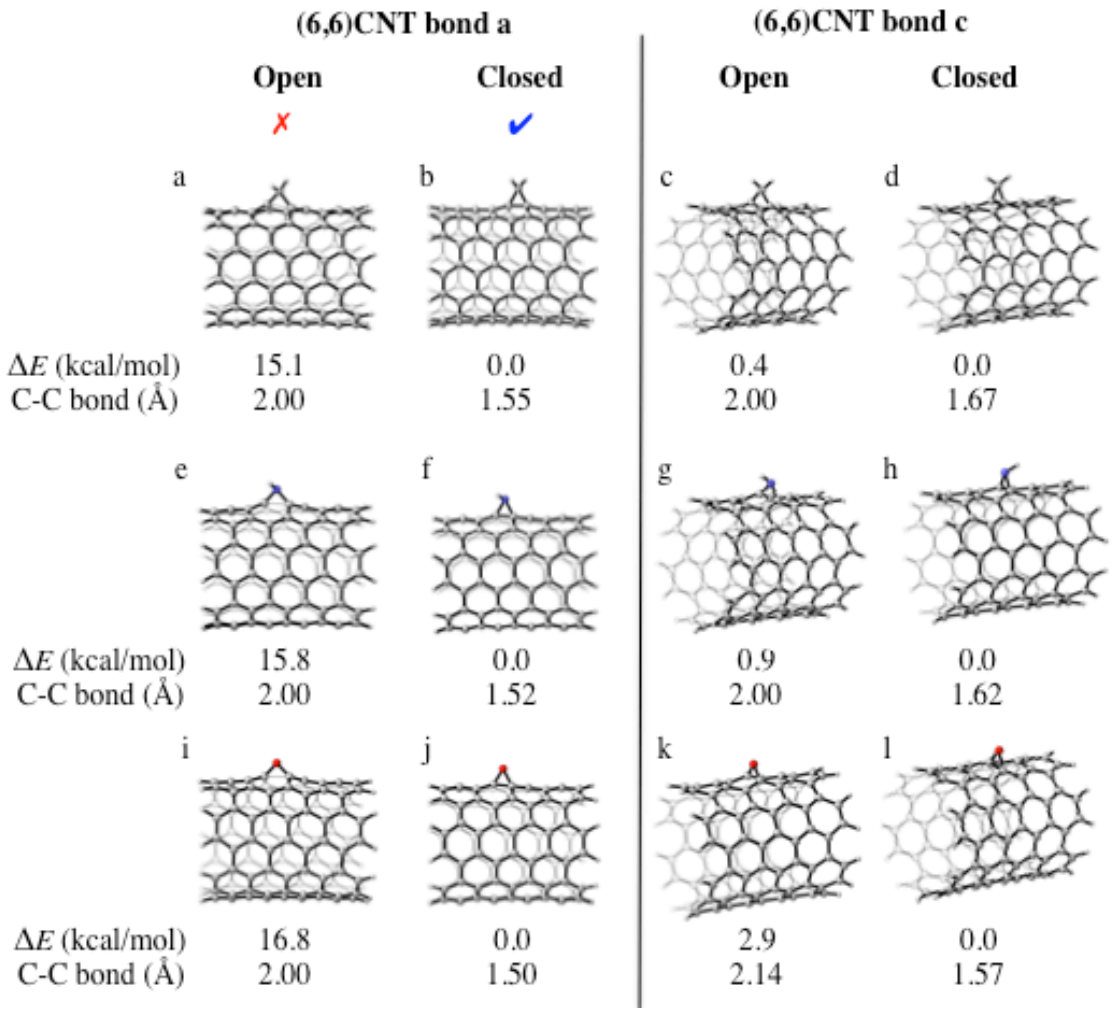

Figure 5 4 The (a) opened and (b) closed adduct structures formed by the (1+2) cycloaddition of carbene, CH_2, with bond a of (6,6)CNT. The (c) opened and (d) closed adduct structures formed by the (1+2) cycloaddition of carbene with bond c of (6,6)CNT. The (e) opened and (f) closed adduct structures formed by the (1+2) cycloaddition of nitrene, NH, with bond a of (6,6)CNT. The (g) opened and (h) closed adduct structures formed by the (1+2) cycloaddition of nitrene with bond c of (6,6)CNT. The (i) opened and (j) closed adduct structures formed by the (1+2) cycloaddition of oxene, O, with bond a of (6,6)CNT. The (k) opened and (l) closed adduct

structures formed by the (1+2) cycloaddition of oxene with bond c of (6,6)CNT. Reaction electronic energies are given in kcal/mol. The C-C bond lengths are given in Å.

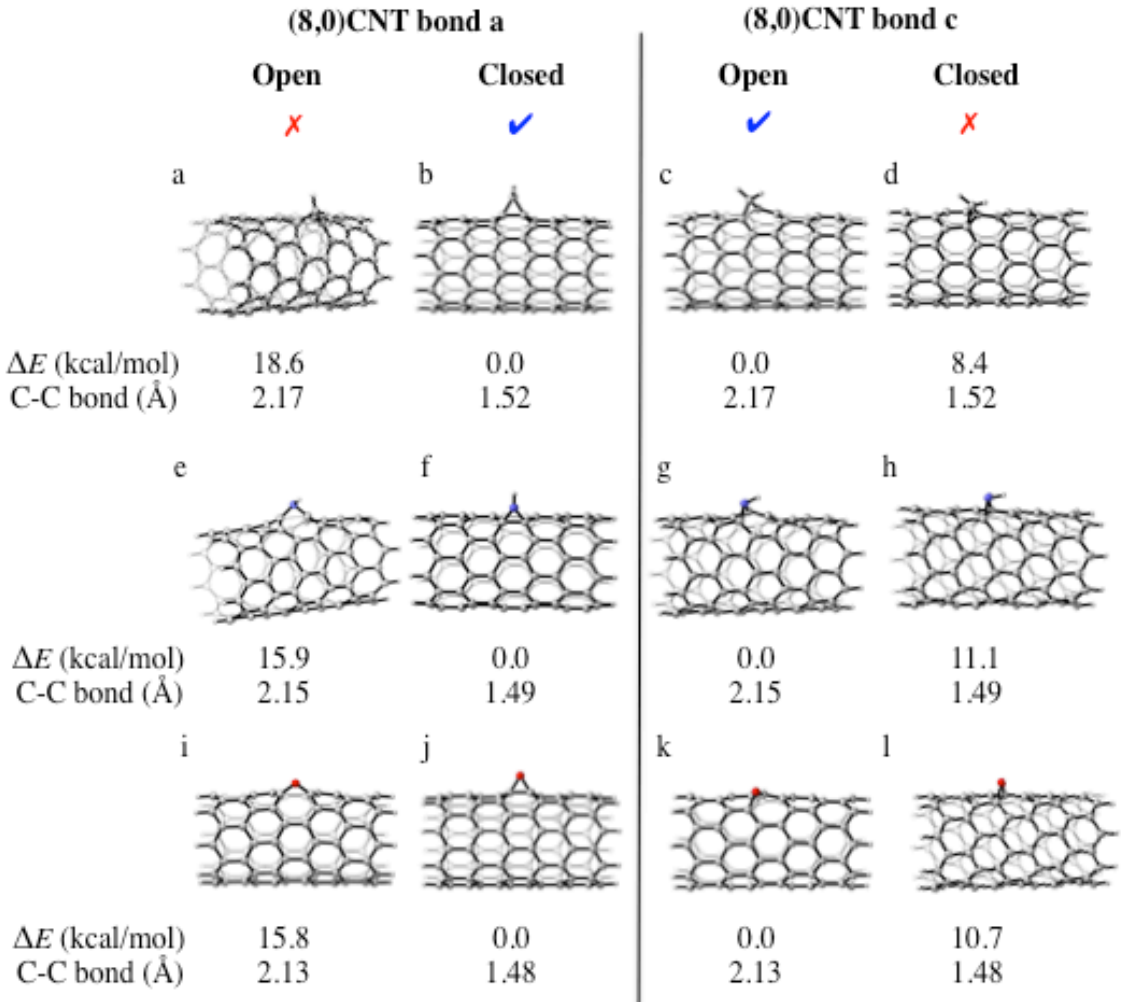

Figure 5.5 The (a) opened and (b) closed adduct structures formed by the (1+2) cycloaddition of carbene, CH_2, with bond a of (8,0)CNT. The (c) opened and (d) closed adduct structures formed by the (1+2) cycloaddition of carbene with bond c of (8,0)CNT. The (e) opened and (f) closed adduct structures formed by the (1+2) cycloaddition of nitrene, NH, with bond a of (8,0)CNT. The (g) opened and (h) closed adduct structures formed by the (1+2) cycloaddition of nitrene with bond c of (8,0)CNT. The (i) opened and (j) closed adduct structures formed by the (1+2)

cycloaddition of oxene, O, with bond a of (8,0)CNT. The (k) opened and (l) closed adduct structures formed by the (1+2) cycloaddition of oxene with bond c of (8,0)CNT. Reaction electronic energies are given in kcal/mol. The C-C bond lengths are given in Å.

5.5 The (1+2) cycloaddition to graphene

Similar, the center bond on graphene model 5x5 (Figure 5.1(e)) was studied. As shown in Figure 5.6, closed structures of the (1+2) addition adducts on graphene are all preferred by 9-10 kcal/mol than opened structures.

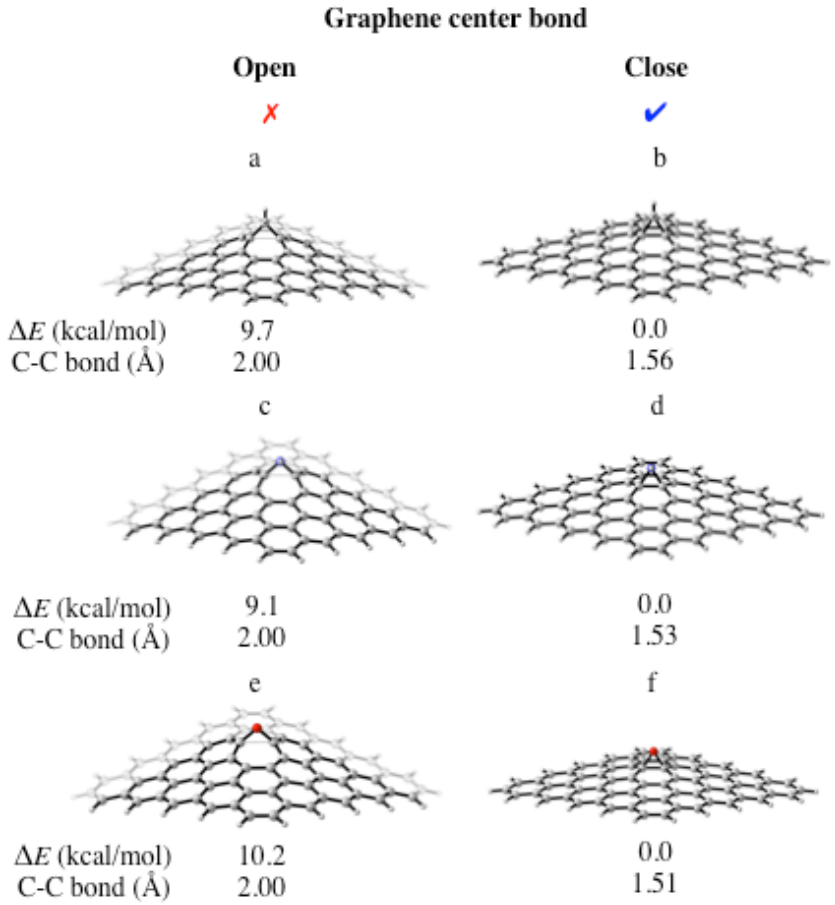

Figure 5.6 The (a) opened and (b) closed adduct structures formed by the (1+2) cycloaddition of carbene, CH_2, with graphene center bond. The (c) opened and (d) closed adduct structures

formed by the (1+2) cycloaddition of nitrene with graphene center bond. The (e) opened and (f) closed adduct structures formed by the (1+2) cycloaddition of oxene with graphene center bond. Reaction electronic energies are given in kcal/mol. The C-C bond lengths are given in Å.

5.6 Reference

1. Frisch, M. J.; Trucks, G. W.; Schlegel, H. B.; Scuseria, G. E.; Robb, M. A.; Cheeseman, J. R.; Scalmani, G.; Barone, V.; Mennucci, B.; Petersson, G. A.; Nakatsuji, H.; Caricato, M.; Li, X.; Hratchian, H. P.; Izmaylov, A. F.; Bloino, J.; Zheng, G.; Sonnenberg, J. L.; Hada, M.; Ehara, M.; Toyota, K.; Fukuda, R.; Hasegawa, J.; Ishida, M.; Nakajima, T.; Honda, Y.; Kitao, O.; Nakai, H.; Vreven, T.; Montgomery, J. A., Jr.; Peralta, J. E.; Ogliaro, F.; Bearpark, M.; Heyd, J. J.; Brothers, E.; Kudin, K. N.; Staroverov, V. N.; Kobayashi, R.; Normand, J.; Raghavachari, K.; Rendell, A.; Burant, J. C.; Iyengar, S. S.; Tomasi, J.; Cossi, M.; Rega, N.; Millam, J. M.; Klene, M.; Knox, J. E.; Cross, J. B.; Bakken, V.; Adamo, C.; Jaramillo, J.; Gomperts, R.; Stratmann, R. E.; Yazyev, O.; Austin, A. J.; Cammi, R.; Pomelli, C.; Ochterski, J. W.; Martin, R. L.; Morokuma, K.; Zakrzewski, V. G.; Voth, G. A.; Salvador, P.; Dannenberg, J. J.; Dapprich, S.; Daniels, A. D.; Farkas, O.; Foresman, J. B.; Ortiz, J. V.; Cioslowski, J.; Fox, D. J.; Gaussian 09, revision C.01; Gaussian Inc.: Wallingford, CT, 2010.
2. Zhao, Y.; Truhlar, D. G. *Theor. Chem. Acc.* **2008**, *120*, 215-241.
3. Zhao, Y.; Truhlar, D. G. *Acc. Chem. Res.* **2008**, *41*, 157-167.
4. Hehre, W. J.; Radom, L.; Schleyer, P. v. R.; Pople, J. A. *Ab Initio Molecular Orbital Theory*, Wiley: New York, 1986.
5. Tsuda, M.; Ishida, T.; Nogami, T.; Kurono, S.; Ohashi, M. *Tetrahedron Lett.* **1993**, *34*, 6911.
6. Bettinger, H. F. *Chem. Eur. J.* **2006**, *12*, 4372.

Chapter 6 A method for the rapid estimation of energetics of addition and cycloaddition reactions of carbon nanomaterials

6.1 Introduction

In previous chapters, we have applied the Hückel Molecular Orbital (HMO) calculations on graphene and acene models and found that the HMO localization energies could predict the reactivities of different polycyclic aromatic hydrocarbon sites. Table 2.1 in Chapter 2 lists HMO localization energies for two graphene models. In both models, HMO results show that interior regions of graphene are more inert than active edges, which are in agreement with the DFT calculations. Figure 4.10 in Chapter 4 show the linear correlation between HMO method and DFT activation free energies and reaction free energies of the DA reactions on seven reaction sites in pentacene and bistetracene molecules. The applicability of the simple method was tested on a set of different acenes in Figure 4.9. The derived activation free energies and reaction free energies based on HMO localization energies are compared with M06-2X calculation results in Table 4.2, showing small energy differences. The good correlation between simple HMO and DFT demonstrated that the reactivities of different sites in polycyclic aromatic hydrocarbons are mainly determined by the loss of the resonance energy upon reaction.[1] This conclusion stimulated us to test a method to estimate quickly the reaction energetics on large carbon nanomaterials. We seek to make reliable predictions of energetics of chemical reactions on large aromatic systems, such as graphene and other carbon based nanomaterials. DFT methods, which are well known for their accuracy in energetics and structures in most chemical systems, are our first choice. However, DFT methods quickly reach a bottleneck as the model size increases beyond 100 atom numbers. Here, we show that the energies of reactions in benzene, the basic

unit of graphene, could be utilized as the model system to estimate quickly the reaction energetics of large carbon nanomaterials.

6.2 Calculation results

All calculations were performed with Gaussian 09.[2] The geometry optimizations of all the minima were carried out at the (U)M06-2X level of theory[3-4] with the 6-31G(d) basis set.[5] Single-point energy calculations were subsequently carried on the optimized structures at the (U)M06-2X with a larger basis set 6-311G(d,p). The reaction enthalpy (ΔH) is used to evaluate reactions.

Figure 6.1 shows carbon allotrope models with representative addition sites. Two graphene models (Figure 6.1 a and b) are discussed in details in Chapter 2. The center double bond from Graphene1 and three bonds from Graphene2 are explored here. The [60]fullerene and two carbon nanotube models are discussed in details in Chapter 5. Two C=C bonds from each of the models were studied. These carbon allotrope models as well as the benzene molecule function as 2π components to react with 10 small functional groups shown in Figure 6.1: the 1,2 additions with fluorine and hydrogen; the 1,3-diploar cycloadditions with azomethine ylide and carbonyl ylide; the (2+2) cycloadditions with benzyne, tetracyanoethylene (TCNE) and maleic anhydride (MA); the Diels-Alder reactions with 2,3-dimethoxybutadiene (DMBD), 9-methylanthracene (MeA) and cyclopentadiene.

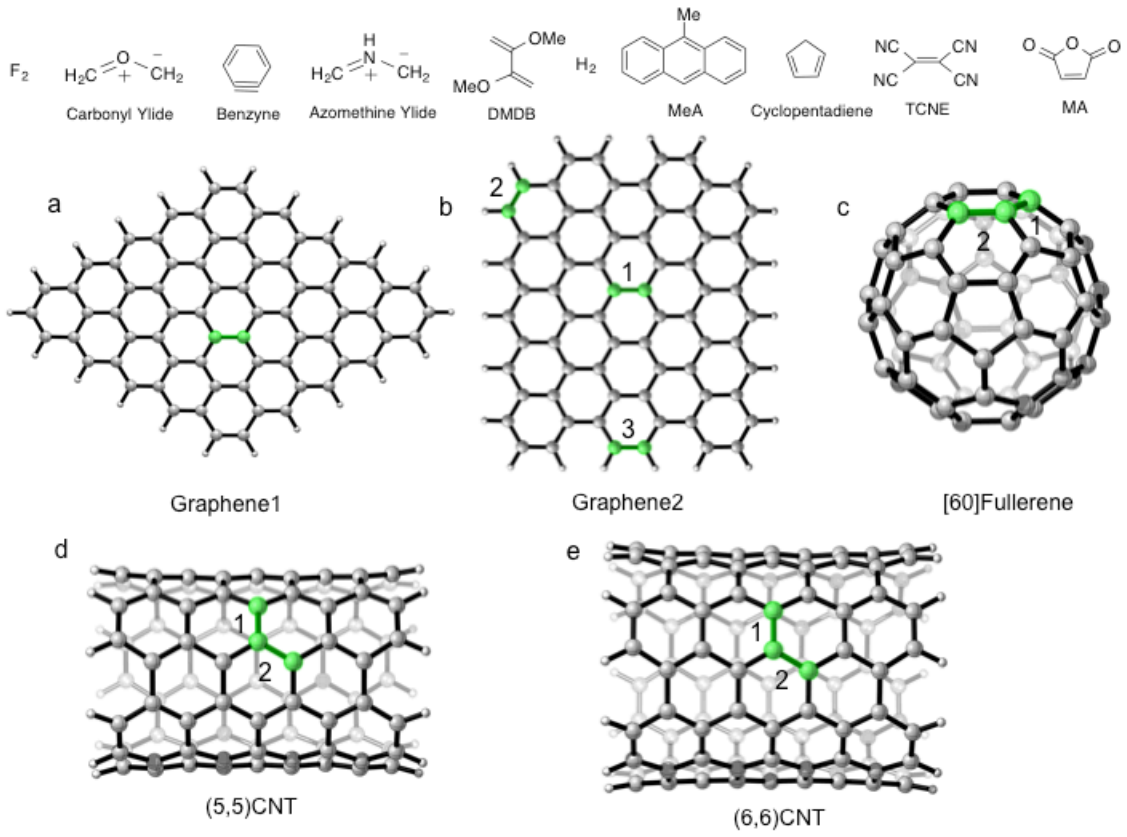

Figure 6.1 Two graphene models (a) and (b) terminated with four reaction bonds. (c) the [60]fullerene model with two reaction bonds. Two carbon nanotube models ((d) (5,5)CNT, (e) (6,6)CNT) with two reaction bonds, respectively. These carbon allotrope models and the benzene molecule function as 2π components to react with 10 small functional groups: the 1,2 additions with fluorine and hydrogen; the 1,3-diploar cycloadditions with azomethine ylide and carbonyl ylide; the (2+2) cycloadditions with benzyne, tetracyanoethylene (TCNE) and maleic anhydride (MA); the Diels-Alder reactions with 2,3-dimethoxybutadiene (DMBD), 9-methylanthracene (MeA) and cyclopentadiene.

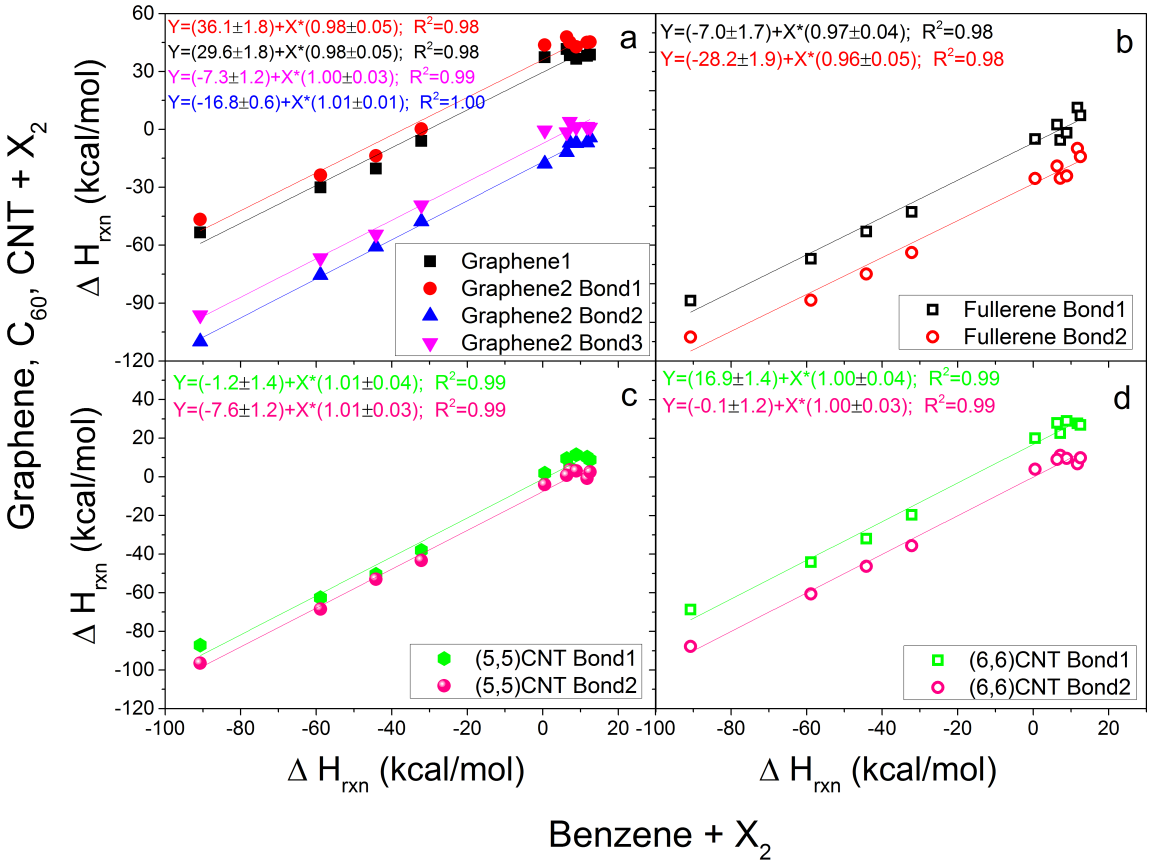

Figure 6.2 Correlation of reaction enthalpies for cycloaddition or addition reactions of 10 small molecule functional groups with C=C bonds on carbon allotropes models and benzene. The X-axis is reaction enthalpies of benzene. The Y-axis is reaction enthalpies of (a) two graphene models, (b) fullerene, (c) (5,5)CNT and (d) (6,6)CNT. Lines are the results from linear fits.

Figure 6.2 gives the correlation of reaction enthalpies between benzene and a series of carbon allotrope models with 10 small molecule functional groups. Ten double bonds from carbon allotrope models were investigated, therefore give 10 linear regression equations. The linear correlation coefficient of determination R^2 are all in the range of 0.98 to 1.00, indicating how well the benzene model results fit with carbon allotrope models'. The slope for the ten

equations are approximately 1. This indicates that for the same addition or cycloaddition reactions, the energetics of benzene are different by a constant number from certain C=C bonds on carbon nanomaterials, regardless of the nanomaterial sizes and shapes. Furthermore, the energy differences are intercepts on Y-axis. Based on these 10 equations, we could quickly estimate cycloaddition or addition reaction enthalpies on different sites of carbon-based nanomaterials by simply calculating their reactions on benzene.

6.3 Reference

1. Hayden, A. E.; Houk, K. N. *J. Am. Chem. Soc.* **2009**, *131*, 4084.
2. Frisch, M. J.; Trucks, G. W.; Schlegel, H. B.; Scuseria, G. E.; Robb, M. A.; Cheeseman, J. R.; Scalmani, G.; Barone, V.; Mennucci, B.; Petersson, G. A.; Nakatsuji, H.; Caricato, M.; Li, X.; Hratchian, H. P.; Izmaylov, A. F.; Bloino, J.; Zheng, G.; Sonnenberg, J. L.; Hada, M.; Ehara, M.; Toyota, K.; Fukuda, R.; Hasegawa, J.; Ishida, M.; Nakajima, T.; Honda, Y.; Kitao, O.; Nakai, H.; Vreven, T.; Montgomery, J. A., Jr.; Peralta, J. E.; Ogliaro, F.; Bearpark, M.; Heyd, J. J.; Brothers, E.; Kudin, K. N.; Staroverov, V. N.; Kobayashi, R.; Normand, J.; Raghavachari, K.; Rendell, A.; Burant, J. C.; Iyengar, S. S.; Tomasi, J.; Cossi, M.; Rega, N.; Millam, J. M.; Klene, M.; Knox, J. E.; Cross, J. B.; Bakken, V.; Adamo, C.; Jaramillo, J.; Gomperts, R.; Stratmann, R. E.; Yazyev, O.; Austin, A. J.; Cammi, R.; Pomelli, C.; Ochterski, J. W.; Martin, R. L.; Morokuma, K.; Zakrzewski, V. G.; Voth, G. A.; Salvador, P.; Dannenberg, J. J.; Dapprich, S.; Daniels, A. D.; Farkas, O.; Foresman, J. B.; Ortiz, J. V.; Cioslowski, J.; Fox, D. J.; Gaussian 09, revision C.01; Gaussian Inc.: Wallingford, CT, 2010.
3. Zhao, Y.; Truhlar, D. G. *Theor. Chem. Acc.* **2008**, *120*, 215-241.
4. Zhao, Y.; Truhlar, D. G. *Acc. Chem. Res.* **2008**, *41*, 157-167.

5. Hehre, W. J.; Radom, L.; Schleyer, P. v. R.; Pople, J. A. *Ab Initio Molecular Orbital Theory*, Wiley: New York, 1986.